FIU Electronic Theses and Dissertations                    University Graduate School

11-6-2013

# Development of Effective Approaches to the Large-Scale Aerodynamic Testing of Low-Rise Building

Tuan-Chun Fu
tfu001@fiu.edu

FLORIDA INTERNATIONAL UNIVERSITY

Miami, Florida

DEVELOPMENT OF EFFECTIVE APPROACHES TO THE LARGE-SCALE AERO-

DYNAMIC TESTING OF LOW-RISE BUILDINGS

A dissertation submitted in partial fulfillment of the

requirements for the degree of

DOCTOR OF PHILOSOPHY

in

CIVIL ENGINEERING

by

Tuan-Chun Fu

2013

To:     Dean Amir Mirmiran
        College of Engineering and Computing

This dissertation, written by Tuan-Chun Fu, and entitled Development of Effective Approaches to the Large-Scale Aerodynamic Testing of Low-Rise Building, having been approved in respect to style and intellectual content, is referred to you for judgment.

We have read this dissertation and recommend that it be approved.

_____
Girma Bitsuamlak

_____
Nakin Suksawang

_____
Yimin Zhu

_____
Arindam Gan Chowdhury, Major Professor

Date of Defense: November 6, 2013

The dissertation of Tuan-Chun Fu is approved.

_____
Dean Amir Mirmiran
College of Engineering and Computing

_____
Dean Lakshmi N. Reddi
University Graduate School

Florida International University, 2013

DEDICATION

I dedicate this dissertation to my wonderful family, especially my parents and my

wife for encouraging me to pursue my dreams and supporting me in every way for all

these years. Thank you for all of your love, patience and sacrifice.

ACKNOWLEDGMENTS

ABSTRACT OF THE DISSERTATION

DEVELOPMENT OF EFFECTIVE APPROACHES TO THE LARGE-SCALE AERO-

DYNAMIC TESTING OF LOW-RISE BUILDINGS

by

Tuan-Chun Fu

Florida International University, 2013

Miami, Florida

Professor Arindam Gan Chowdhury, Major Professor

Low-rise buildings are often subjected to high wind loads during hurricanes that lead to severe damage and cause water intrusion. It is therefore important to estimate accurate wind pressures for design purposes to reduce losses. Wind loads on low-rise buildings can differ significantly depending upon the laboratory in which they were measured. The differences are due in large part to inadequate simulations of the low-frequency content of atmospheric velocity fluctuations in the laboratory and to the small scale of the models used for the measurements. A new partial turbulence simulation methodology was developed for simulating the effect of low-frequency flow fluctuations on low-rise buildings more effectively from the point of view of testing accuracy and repeatability than is currently the case. The methodology was validated by comparing aerodynamic pressure data for building models obtained in the open-jet 12-Fan Wall of Wind (WOW) facility against their counterparts in a boundary-layer wind tunnel. Field measurements of pressures on Texas Tech University building and Silsoe building were also used for validation purposes. The tests in partial simulation are freed of integral length scale constraints, meaning that model length scales in such testing are only limited by blockage

considerations. Thus the partial simulation methodology can be used to produce aerody-namic data for low-rise buildings by using large-scale models in wind tunnels and WOW-like facilities. This is a major advantage, because large-scale models allow for accurate modeling of architectural details, testing at higher Reynolds number, using greater spatial resolution of the pressure taps in high pressure zones, and assessing the performance of aerodynamic devices to reduce wind effects. The technique eliminates a major cause of discrepancies among measurements conducted in different laboratories and can help to standardize flow simulations for testing residential homes as well as significantly improv-ing testing accuracy and repeatability. Partial turbulence simulation was used in the WOW to determine the performance of discontinuous perforated parapets in mitigating roof pressures. The comparisons of pressures with and without parapets showed signifi-cant reductions in pressure coefficients in the zones with high suctions. This demonstrat-ed the potential of such aerodynamic add-on devices to reduce uplift forces.

Keywords: Hurricane; Low-rise buildings; Parapets; Mitigation; Partial simulation; Silsoe; TTU; Wall of Wind; Wind Tunnel

TABLE OF CONTENTS

LIST OF FIGURES

**CHAPTER I**

INTRODUCTION

# CHAPTER I

## INTRODUCTION

### 1.1 Wind Induced Damages to Low-Rise Buildings

About 39% of the United States population lives in the counties directly on the shorelines prone to hurricanes (National Oceanic and Atmospheric Administration (NOAA. 2013). High wind events, such as hurricanes, cause the largest losses due to natural disasters in the United States. Low-rise buildings such as single-family residences and small commercial structures, which constitute over 70 % of the U.S. building stock, account for a majority of these losses. Although wind forces may not damage the building structure significantly, they inflict severe effects on the building envelope, especially the roofing components on low-rise buildings (MDC-BCCO, 2006). Building envelope damage due to high winds account for about 70% of the total insured losses (Holmes 2007). Most of the wind-induced damages are due the strong corner suction pressure on the roofs. Therefore, the shingles, tiles, or pavers placed on roofs are most vulnerable to being dislodged and becoming wind-borne debris (Aly et al. 2012, Tecle et al. 2013). In addition, losing roofing components could lead to rain water intrusion and losses to interior appliances and building contents (Bitsuamlak et al. 2009). Therefore, the need to reduce roof damages due to wind effects has recently become one of the most important challenges for designers, building component manufacturers, and building code officials. Understanding the relationship between natural wind loads and wind-induced uplift on roofs is required for developing passive mitigation devices that reduce suctions.

**1.2 Challenges in Estimating Wind Effects on Low-Rise buildings**

The reduction of wind induced damages to low-rise buildings requires the development of appropriate design and retrofitting provisions for such buildings, which currently are limited due to aerodynamic measurement difficulties in the current state of the art. To determine wind loading on buildings and other structures, model-scale testing is performed in aerodynamic testing facilities whose flows have properties such as mean wind profile, turbulence intensity, turbulence spectrum, and integral length scale similar to those of atmospheric boundary layer (ABL) flows. Such flows are generally appropriate for small-scale models (e.g., 1:100 to 1:400 scales). Kozmar (2010) found that flows with integral turbulence scales typically used for testing high-rise structures were inadequate for testing low-rise buildings. Low-rise buildings and other small structures such as residential buildings and small warehouses need to be modeled at larger scales (of the order of, say, 1:10 to 1:50) to replicate the effects of architectural details, achieve adequate spatial resolution of pressures taps, and reduce Reynolds number effects. Such large-scale model testing is often constrained by the difficulty of simulating adequately the low-frequency content of the turbulence spectrum and, in particular, the integral length scale parameter. For this reason, large-scale testing may appear to be inconsistent with wind testing provisions specified by ASCE 7-10 (2010), which, among other criteria, state: "*The relevant macro- (integral) length and micro-length scales of the longitudinal component of atmospheric turbulence are modeled to approximately the same scale as that used to model the building or structure.*"

Wind loads on low-rise buildings can differ significantly depending upon the laboratory in which they were measured. The differences are due in large part to inadequate

simulations of the low-frequency content of atmospheric velocity fluctuations in the laboratory and to the small scale of the models used for the measurements. Owing in part to such differences  aerodynamic pressures on low-rise structures specified in the ASCE 7 Standard (ASCE 7-2010) can be smaller by as much as 50 % than those measured in the wind testing laboratories or specified in the literature (Surry et al., 2003; St. Pierre et al., 2005; Ho et al., 2005; Coffman et al., 2009).

## 1.3 Development of Effective Approaches to Large-Scale Testing of Low-Rise Buildings

To address the above mentioned challenges the objective of the current work is to achieve flow simulations aimed to determine aerodynamic pressures on residential homes that are more effective from the point of view of testing accuracy and repeatability than is the case for conventional simulations in most wind testing facilities, including wind tunnels (Cermak, 1995) and large scale open jet facilities (Huang et al., 2009, Bitsuamlak et al., 2009, Bitsuamlak et al., 2010, Gan Chowdhury et al., 2009, Masters and Lopez, 2010, Smith et al., 2010). The approach for achieving this goal is the following. A new partial turbulence simulation method, which is an approach freed from the integral length constraint stated above, is developed to perform aerodynamic testing on large-scale residential building models and investigate the effectiveness of attenuating uplift pressure by installing passive devices. It was hypothesized that similar peak wind speeds in two flows, one characterized by a full turbulence spectrum and the other characterized by a partial turbulence spectrum with weak low frequency fluctuations and similar high frequency fluctuations, result in similar peak aerodynamic effects (i.e., in similar peak pressure coefficients). This hypothesis was partly based on previous studies that examined the role of

4

small scale (high frequency) turbulence on local aerodynamic effects such as peak pressures on low-rise structures (Melbourne 1980, Saathoff and Melbourne, 1997, Suresh and Stathopoulos 1998, Tieleman 2003, Richards et al. 2007, Banks 2011, Yamada and Katsuchi 2008, Irwin 2009, Kopp et al 2013, Kopp and Banks 2013).

The new approach amounts in effect to substituting for the low-frequency fluctuations of the flow with mean speed $U(z)$ an incremental speed $(c-1)U(z)$ constant in time. This incremental speed may be viewed as a conceptual flow fluctuation with vanishing frequency (i.e., with infinite period). The spatial coherence for this conceptual fluctuation is unity. It is to be noted that for large buildings, imperfect spatial coherence of atmospheric flows results in significant reductions of the overall wind effects with respect to the case of perfectly coherent flows. However, the smaller the building dimensions, the smaller are those reductions. In particular, the reductions can be expected to be small for residential homes.

In addition to eliminating a cause of discrepancies among measurements conducted in different laboratories, the proposed approach allows the use of considerably larger model scales than are possible in conventional testing, since it eliminates restrictions imposed by integral turbulence scales achievable in the laboratory. This is a major advantage, because large-scale models allow for accurate modeling of architectural details, testing at higher Reynolds number, using greater spatial resolution of the pressure taps in high pressure zones, and assessing the performance of aerodynamic devices to reduce wind effects.

## 1.4 Thesis Organization

The current dissertation is written in the format of 'Thesis Containing Journal Papers.' The dissertation contains four manuscripts out of which one is published, one is under review, and the other two will be submitted to scholarly journals. In addition, a general introduction chapter appears at the beginning and a general conclusion chapter appears at the end of dissertation.

The first paper, published in the International Journal of Wind and Structures, describes the concept for simulating the effect of low-frequency flow fluctuations on low-rise buildings more effectively. Experimental results are presented for two flows with and without low-frequency flow fluctuations. The results validated the hypothesis that missing low-frequency fluctuations can be compensated using incremental mean wind speed. The new technique can help standardize flow simulations and is applicable to wind tunnels and large scale open jet facilities.

The second paper, under review for the International Journal of Wind and Structures, describes the new partial turbulence simulation approach considering only high frequency part of the turbulent fluctuations spectrum in the small-scale 12-Fan Wall of Wind (WOW) facility. For the validation of aerodynamic pressures a series of tests were conducted in both wind tunnel and the small-scale 12-fan WOW facilities on low-rise buildings including two gable roof and two hip roof buildings with two different slopes. Testing was performed to investigate the mean and peak pressure coefficients at various locations on the roofs including near the corners, edges, ridge and hip lines.

The third paper, under review for the Journal of Wind Engineering and Industrial Aerodynamics, describes the iteration procedure for the partial turbulence simulation ap-

proach for simulating realistic aerodynamic loads on low-rise buildings. The paper also presents comparisons of pressure coefficients obtained in the prototype 12-fan Wall of Wind (WOW) facility on large-scale models of Texas Tech University (TTU) and Silsoe experimental buildings. Pressure data using the partial simulation approach were compared with field measurements on the prototype TTU and Silsoe buildings in ABL flows. The comparisons validate the efficacy of that approach for aerodynamic testing purposes.

The fourth paper, under review for the Engineering Structures, presents the comparisons of pressure coefficients obtained by (1) using the partial simulation approach in the FIU 12-fan Wall of Wind (WOW) facility on 1:6 models of prototype two-story residential buildings, and (2) wind tunnel measurements on 1:50 models of those prototype buildings in ABL flows. The large-scale models were then retrofitted with discontinuous perforated parapets at critical locations and tested in the WOW to assess their effectiveness in mitigating the mean and peak roof pressures.

**Reference**

Aly, A. M., Bitsuamlak, G. T., and Gan Chowdhury, A. (2012). "Full-scale aerodynamic testing of a loose concrete roof paver system." J. Eng. Struct., 44, 260-270.

ASCE. (2010). "Minimum design loads for buildings and other structures." ASCE/SEI 7-10, Reston, VA.

Banks D. (2011), "Measuring peak wind loads on solar power assemblies", The 13th International Conference on Wind Engineering, Amsterdam, Netherlands.

Bitsuamlak, G.T., Gan Chowdhury, A., and Sambare, D. (2009). "Application of a full-scale testing facility for assessing wind-driven-rain intrusion." J. Building Environm., 44(12), 2430-2441.

Bitsuamlak, G.T, Dagnew, A, Gan Chowdhury, A (2010). "Computational blockage and wind sources proximity assessment for a new full-scale testing facility." Wind and Structures, 13(1), 21-36.

Cermak, J.E. (1995). "Development of wind tunnels for physical modeling of the atmospheric boundary layer (ABL). A state of the art in wind engineering." Proceedings of the 9th International Conference on Wind Engineering. New Age International Publishers Limited, London, U.K., 1995, pp. 1-25.

Coffman, B.F., Main, J.A., Duthinh, D., Simiu, E. (2010). "Wind effects on low-rise buildings: Database-assisted design vs. ASCE 7-05 Standard estimates." J. Struct. Eng. (in press).

Gan Chowdhury, A., Simiu, E. and Leatherman, S.P. (2009), "Destructive testing under simulated hurricane effects to promote hazard mitigation," Nat. Hazards Review J. ASCE, 10(1), 1-10.

Ho, T.C.E., Surry, D., Morrish, D., and Kopp, G.A. (2005). "The UWO contribution to the NIST aerodynamic database for wind loads on low buildings: Part I. Archiving format and basic aerodynamic data," J. Wind Eng. Ind. Aerodyn. 93, 1-30.

Holmes, J.D. (2007). Wind Loading of Structures, 2nd Ed. Taylor & Francis, London.

Huang, P., Gan Chowdhury, A., Bitsuamlak G., and Liu. R. (2009). "Development of devices and methods for simulation of hurricane winds in a full-scale testing facility," Wind and Structures, 12 (2), 151-177.

Irwin, P. (2009), "Wind engineering research needs, building codes and project specific studies", 11th Americas Conference on Wind Engineering, San Juan, Puerto Rico.

Kopp, G. A. and Banks, D. (2013), "Use of the wind tunnel test method for obtaining design wind loads on roof-mounted solar arrays", J. Struct. Eng., 139, 284-287.

Kozmar, H. (2010), "Scale effects in wind tunnel modeling of an urban atmospheric boundary layer", Theor. Appl. Climatol., 100, 153-162.

Masters, F.J., Lopez, C. (2010). "Progress Update on Wind-Driven Rain Ingress Research at the University of Florida." Proceedings of the 2nd Workshop of the American Association for Wind Engineering (AAWE) (Marco Island, Florida, USA), (CD-ROM).

MDC-BCCO. Post hurricane Wilma progress assessment. Miami-Dade County Building Code Compliance Office, Miami, FL, 2006:1-22.

Melbourne W. H. (1980), "Turbulence effects on maximum surface pressures – a mechanism and possibility of reduction", Wind Engineering, 1, 521-551.

National Oceanic and Atmospheric Administration (2013). Population trends from 1970 to 2020. National Costal Population Report.

Richards, P.J., Hoxey, R.P., Connell, R.P., and Lander, D.P. (2007), "Wind-tunnel modelling of the Silsoe Cube", J. Wind Eng. Ind. Aerod., 95, 1384-1399.

Smith, J., Liu, Z., Masters, F.J., Reinhold, T. (2010). "Validation of facility configuration and investigation of control systems for the 1:10 scaled Insurance Center for Building Safety Research." Proceedings of the 2nd Workshop of the American Association for Wind Engineering (AAWE) (Marco Island, Florida, USA), (CD-ROM).

Saathoff, P. J. and Melbourne, W. H. (1997). "Effects of free-stream turbulence on surface pressure fluctuation in a separation bubble', J Fluid Mech., 337, 1-24.

Suresh Kumar, K. and Stathopoulos, T. (1998), "Spectral Density Functions of Wind Pressures on Various Low Building Roof Geometries", Wind and Structures, 1(3), 203-223.

Tecle, A., Bitsuamlak, G., Suksawang N., Gan Chowdhury, A., and Fuez, S. (2013). "Ridge and field tile aerodynamics for a low-rise building: a full-scale study." Wind and Struct., 16(4), 301-322.

Tieleman, H. W. (2003), "Wind tunnel simulation of wind loading on low-rise structures: a review", J. Wind Eng. Ind. Aerod., 91, 1627-1649.

Yamada, H. and Katsuchi, H. (2008), "Wind-tunnel study on effects of small-scale turbulence on flow patterns around rectangular cylinder", Proceeding of the 4th International Colloquium on Bluff Bodies Aerodynamics & Applications, Italy.

# CHAPTER II

A PROPOSED TECHNIQUE FOR DETERMINING AERODYNAMIC PRESSURES

ON RESIDENTIAL HOMES

(A paper published in *The Journal of Wind and Structure*)

# CHAPTER II

# A PROPOSED TECHNIQUE FOR DETERMINING AERODYNAMIC PRESSURES ON RESIDENTIAL HOMES

Tuan-Chun Fu[1], Aly Mousaad Aly[2], Arindam Gan Chowdhury[3], Girma Bitsuamlak[4],

DongHun Yeo[5], Emil Simiu[6]

## 2.1 Abstract

Wind loads on low-rise buildings in general and residential homes in particular can differ significantly depending upon the laboratory in which they were measured. The differences are due in large part to inadequate simulations of the low-frequency content of atmospheric velocity fluctuations in the laboratory and to the small scale of the models used for the measurements. The imperfect spatial coherence of the low frequency velocity fluctuations results in reductions of the overall wind effects with respect to the case of perfectly coherent flows. For large buildings those reductions are significant. However, for buildings with sufficiently small dimensions (e.g., residential homes) the reductions

[1] Graduate Student, Dept. of Civil & Environ. Engineering, Florida International University, Miami, Florida 33174, E-mail: tfu001@fiu.edu.

[2] Former Post Doctoral Research Scholar, Intl. Hurricane Research Center, Florida International University, Miami, Florida 33174, E-mail: aly.mousaad@polimi.it.

[3] *Corresponding Author*: Assistant Professor, Dept. of Civil & Environ. Engineering, Florida International University, Miami, Florida 33174, Tel: (305)348-0518, Fax: (305)348-2802, E-mail: chowdhur@fiu.edu.

[4] Assistant Professor, Dept. of Civil & Environ. Engineering, Florida International University, Miami, Florida 33174, E-mail: bitsuamg@fiu.edu.

[5] Research Engineer, National Institute of Standards and Technology, Gaithersburg, Maryland 20899, E-mail: donghun.yeo@nist.gov.

are relatively small. A technique is proposed for simulating the effect of low-frequency flow fluctuations on such buildings more effectively from the point of view of testing accuracy and repeatability than is currently the case. Experimental results are presented that validate the proposed technique. The technique eliminates a major cause of discrepancies among measurements conducted in different laboratories. In addition, the technique allows the use of considerably larger model scales than are possible in conventional testing. This makes it possible to model architectural details, and improves Reynolds number similarity. The technique is applicable to wind tunnels and large scale open jet facilities, and can help to standardize flow simulations for testing residential homes as well as significantly improving testing accuracy and repeatability. The work reported in this paper is a first step in developing the proposed technique. Additional tests are planned to further refine the technique and test the range of its applicability.

**KEY WORDS:** Aerodynamics; atmospheric surface layer; building technology; low-rise structures; open jet facilities; residential buildings;  wind engineering; wind tunnels.

### 2.2 Introduction

High winds cause the largest losses due to natural disasters in the U.S. Annual losses due predominantly to high winds from hurricanes alone averaged on the order of $10 billion from 1990-1995. Low-rise buildings such as single-family residences and small commercial structures, which constitute over 70 % of the U.S. building stock, account for a majority of these losses. The reduction of these losses requires the development of appropriate design and retrofitting provisions for such buildings, which currently

---

[6] NIST Fellow, National Institute of Standards and Technology, Gaithersburg, Maryland.

are limited due to aerodynamic measurement difficulties in the current state of the art. An international round-robin set of wind tunnel tests of low-rise structures conducted at six reputable laboratories showed that wind-induced internal forces in structural frames, and pressures at individual taps, can differ from laboratory to laboratory by factors larger than two (Fritz et al., 2008). This variation is a barrier to the development of rational building standards. Owing in part to such differences  aerodynamic pressures on low-rise structures specified in the ASCE 7 Standard (ASCE 7-2005) can be smaller by as much as 50 % than those measured in the wind testing laboratories or specified in the literature (Surry et al., 2003; St. Pierre et al., 2005; Ho et al., 2005; Coffman et al., 2009).

Among the reasons for the non-repeatability of conventional tests across laboratories are two facts. First, the low-frequency fluctuations of the oncoming flow turbulence in the atmospheric surface layer are difficult to simulate in the laboratory, and second, the techniques for their production in the laboratory are not standardized. Since those fluctuations contain the bulk of the turbulent energy, they contribute overwhelmingly to the turbulence intensity and the integral turbulence scale.

For large buildings, imperfect spatial coherence of atmospheric flows results in significant reductions of the overall wind effects with respect to the case of perfectly coherent flows. However, the smaller the building dimensions, the smaller are those reductions. In particular, the reductions can be expected to be small for residential homes. It is hypothesized that peak aerodynamic effects experienced by a small building subjected to flows whose velocities have significant low-frequency fluctuations (hereinafter called "*atmospheric boundary layer-type or ABL-type flows*") are not substantially different from those induced by flows hereinafter called "*simplified flows*;" that is, for flows for

which (a) the low-frequency content is negligible, while (b) the mean velocities are larger than their counterparts in atmospheric boundary layer flows by amounts that make up for the absence of low-frequency fluctuations.

The objective of the proposed technique is to achieve flow simulations aimed to determine aerodynamic pressures on residential homes that are more effective from the point of view of testing accuracy and repeatability than is the case for conventional simulations in most wind testing facilities, including wind tunnels (Cermak, 1995) and large scale open jet facilities (Huang et al., 2009, Bitsuamlak et al., 2009, Bitsuamlak et al., 2010, Gan Chowdhury et al., 2009, Masters and Lopez, 2010, Smith et al., 2010). The approach for achieving this goal is the following. No attempt is made to simulate low-frequency components, i.e., components with non-dimensional frequencies $nz / U(z)$ less than say, 0.1 or 0.2, for which it is commonly accepted that inertial subrange assumptions are no longer applicable ($n$ = frequency, $z$ = height above the surface, $U$ = mean wind speed of the turbulent flow averaged over, say, 10 min or 1 hour) (Fichtl and McVehil, 1970). Rather, the mean speed of the laboratory flow is augmented from $U(z)$ to $cU(z)$, where $c > 1$ is determined as shown in the Appendix. Note that the vertical profile of the simulated flow speeds $U(z)$ and $cU(z)$ is the same. This approach amounts in effect to substituting for the low-frequency fluctuations of the flow with mean speed $U(z)$ an incremental speed $(c-1)U(z)$ constant in time. This incremental speed may be viewed as a conceptual flow fluctuation with vanishing frequency (i.e., with infinite period). The spatial coherence for this conceptual fluctuation is unity. Methodology for the determination of factor $c$ is described in the Appendix.

In addition to eliminating a cause of discrepancies among measurements conducted in different laboratories, the proposed approach allows the use of considerably larger model scales than are possible in conventional testing, since it eliminates restrictions imposed by integral turbulence scales achievable in the laboratory.

Provided that the spatial separations are of the order of, say, 20 m or less, for the low-frequency components of the atmospheric flow fluctuations, the spatial coherences are relatively large. This is shown in the Appendix by using the expression for spatial coherence (Vickery, 1970):

$$Coh(r,n) = e^{-f} \tag{1}$$

$$f = \frac{n[C_z^2(z_1 - z_2)^2 + C_y^2(y_1 - y_2)^2]^{1/2}}{\frac{1}{2}[U(z_1) + U(z_2)]} \tag{2}$$

where $n$ is the frequency of atmospheric flow fluctuations, $U(z)$ is the mean wind speed at height $z$, $y_1$, $y_2$ and $z_1$, $z_2$ are horizontal and vertical coordinates of points $M_1$ and $M_2$ (the distance between which is denoted by $r$), and the line $M_1$, $M_2$ is assumed to be perpendicular to the direction of the mean wind speed. $C_y$ and $C_z$ are exponential decay coefficients that are determined experimentally. The proposed testing procedure for low-rise buildings is based on the hypothesis that the spatial coherences of interest are indeed sufficiently large.

To test the hypothesis that peak aerodynamic effects experienced by a small building subjected to ABL-type flows are not substantially different from the aerodynamic effects induced by simplified flows, two sets of tests were carried out as follows. One set of tests used a model of the Silsoe building (Murakami and Mochida, 1990; Richards et al., 2001), while the second set used a model of the Texas Tech University (TTU) test

building (Okada and Ha, 1992). Each set of tests was based on two types of flow. The ABL-type flow was simulated by imparting to the fans quasi-periodic rotations induced by a quasi-periodic waveform signal (for details see Huang et al., 2009). The simplified flow contained negligible low-frequency fluctuations (substituting for the low-frequency fluctuations an incremental speed $(c-1)U(z)$ constant in time), as explained earlier. A methodology for estimating the factor $c$ is presented in some detail in the Appendix. As is shown subsequently in the section "Results", the pressure measurement results obtained under these two types of flows support the hypothesis on which this paper is based.

**2.3 Description of Tests**

The experiments were carried out by utilizing the 12-fan small-scale Wall of Wind (WoW) (Fu et al., 2010, Gan Chowdhury et al., 2010), an open jet test facility at Florida International University (Figure 1). Two specimens were built as follows:

(1) 8.9 x 8.9 x 8.9 cm (3.5 x 3.5 x 3.5 in) Silsoe cube (length scale being 1:67.5),

(2) 17.5 x 26.0 x 7.7 cm (6.89 x 10.24 x 3.03 in) TTU building (length scale being 1:52).

High frequency cobra probes were used for wind speed measurements and set at 625 Hz sampling rate. A 64 channels pressure transducer was used at a 100 Hz sampling rate. For specimens (1) and (2), all the pressure taps were distributed over the external surface, covering the windward, roof, leeward, and side walls as shown in Figure 2. Pressures were measured for wind angles of attack of 0˚ and 45˚.

Two types of wind flows were generated to simulate the wind stream without and with low frequency turbulence. To simulate the wind flow without low frequency turbulence components, a flat waveform signal was input into the WoW controller. To simu-

late the wind flow with low frequency components, a quasi-periodic waveform signal was input into the WoW controller, based on the spectrum of the longitudinal velocity fluctuations for real hurricanes (Yu et al., 2008). The waveform generation details are described in Huang et al. (2009). Figure 3 presents the input waveforms for generating the airflows without and with low-frequency turbulence. The peak of the input signal for the quasi-periodically driven fans (generating ABL-type flows) was equal to the constant input signal for the uniformly driven fans (generating simplified flows). Simplified estimation of increased mean wind speed $c'U(z)$ (for uniform flow) was estimated by using Step 4, variant (b), of the Appendix. To ensure stability and repeatability of the peak pressure values, all the tests were carried out for 5 min. For the TTU model this duration corresponds at full scale to 90 min, as shown by Eqs. 3 and 4:

$$\frac{T_p U_p}{L_p} = \frac{T_m U_m}{L_m} \tag{3}$$

$$T_p = \left(\frac{L_p}{L_m}\right)\left(\frac{U_m}{U_p}\right)T_m = (52)\left(\frac{16.9(m/s)}{50(m/s)}\right) \times 5(\text{min}) = 87.9\,\text{min} \tag{4}$$

where $T$, $U$, and $L$ are the time, mean wind speed, and characteristic length, respectively, and the subscript $p$ and $m$ refer to the prototype and the model, respectively. The length scale of 1:52 was based on the scale of the TTU model and the full-scale wind speed is considered as 50 m/s. For the quasi-periodic flow the mean wind speed was 16.9 m/s. For the Silsoe model the 5 min. duration corresponded to about 2 hrs at full-scale.

To simulate atmospheric boundary layer (ABL) wind profiles, a passive device was used to generate the vertical profile of wind flows (Gan Chowdhury et al., 2010).

This device consisted mainly of a set of planks. The inclination of each plank was adjusted by trial and error to ensure that the mean speeds of the air flow match reasonably well the mean flow in typical open terrain (power law exponential $\bar{\alpha}$ = 1/6 pertaining to mean flow, see Figure 4).

The measured turbulence intensity at 89 mm (3.5 in) above ground (corresponding to the roof height of the Silsoe model) was about 6 % for the flat flow and 26 % for the quasi-periodic flow. Mean wind speeds were 24.8 m/s and 16.9 m/s for the flat and quasi-periodic flows, respectively. This ensured that the flow with negligible low-frequency content had a mean velocity equal to the sum, in the flow with significant low-frequency content, of (a) the mean velocity, and (b) the peak fluctuating velocity induced by the low-frequency fluctuations. The optimal distance between the exit of the WoW and the windward wall surface of the test models was 22.0 cm (8.6 in). Figure 5 shows the wind velocity time histories of the flows without and with low-frequency components. Figure 6 shows the dimensional spectra for both flows. For comparison purposes the figure also shows the spectrum proposed by Yu et al. (2008) for hurricane wind data in open terrain exposure, obtained within the framework of the Florida Coastal Monitoring Program (Masters, 2004) [mean wind speed of 16.9 m/s, turbulence intensity of 26 %, and parameter $\beta$ = 6.0 (Table 2.3.1, Simiu and Scanlan, 1996)]. The spectrum for the flat flow shows significantly lower ordinates than those of the FCMP spectrum. The spectrum for the flow with low-frequency fluctuations (i.e., the quasiperiodic flow) has ordinates comparable to those of the FCMP spectrum for the interval of $n$ = 0.03 Hz to $n$ = 1 Hz. The small-scale fans were not capable of producing significant fluctuations beyond $n$ = 1 Hz, hence the deficit in the quasiperiodic flow spectrum ordinates beyond $n$ = 1 Hz.

Because of the limitations of the small scale WoW fan's performance, it was possible to obtain spectra covering only the dimensional interval $n = 0.03$ Hz to $n = 10$ Hz, that is, the non-dimensional interval up to $f = 0.06$. The turbulence intensities achieved in the experiments increased from 6 % in the absence of low-frequency fan rotations to 26 % when quasiperiodic fan rotations were activated. The results of the experiments presented in the paper show that the effect of increments in the mean speeds (i.e., the effect of incremental "zero frequency" fluctuations) was a reasonable substitute for the effect of low-frequency fluctuations. This was the case not only for the aerodynamics of the windward face of the structure, but also for the aerodynamics of the structure as a whole. Quantitative experimental information (a) corresponding to other non-dimensional frequency intervals and (b) on the sizes of the windward face for which the assumption of perfect coherence of the oncoming low-frequency fluctuations is not overly conservative, will require large-scale WoW testing used in conjunction with analytical calculations in which the parameters of the flow coherence are based on measurements of the large-scale turbulent flow.

Figure 1. Small-Scale 12-Fan Wall-of-Wind (WoW)

(a)
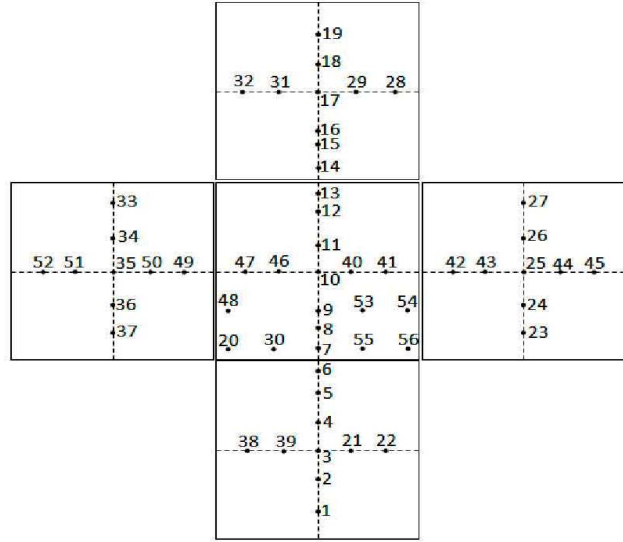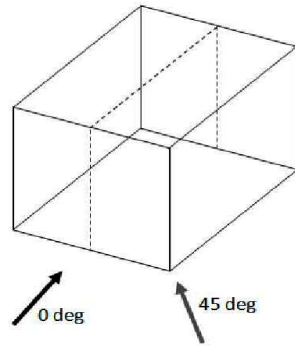


(b)
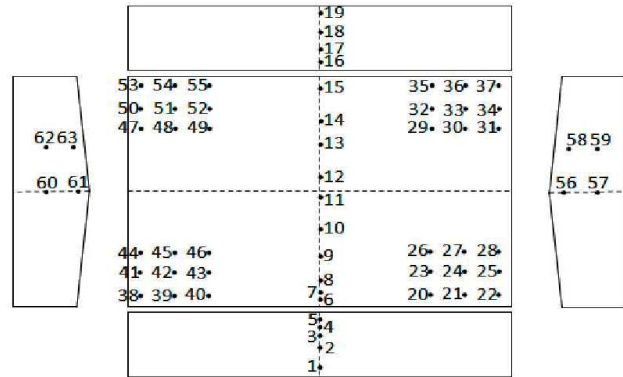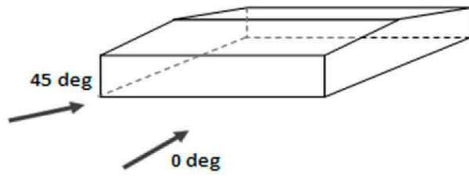


Figure 2. Tap Layout for the Two Test Specimens: (a) 8.9 x 8.9 x 8.9 cm Silsoe Cube, and (b) 17.5 x 26.0 x 7.7 cm TTU Building
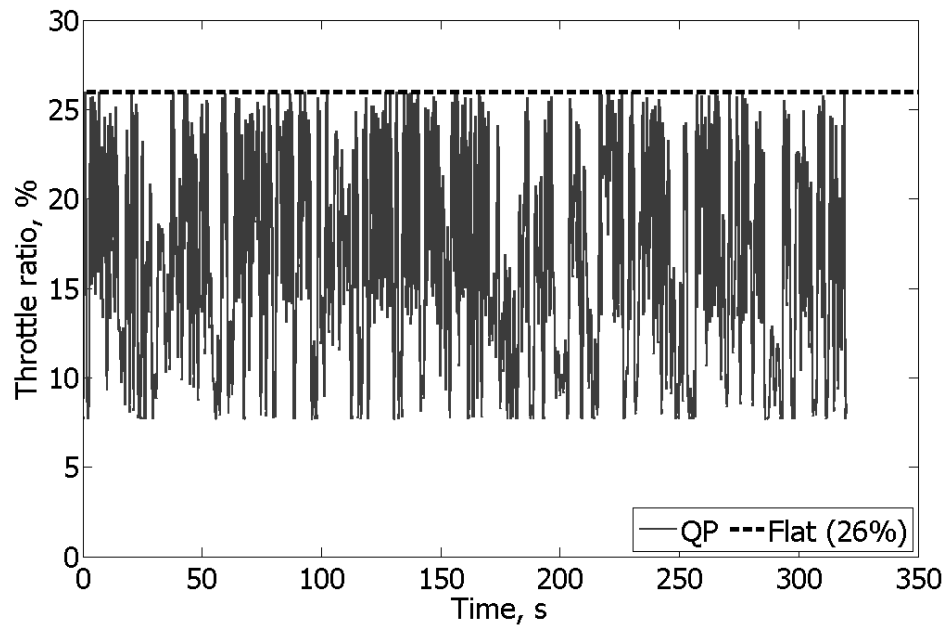
Figure 3. Input Waveforms of Flat Flow (without Low-Frequency Content) and Quasi-Periodic (QP) Flow (with Low-Frequency Content)
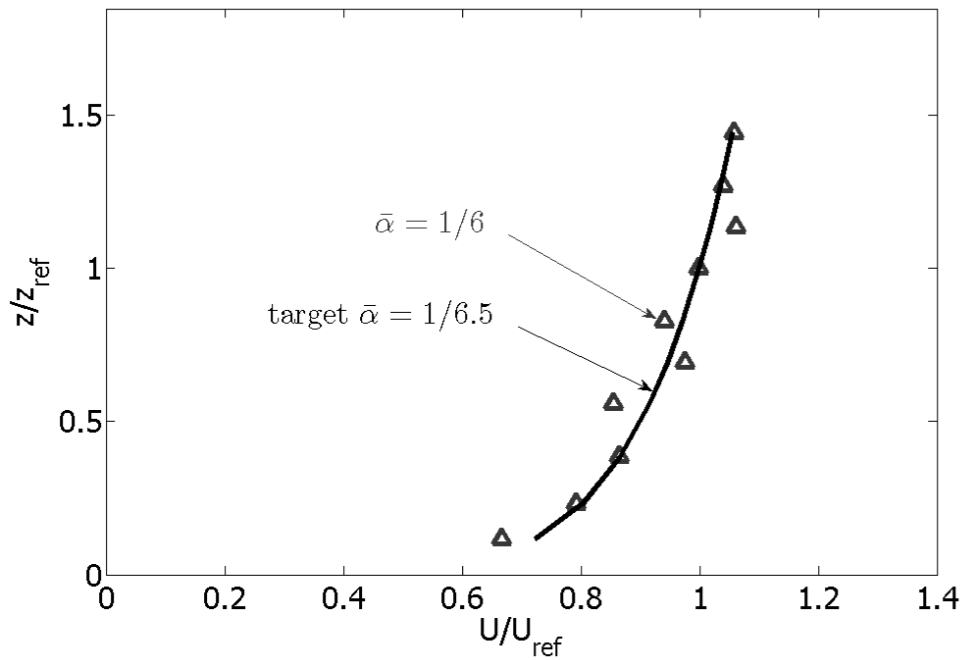


Figure 4. Mean Wind Speed Profile
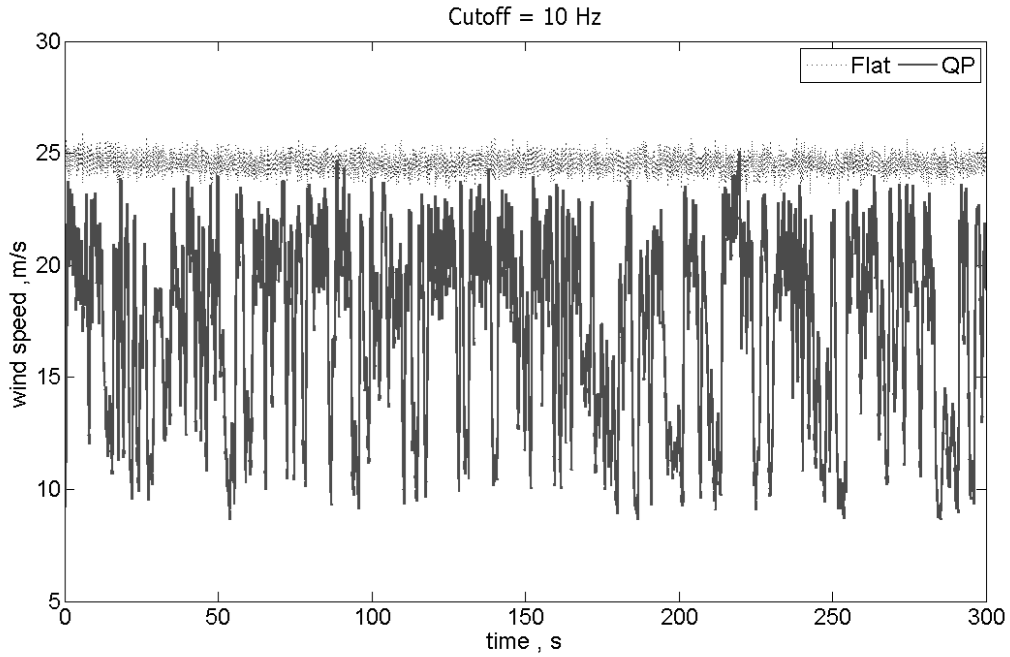
Figure 5. Time History of Flat Flow (Without Low-Frequency Content), and Quasi-Periodic (QP) Flow (With Low-Frequency Content)
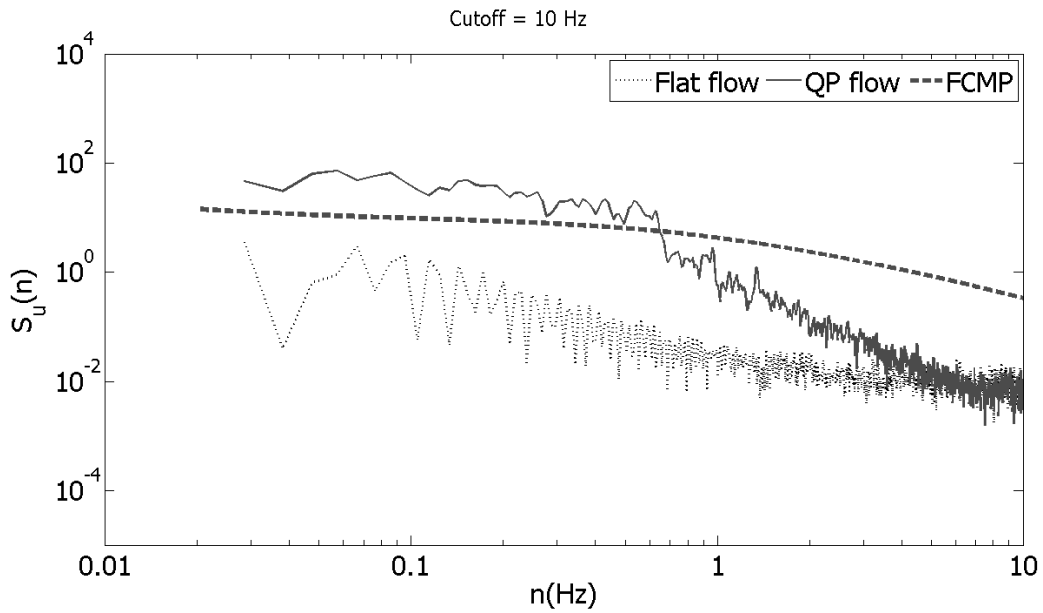


Figure 6. Dimensional Spectra of Longitudinal Wind Flow Fluctuations

23

**2.4 Results**

Typical time histories of roof pressures are shown in Figure 7. The observed peaks can exhibit wide variability from one realization to another due to their random nature. To remove the uncertainties inherent in the randomness of the peaks, probabilistic analyses were performed using the procedure developed by Sadek and Simiu (2002) (www.nist.gov/wind) for obtaining statistics of pressure peaks from observed pressure time histories. Because estimates obtained by this procedure are based on the entire information contained in the time series, they are more stable than estimates based on observed peaks and provide a clearer and more meaningful basis for the comparisons. The comparisons were in all cases based on the 95th percentile of the estimated distributions of the peaks.

Figure 8 shows the ratio (R) of the 95th percentile estimates of peak pressures measured for the Silsoe model under flow with no low-frequency content to peak pressures measured with low frequency content. The experiments were repeated 5 times. As the results show, the ratios are typically close to unity. In a few cases they are higher than unity by approximately 20 %, and lower than unity by approximately 17 %.

Table 1 lists means and standard deviations of the ratio R obtained for each of the selected taps on the Silsoe model for two wind azimuths (0 ˚ and 45 ˚) in five repeated tests. Taps were chosen to represent windward wall, roof, leeward wall, top corner, and side walls. Results show that the mean value of the ratio R for the five trials is also close to one. Low standard deviation values indicate that the repeatability of the tests is satisfactory.

Figure 9 shows peak pressure ratios for TTU model. The largest ratio R at the roof is about 20 % higher than unity. Table 2 lists mean and standard deviation of the ratio R obtained for five repeated tests with the TTU model for two wind azimuths (0 ˚ and 45 ˚). Arbitrary taps were chosen to represent windward, roof, leeward, top corner, and side wall. Results show that the mean value of the ratio, R, for the five trials is close to one. The standard deviations of the results are in all cases small. This establishes the repeatability of the tests performed in accordance with the procedure proposed in this paper.

Future tests are planned in FIU's large-scale 12-fan WoW facility currently under construction, with a view to validating the proposed procedure for a wide range of model-to-full-scale ratios. For these tests, attendant skewness and kurtosis calculations will be performed to determine possible deviations of the distributions from normality.
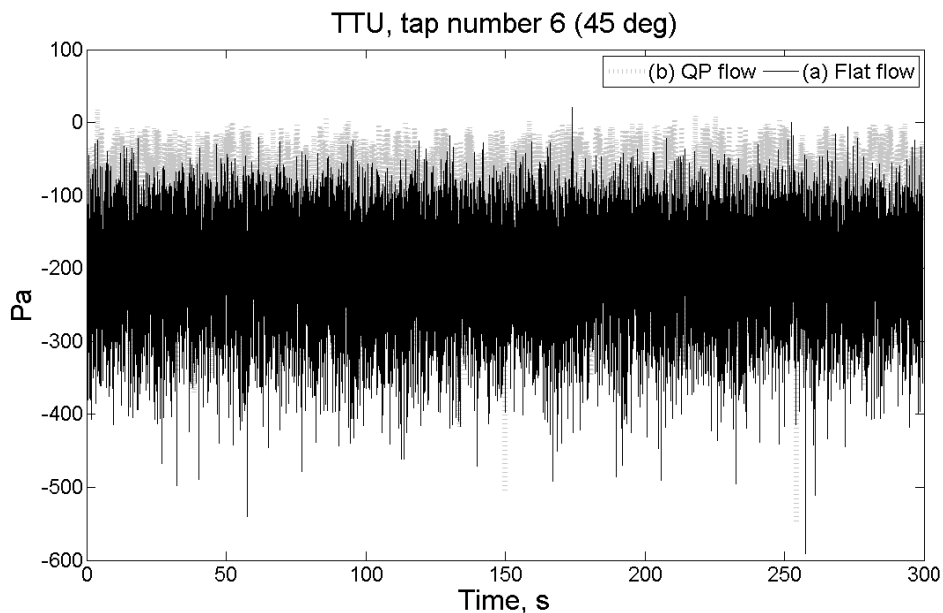


Figure 7. Typical Roof Pressure Time History Data under (a) Flat Wind Flow and (b) Quasi-Periodic (QP) Wind Flow
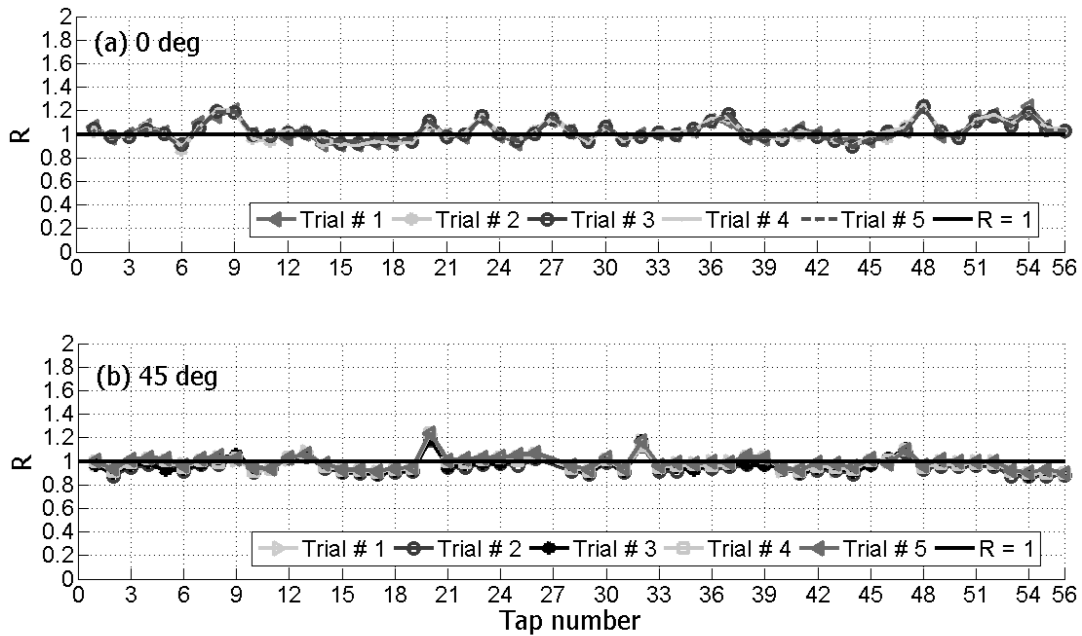
Figure 8. Peak Pressure Ratio for Flat to Quasi-Periodic (QP) Flows vs. Tap Number (Silsoe Cube)

Table 1. Mean and Standard Deviation of the Ratio R Obtained for Five Repeated Tests with the Silsoe Cube Model for Two Wind Azimuths

| Azimuth | Ratio | Tap # 5 | Tap # 7 | Tap # 14 | Tap # 49 | Tap # 56 |
|---------|-------|---------|---------|----------|----------|----------|
| 0 deg | $R_{mean}$ | 1.0092 | 1.0650 | 0.9439 | 1.0166 | 1.0308 |
|  | $R_{std}$ | 0.0028 | 0.0164 | 0.0257 | 0.0148 | 0.0021 |
| 45 deg | $R_{mean}$ | 0.9796 | 0.9946 | 0.9557 | 0.9854 | 0.8907 |
|  | $R_{std}$ | 0.0391 | 0.0228 | 0.0160 | 0.0198 | 0.0070 |
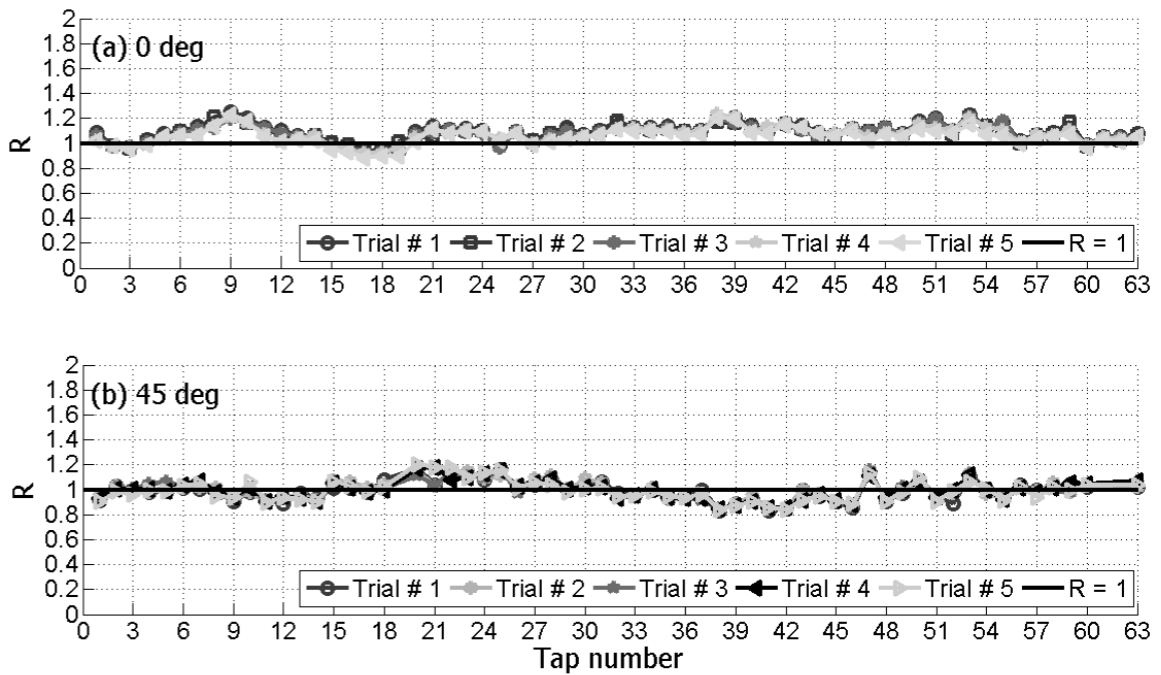
Figure 9. Peak Pressure Ratio for Flat to Quasi-Periodic (QP) Flows vs. Tab Number (TTU Model)

Table 2. Mean and Standard Deviation of the Ratio R Obtained for Five Repeated Tests with the TTU Test Model for Two Wind Azimuths

| Azimuth | Ratio | Tap # 4 | Tap # 8 | Tap # 16 | Tap # 38 | Tap # 60 |
|---------|-------|---------|---------|----------|----------|----------|
| 0 deg | $R_{mean}$ | 1.0060 | 1.1528 | 0.9607 | 1.2052 | 0.9786 |
| | $R_{std}$ | 0.0191 | 0.0338 | 0.0230 | 0.0235 | 0.0107 |
| 45 deg | $R_{mean}$ | 1.0017 | 0.9773 | 1.0260 | 0.8384 | 1.0320 |
| | $R_{std}$ | 0.0271 | 0.0218 | 0.0210 | 0.0059 | 0.0117 |

**2.5 Conclusions**

Flows that attempt to simulate low-frequency fluctuations for the testing of residential homes and other low-rise buildings or portions thereof have the following drawbacks. First, they tend to induce significant errors in the estimation of the pressures. These errors are typically much larger than errors inherent in the use of flows with no low-frequency fluctuations, and affect adversely the repeatability of the tests. To achieve better agreement among results across different laboratories, a standard flow simulation protocol for low-rise buildings will have to be developed for both wind tunnels and large scale open jet facilities. The standardized flow simulations will result in improved testing accuracy and repeatability for residential homes.

Second, the simulation of low-frequency turbulent fluctuations imposes severe constraints on the geometric model scale, which unavoidably entail additional errors in the estimation of aerodynamic effects. For flows with no low-frequency fluctuations these constraints are eliminated, the only subsisting constraints on model scale being those associated with blockage.

The results of the tests presented in this paper support the hypothesis that flows with no low-frequency content that simulate correctly the mean wind profile in the atmospheric boundary layer are adequate for the simulation of pressures induced by atmospheric flows on low-rise buildings with dimensions comparable to those of individual homes. The errors inherent in such flows are far smaller than those that can occur in conventional wind tunnel tests. The proposed technique allows the use of larger test models allowing the modeling of architectural details, Reynolds number improvements enhanc-

ing aerodynamic accuracy, and higher spatial resolution of pressure measurements. The work reported in this paper is viewed as a first step in developing the proposed technique.

Future tests are planned to further refine the technique and validate it for a wide range of model-to-full-scale ratios. For these tests, attendant skewness and kurtosis calculations will be performed to determine possible deviations of the distributions from normality.

The principle of the methodology is applicable not only to the proposed experimental technique but to Computational Fluid Dynamics (CFD) calculations as well. Such application would have the considerable advantage of simplifying the simulation of the oncoming flow, whose conventional representation, entailing as it does fluctuations with imperfectly correlated low-frequency fluctuations, is a major barrier to the performance of effective numerical computations.

## 2.6 Acknowledgements

## Appendix. Determination of factor *c*

This Appendix proposes an answer to the question: how large should the increment of the mean velocity be in order to provide a correct approximate substitute for the missing low-frequency fluctuations?

Consider the simple case of the total wind force acting on the windward face of a rectangular building acted upon by wind normal to that face. For this case it is possible to calculate approximately that force both for flow nominally conforming to the conventional ABL model, and for flow conforming to the simplified model described earlier. The study also proposes an answer to the following question: what is the definition of "low-frequency fluctuations?" The answers based on the present study are intended to provide guidance required for aerodynamic testing of small buildings in simplified flows.

The wind speed $U(y, z, t)$ is assumed to vary with time $t$, width $y$, and height $z$, and consists of the mean wind speed $U(z)$ and the wind speed longitudinal fluctuations about the mean, $u(y, z, t)$. The velocity $U(y, z, t)$ is assumed to be normal to the wider face of the building.

The objective is to create a simplified flow such that the peak total aerodynamic force $F_{peak}$ it induces on the windward face of a building is approximately equal to the peak force induced by the ABL-type. The calculations entail the following steps:

*Step 1*: Estimation of peak force $F_{peak}$ induced by the ABL flow on the windward building face:

The calculation of the peak total aerodynamic force $F_{peak}$ is performed here under the following assumptions:

1. The spectral density of the longitudinal flow fluctuations $u$ is described by the expression for the modified Kaimal spectrum:

$$\frac{n\, S_u(z,n)}{u_*^2} = \frac{200 f}{(1 + 50 f)^{5/3}} \tag{A1}$$

where $f$ is the reduced frequency defined as $nz/U(z)$ and $u_*$ is the friction velocity (Simiu and Scanlan, 1996, p. 59). This expression is valid for frequencies $0 < f \leq f_c$ in which it is reasonable to assume a cut-off frequency $f_c = 10$ (i.e., $S_u(z, n) = 0$ for $f > f_c$). If appropriate, different expressions for the spectrum may be employed.

2. The expression for the spatial coherence of the longitudinal wind velocity fluctuations $u$ is given by Eqs. 1 and 2.

3. The longitudinal flow fluctuations and the flow-induced forces on the windward wall are approximately Gaussian.

Using these assumptions, the total wind-induced peak force $F_{peak}$ on the windward wall can be expressed as the sum of the mean force and the peak force due to all fluctuations:

$$F_{peak} \approx F_U + \kappa_{Fp} \sigma_{Fp} \tag{A2}$$

where

$$F_U = \int_0^h \int_0^b \tfrac{1}{2} \rho C_p U^2(z) \, dy \, dz \tag{A3}$$

$b$ is the width of the building, $h$ is the height, $\rho$ is the air density, $C_p = P(z) / \left[ \tfrac{1}{2} \rho U^2(z) \right] \approx 0.8$ is the mean pressure coefficient where $P(z)$ is the mean pressure at height z, $K_{Fp}$ is the peak factor, and $\sigma_{Fp}$ is the r.m.s. of the fluctuating force $F'$.

The peak factor for a flow with a duration of $T$ seconds is approximately (Davenport 1964)

$$\kappa_{Fp} \approx \sqrt{2\ln(\nu_{Fp}T)} + \frac{0.577}{\sqrt{2\ln(\nu_{Fp}T)}}$$

$$\text{where} \quad \nu_{Fp} = \left[ \frac{\int_0^{n_c} n^2 S_{Fp}\, dn}{\int_0^{n_c} S_{Fp}\, dn} \right]^{1/2} \tag{A4}$$

where $\nu_{Fp}$ is the expected frequency for the peak force, and $n_c$ is the dimensional cut-off

frequency corresponding to $f_c$, $S_{Fp}$ is the spectral density of the fluctuating force $F_p$ on the

windward wall. The r.m.s. of the fluctuating force $F_p$ is obtained by integration as

follows:

$$\sigma_{Fp} =$$
$$\left[ \int_0^{n_c} \int_0^h \int_0^h \int_0^b \int_0^b \rho^2 C_p^2 U(z_1) U(z_2) S_u^{1/2}(z_1,n) S_u^{1/2}(z_2,n) \times \atop \text{Coh}(y_1,y_2,z_1,z_2,n)\, dy_1\, dy_2\, dz_1\, dz_2 dn \right]^{1/2} \tag{A5}$$

(Simiu and Scanlan,1996, p. 208). This completes the calculation of the peak force $F_{peak}$

induced by the ABL flow.

*Step 2*: Estimation of peak force $F_{peak1}$ induced by the simplified flow.

The estimation process is similar to Step 1 except that:

1. The spectral density of the longitudinal velocity fluctuations $u$ in the simplified flow is

$$S_u(z,n) = 0 \qquad \text{for } 0 < f \le f_{low}$$

$$\frac{n\, S_u(z,n)}{u_*^2} = \frac{200 f}{(1+50f)^{5/3}} \quad \text{for } f_{low} < f \le f_c \tag{A6}$$

32

where $f_{low}$ can be selected near the lower limit of the interval within which the Kolmogorov inertial subrange hypothesis holds in the ABL wind, and $f_c = 10$ as explained earlier. Recall that the reduced frequency $f$ is based on mean wind speed $U(z)$.

The simplified flow has no (or weak) low-frequency fluctuations (area $A$ in Fig. A1) (see Eq. A6), and has an increased mean speed $cU$ which is required so that the peak force generated by the ABL flow (with speed $U$ and spectral content denoted by $A$ and $B$ in Fig. A1) be the same as the peak force generated by the simplified flow (with speed $cU$ and spectral content denoted by $B$). Note that wind-induced pressures on buildings are affected by high-frequency fluctuations, which should be simulated in the simplified flow.

The calculation of the peak force $F_{peak1}$ ($= F_{cU}$) due to the simplified flow is similar to the calculation of the force $F_{peak}$ in Step 1.

*Step 3*: Estimation of the upper limit of low-frequency fluctuations $f_{low}$.

To generate approximately equivalent peak forces due to the ABL flow (Step 1) and the simplified flow (Step 2), the low-frequency fluctuations must have sufficiently high spatial coherence so that the force they generate can be replaced by the mean force due to the incremental speed $\Delta U$. For small structures, e.g., residential homes, a reasonable approximate estimate of the upper limit of low-frequency fluctuations is $f_{low} = 0.1$ (Yeo, 2010).

*Step 4*, variant (a): Estimation of increased mean wind speed $cU$.

Given $f_{low}$, the increased mean wind speed $cU = U + \Delta U$ can be determined by equating the peak force due to the ABL flow and the peak force due to the simplified flow (i.e.,

$F_{peak} = F_{peak1}$). The requisite factor $c$ and the corresponding mean wind speed increment $\Delta U$ are therefore estimated as follows:

$$F_{cU} = c^2 F_U \tag{A7}$$

$$c = \sqrt{\frac{\kappa_{Fp}\sigma_{Fp} - \kappa_{Fph}\sigma_{Fph}}{F_U} + 1} \tag{A8}$$

$$\Delta U = (c-1)U \tag{A9}$$

where $\kappa_{Fp}$ is the peak factor and $\sigma_{Fp}$ is the r.m.s. of the fluctuating force, for the high frequency fluctuations $f_{low} < f \le f_c$.

*Step 4*, variant (b): Simplified estimation of increased mean wind speed $c'U = U + \Delta U'$. An alternative estimate of the increased speed, denoted by $c'U$, can be performed by equating the peak wind speed due to the low-frequency fluctuations in the ABL flow and the increment in the mean speed $\Delta U'$ in the simplified flow. The results are then

$$U + \kappa_u \sigma_u = c'U + \kappa_{uh}\sigma_{uh} \tag{A10}$$

$$c' = \frac{\kappa_u \sigma_u - \kappa_{uh}\sigma_{uh}}{U} + 1 \tag{A11}$$

$$\Delta U' = \kappa_u \sigma_u - \kappa_{uh}\sigma_{uh} \tag{A12}$$

where $\kappa_u$ and $\sigma_u$ are the peak factor and the r.m.s. of the longitudinally fluctuating wind speed corresponding to all frequency fluctuations $0 < f \le f_c$, and $\kappa_{uh}$ and $\sigma_{uh}$ are their counterparts corresponding to high frequency $f_{low} < f \le f_c$. The calculated $\Delta U'$ is

slightly more conservative (i.e., larger) and less accurate than $\Delta U$ calculated in Step

4(a). The larger the building, the less accurate the simplified calculation is.

The software for the numerical implementation of the calculation is provided in

Yeo (2010).
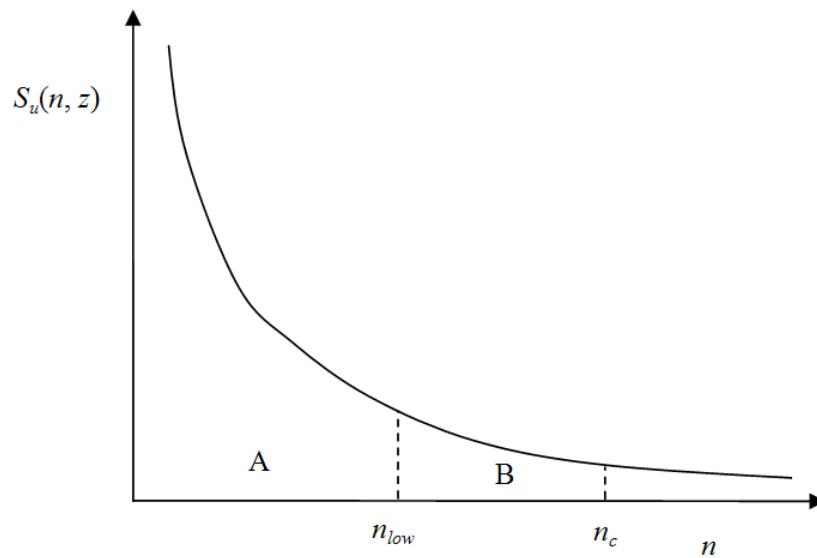
Figure 10. Spectrum of the Longitudinal Velocity Fluctuations [ n = fU(z)/z ]

## 2.7 Reference

American Society of Civil Engineers (ASCE) Standard. *Minimum Design Loads for Buildings and Other Structures*. American Society of Civil Engineers, New York, 2005, ASCE/SEI 7-05.

Bitsuamlak, G.T, Gan Chowdhury, A, Sambare, D (2009). "Development of full-scale testing facility for water intrusion." *Building and Environment*, 44 (12), 2430-2441.

Bitsuamlak, G.T, Dagnew, A, Gan Chowdhury, A (2010). "Computational blockage and wind sources proximity assessment for a new full-scale testing facility." *Wind and Structures*, 13(1), 21-36.

Cermak, J.E. (1995). "Development of wind tunnels for physical modeling of the atmospheric boundary layer (ABL). A state of the art in wind engineering." *Proceedings of the 9th International Conference on Wind Engineering.* New Age International Publishers Limited, London, U.K., 1995, pp. 1-25.

Coffman, B.F., Main, J.A., Duthinh, D., Simiu, E. (2010). "Wind effects on low-rise buildings: Database-assisted design vs. ASCE 7-05 Standard estimates." *J. Struct. Eng.* (in press).

Endo, M., Bienkiewicz, B., Ham, H.J. (2006). "Wind-tunnel investigation of point pressure on TTU test building." *J. Wind Eng. Ind. Aerodyn.,* 94, 553-578.

B. Bienkiewicz, M. Endo, and J.A. Main. (2009), "Comparative inter-laboratory study of wind loading on low-rise industrial buildings," *ASCE/SEI Structural Congress*, American Society of Civil Engineers, Austin Texas.

Davenport, A. G. (1964), "Note on the distribution of the largest value of a random function with application to gust loading." Institution of Civil Engineers, London, England, 187-196.

Fichtl, G.H., and McVehil, G.E. (1970), "Longitudinal and lateral spectra of turbulence in the atmospheric boundary layer at the Kennedy Space Center," *J. Appl. Meteor.* 51-63

Fritz, W.P., Bienkiewicz B., Cui B., Flamand O., Ho T. C. E., Kikitsu H., Letchford C.W., and Simiu E. (2008). "International comparison of wind tunnel estimates of wind effects in low-rise buildings: test-related uncertainties," *Journal of Structural Engineering*, 134, 1887-1880.

Fu, T-C., Aly, A.M., Bitsuamlak, G., Gan Chowdhury, A., Simiu, E. (2010). "Flow simulation in    12-fan Wall of Wind testing facility." *Proceedings of the 2nd Workshop of the American Association for Wind Engineering* (AAWE) (Marco Island, Florida, USA), (CD-ROM).

Gan Chowdhury, A., Aly, A.M., Bitsuamlak, G. (2010). "Full- and large-scale testing to promote wind disaster mitigation." *Proceedings of the Fifth U.S.-Japan Workshop on Wind Engineering* (Chicago, Illinois, USA), (CD-ROM).

Gan Chowdhury, A., Simiu, E. and Leatherman, S.P. (2009), "Destructive testing under simulated hurricane effects to promote hazard mitigation," *Nat. Hazards Review J. ASCE*, 10(1), 1-10.

Ginger, J. D. and Letchford, C.W. (1999). "Net pressure on a low-rise full-scale building," *J. Wind Eng. Ind. Aerodyn.* 83, 239-250.

Ho, T.C.E., Surry, D., Morrish, D., and Kopp, G.A. (2005). "The UWO contribution to the NIST aerodynamic database for wind loads on low buildings: Part I. Archiving format and basic aerodynamic data," *J. Wind Eng. Ind. Aerodyn.* 93, 1-30.

Huang, P., Gan Chowdhury, A., Bitsuamlak G., and Liu. R. (2009). "Development of devices and methods for simulation of hurricane winds in a full-scale testing facility," *Wind and Structures*, 12 (2), 151-177.

Letchford, C. W. and Chay, M. T. (2002). "Pressure distributions on a cube in a simulated thunderstorm downburst. Part B: moving downburst observations," *J. Wind Eng. Ind. Aerodyn.*, 90, 733-753.

Li Q.S. and Melbourne W.H. (1995). "An experimental investigation of the effects of fee-stream turbulence on streamwise surface pressure in separated and reattaching flows," *J. Wind Eng. Ind. Aerodyn.* 54/55, 313-323.

Okada, H. and Ha, Y.C. (1992), "Comparison of wind tunnel and full-scale pressure measurement tests on the Texas Tech Building", *J. Wind Eng. Ind. Aerodyn.*, 43(1-3), 1601-1612.

Orwig, K.D. and Chroeder J. L. (2007). "Near-surface win characteristics of extreme thunderstorm outflows," *J. Wind Eng. Ind. Aerodyn.*, 95, 565-584.

Masters, F.J. *Measurement, Modeling and Simulation of Ground-Level Tropical Cyclone Winds*. PhD Dissertation, University of Florida, Gainesville, 2004.

Masters, F.J., Lopez, C. (2010). "Progress Update on Wind-Driven Rain Ingress Research at the University of Florida." *Proceedings of the 2nd Workshop of the American Association for Wind Engineering* (AAWE) (Marco Island, Florida, USA), (CD-ROM).

Murakami, S. and Mochida, A. (1990) "3-D numerical simulation of airflow around a cubic model by means of the k-ε model," *J. Wind Eng. Ind. Aerodyn.*, 31, pp. 283-303.

National Institute of Standards and Technology (NIST), May (2010), http://www.itl.nist.gov/div898/winds/peakest_files/peakest.htm

Richards, P.J., Hoxey, R.P. and Short, L.J. (2001) "Wind pressures on a 6m cube," *J. Wind Eng. Ind. Aerodyn.*, 89, 1553-1564.

Sadek, F. and Simiu, E. (2002), "Peak non-Gaussian wind effects for database-assisted low-rise building design," *J. Eng. Mech.*, 128( 5), 530-539.

Smith, J., Liu, Z., Masters, F.J., Reinhold, T. (2010). "Validation of facility configuration and investigation of control systems for the 1:10 scaled Insurance Center for Building Safety Research." *Proceedings of the 2nd Workshop of the American Association for Wind Engineering* (AAWE) (Marco Island, Florida, USA), (CD-ROM).

St. Pierre, L.M., Kopp, G.A., Surry, D., and Ho, T.C.E. (2005). "The UWO contribution to the NIST aerodynamic database for wind loads on low buildings: Part II. Comparison of data with wind load provisions," *J. Wind Eng. Ind. Aerodyn.* 93, 31-59.

Surry, D., Ho, T.C.E., and Kopp, G.A. (2003). "Measuring pressures is easy, isn't it?" *Proceedings, International Conf. on Wind Engineering*, Texas Tech University, Lubbock, TX, 2, 2618-2623.

Tieleman, H.W., Surry, D., Mehta, K.C. (1996), "Full/model-scale comparison of surface pressures on the Texas Tech experimental building", *J. Wind Eng. Ind. Aerodyn.* 61(1–23), 1–23.

Vickery, B. J. (1970). "On the reliability of gust loading factors." the Technical Meeting Concerning Wind Loads on Buildings and Structures, Building Science Series 30, National Bureau of Standards, Washington, DC.

Yeo, D. (2010). "Numerical simulation of along-wind loading on small structures using a simplified wind flow model." NIST Technical Note 1683, National Institute of Standards and Technology, Gaithersburg, MD, (available at publications in www.nist.gov/wind).

Yu, B., Chowdhury A.G., and Masters F.J. (2008). "Hurricane wind power spectra, co-spectra, and integral length scales," *Boundary-Layer Meteorol*, 129, 411-430.

**CHAPTER III**

PARTIAL TURBULENCE SIMULATION AND AERODYNAMIC PRESSURES VAL-

IDATION FOR AN OPEN-JET TESTING FACILITY

(A paper under review for *The Journal of Wind and Structure*)

# CHAPTER III

# PARTIAL TURBULENCE SIMULATION AND AERODYNAMIC PRESSURES

# VALIDATION FOR AN OPEN-JET TESTING FACILITY

Tuan-Chun Fu[1], Arindam Gan Chowdhury*[2], Girma Bitsuamlak[3], Thomas Baheru[4]

[1]*Department of Civil and Environmental Engineering, Florida International University, 10555 West Flagler St., Miami, FL, 33174, U.S.A.*
[2]*Department of Civil and Environmental Engineering, International Hurricane Research Center,*
*Florida International University, 10555 West Flagler St., Miami, FL, 33174, U.S.A.*
[3]*Department of Civil and Environmental Engineering,*
*The University of Western Ontario, London, ON, Canada*
[4] *Department of Civil and Environmental Engineering, Florida International University, 10555 West Flagler St., Miami, FL, 33174, U.S.A.*

### 3.1 Abstract

This paper describes partial turbulence simulation and validation of the aerodynamic pressures on building models for an open-jet small-scale 12-Fan Wall of Wind (WOW) facility against their counterparts in a boundary-layer wind tunnel. The wind characteristics pertained to the Atmospheric Boundary Layer (ABL) mean wind speed profile and turbulent fluctuations simulated in the facility. Both in the wind tunnel and the small-scale 12-Fan WOW these wind characteristics were produced by using spires and roughness elements. It is emphasized in the paper that proper spectral density parameterization is required to simulate turbulent fluctuations correctly. Partial turbulence considering only high frequency part of the turbulent fluctuations spectrum was simulated in the small-scale 12-Fan WOW. For the validation of aerodynamic pressures a series of tests were conducted in both wind tunnel and the small-scale 12-fan WOW facilities on low-rise buildings including two gable roof and two hip roof buildings with two different

40

slopes. Testing was performed to investigate the mean and peak pressure coefficients at various locations on the roofs including near the corners, edges, ridge and hip lines. The pressure coefficients comparisons showed that open-jet testing facility flows with partial simulations of ABL spectrum are capable of inducing pressures on low-rise buildings that reasonably agree with their boundary-layer wind tunnel counterparts.

**KEYWORDS**: Wall of Wind; low-rise building; spectrum; roof; partial turbulence; pressure coefficient

### 3.2 Introduction

Observations of damage have shown that residential low-rise buildings are typically vulnerable to powerful wind storms. An improved understanding of wind effects on low-rise buildings is therefore needed.  Simulations of wind effects on structures are primarily performed on small-scale (say, 1:100) building models, in wind tunnels that simulate atmospheric boundary layer (ABL) flows. However, there are some scaling issues while using boundary layer wind tunnel facilities, primarily constructed for high rise buildings, to study low-rise buildings. Kozmar (2010) found that flows with integral turbulence scales typically used for testing high-rise structures were inadequate for testing low-rise buildings. Nevertheless, wind tunnel studies remains industry wide accepted tools and test results so obtained are the main source for building code specifications on wind pressures.

With a view to testing of low-rise buildings at large scales for high resolution wind pressure measurements, testing of actual material characteristics, and coupled wind and wind driven rain tests, a large-scale 6-Fan Wall of Wind (WOW) open-jet wind engi-

neering test facility (Fig. 1) was developed at Florida International University (FIU) (Huang et al. 2009).
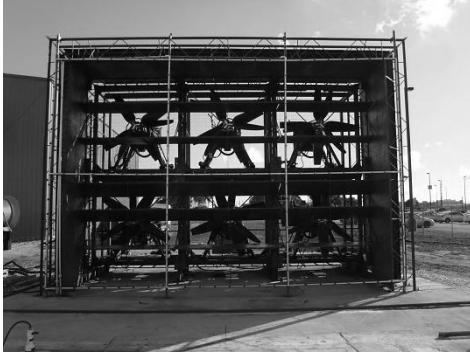


Figure 1. 6-Fan WOW at FIU

The 6-fan WOW was used for performing tests on low-rise buildings subjected to strong winds (Aly et al. 2012, Bitsuamlak et al. 2009, Gan Chowdhury et al. 2009, Gan Chowdhury et al. 2010, Simiu et al. 2011, Tecle et al. 2013). However, the 6-Fan WOW facility was not capable of performing tests in flow speeds associated with higher category hurricanes (Leatherman et al. 2007). A more advanced large-scale 12-Fan WOW (Fig. 2), capable of producing wind velocities associated with Category 5 hurricanes was constructed at FIU and opened in 2012. Each fan has a maximum flow rate of 113.3 cubic meter/second (240,000 cubic foot/minute (cfm)) with a total pressure head of 3736 Pa (15 in. $H_2O$).



Figure 2. Large-Scale 12-Fan WOW

The power rating of each motor driving the fan is 522 kilowatt (700hp). The fan speeds are controlled by variable frequency drives (VFD). The 12 fans are mounted on a steel frame and a contraction section boosts the mean wind speed up to 71.4 m/s (157 mph). It is also necessary to assure that the 12-Fan WOW is capable of simulating reasonably well the main flow characteristics as of ABL winds including the mean wind profile and turbulence parameters. For this reason, flow management devices comprising of spires and roughness elements are to be designed to produce flows with characteristics close to those of natural winds and to those used in the boundary layer wind tunnels.

To save design time and resources, a cost effective small-scale 12-Fan replica (Fig. 3) with a model scale 1:15 was built with a view to developing the requisite flow management devices. In that replica, Aly et al. (2011) successfully reproduced natural wind characteristics for suburban exposure using active controls (i.e. running the fans with waveforms that can vary the fan speeds) and passive controls (using horizontal planks). A quasi-periodic waveform was used to control the fan speeds with a view to generating adequate turbulence intensity. In addition Aly et al. (2011) performed pressure measurements on models of the Silsoe building and the Texas Tech University experimental building, two structures for which measurements of pressures induced by natural wind were available.
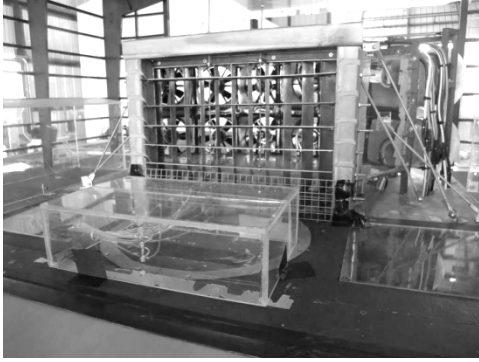
Figure 3. 1:15 Small-Scale 12-Fan WOW

The quasi-periodic waveform used by Huang et al. (2009) and Aly et al. (2011) in the small-scale 12-Fan WOW could not be employed in the large-scale 12-Fan WOW because its electrical components were not capable of generating rapid changes in the rotational velocity of the fans. Therefore, constant rotational speeds of the fans were used to simulate natural wind in the large-scale WOW. This paper describes the passive generation in the small-scale 12-fan WOW of flows simulating natural winds. The paper also reports results of tests in those flows of four typical low-rise buildings, and comparisons of those results with data obtained in wind tunnel tests.  Comparisons between results obtained in the small-scale 12-Fan WOW and the wind tunnel are a useful indication of the capabilities of the WOW and are the initial steps toward  the future validation of test results obtained in the large-scale 12-fan WOW.

### 3.3 Wind Flow Simulation and Pressure Measurements

Flow simulations in both the wind tunnel and the small-scale 12-Fan WOW were performed with a view to reproducing correctly target ABL flows and obtain reliable pressure data for low-rise buildings. In both facilities three spires as well as floor roughness elements (Fig. 4) were used to reproduce suburban wind profiles. Fig. 5 shows pro-

files generated in wind tunnel and the small-scale WOW, as well as the target prototype profile. The exponent of the power law describing the profiles is in all cases α ≈ 0.25. The mean wind velocities at reference height (mean roof height of building model) were approximately 8 m/s and 12.5 m/s for wind tunnel and small-scale WOW, respectively. However, the full longitudinal turbulence spectrum was reproduced in the wind tunnel, whereas in the small-scale WOW only partial longitudinal turbulence spectrum was simulated, as is shown in some detail subsequently in this paper.
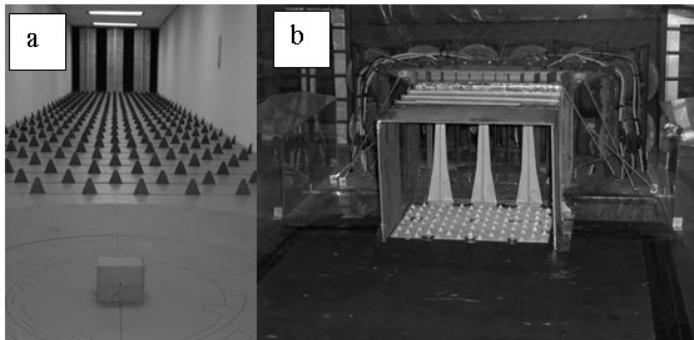


Figure 4. (a) RWDI Wind Tunnel, (b) Small-Scale 12-Fan WOW with Flow Management Devices
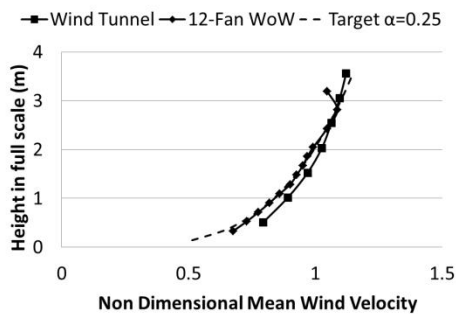


Figure 5. ABL Profile of Wind Tunnel, Small-Scale 12-Fan WOW, and Target ABL Profile

### 3.4 WOW Simulation of Atmospheric Boundary Layer Flow

#### 3.4.1    Partial Turbulence Flow Simulation in WOW

Melbourne (1980) introduced the small scale turbulence parameter $S = [nS_u(n)/\sigma_u^2](\sigma_u/U)^2 \times 10^6$ evaluated at frequency $n = 10U/L_B$ where $S_u(n)$ is the spectral density of the $u$-velocity component, $\sigma_u$ is the RMS (root-mean-square) of the velocity component $u$, $n$ is the frequency, and $U$ is the mean wind velocity. The small scale or high frequency turbulence needs careful consideration for proper simulation of aerodynamic effects on low-rise structures. Saathoff and Melbourne (1997) investigated the effects of free-stream turbulence on surface pressure fluctuations near leading edges of sharp-edged bluff bodies. This experimental study showed that peak pressure fluctuations occur when free-stream perturbations cause the separated shear layer to roll-up near the leading edge. Tieleman (2003) pointed out that in order to conduct correct wind tunnel simulation for fluctuating pressures on a low-rise structure, it is necessary to duplicate the small scale turbulence at the height where the pressures are being measured. The small scale turbulence parameter, $S$, is appropriately based on the content of the turbulence in the incident flow with a wavelength comparable to the thickness of the separated shear layer. The latter is estimated for low-rise structures at 1:10 of their height. Richards et al. (2007) tested the well-known Silsoe building, and showed that wind tunnel flow for which high frequency turbulence components correctly reproduced their prototype counterparts produced mean and peak pressure coefficient ($C_p$) values that compared well with the respective values measured at full scale. Yamada and Katsuchi (2008) also proved that the flow field around a rectangular cylinder can be adequately simulated by adopting "partial simulation" considering only the high frequency turbulence. In their study, a

Von-Karman type power spectral density model was considered to simulate the high-frequency part of the turbulence. More recently, Sangchuwang et al. (2013) observed the effects of "partial simulation" turbulence on sharp-edged bluff bodies. In their study, a new turbulence parameter, reduced turbulence intensity ($I_r$), was adopted to investigate the flow pattern around bluff bodies.

Based on the researches mentioned above it is apparent that the high frequency turbulence generation is important for the WOW simulation. This small scale turbulence affects some of the most critical aerodynamic features causing high suctions due to (1) flow separation from sharp edges creating shear layers and separation bubbles, and (2) conical vortices originating at corners from cornering winds. Fig. 6 shows comparisons of full turbulence spectra for ABL flows (as simulated in the wind tunnel) and the small-scale WOW partial turbulence spectrum. It is seen that the high frequency portion of the WOW spectrum better matches its counterpart in the ABL spectra as compared to the low frequency portion, which is much lower in the WOW. The missing low frequency portion represents the large scale turbulence that can be depicted by slowly moving gusts. As these large scale gusts were missing in the WOW simulation it was proposed by Yeo and Gan Chowdhury (2013) to compensate for the missing low-frequency content by increasing the mean wind speed $U$ by $\Delta U$.
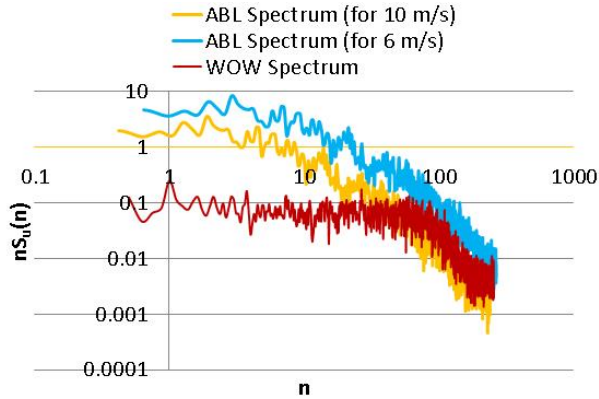
Figure 6. Comparison of WOW Partial Turbulence Spectrum with ABL Full Turbulence Spectra Obtained Using Two Arbitrary Mean Wind Speeds of 10 m/s and 6 m/s

The mean wind speed increment $\Delta U$ may be viewed as a flow fluctuation with zero frequency and perfect spatial coherence and, therefore, as a reasonable approximation of the missing low-frequency fluctuations in the spectrum (for more details see Fu et al. 2012, Yeo and Gan Chowdhury, 2013). As showed in Simiu et al. (2011), these assumptions are valid for small structures (such as single residential buildings and their components) for which, unlike for high-rise and large low-rise buildings, the coherence of the oncoming flow turbulence is close to unity over distances comparable to the dimensions of the structure. This approach is also hypothesized to be appropriate for experimentation on local aerodynamic effects, such as local pressures on roof components and claddings of limited sizes for which high coherence is expected over the component sizes. An example is measuring aerodynamic pressures on tiles, shingles, or roof pavers on building models large enough to accommodate those roof components.

To achieve a Reynolds number close to that in full scale, the WOW tests are conducted mostly at high wind speeds. Let $U_{PS}$ represents the mean wind speed recorded during high speed aerodynamic testing in the WOW. The subscript $PS$ stands for "partial

spectrum," meaning that the low-frequency content of the WOW longitudinal velocity fluctuations spectrum is weaker than in the ABL. Thus the recorded mean wind speed $U_{PS}$ for the WOW partial turbulence simulation, being 12.5 m/s at mean roof height for the current work, can be considered to be higher by $\Delta U$ than the mean wind speed of an ABL full turbulence flow for which the high frequency portion of the WOW and ABL spectra match. Let the mean wind speed in the ABL flow be denoted by $U_{FS}$ at the mean roof height of the building. The subscript $FS$ stands for "full spectrum," meaning that the ABL longitudinal velocity fluctuations spectrum has both the low- and high-frequency content inherent in typical models of ABL flows. Among other widely accepted representations, it is appropriate to represent non-dimensional spectra $nS(n)/U^2$, as functions of the Monin parameter $nz/U$, where $n$ is the frequency and $U$ is the mean wind speed at the reference height $z$ (e.g., Richards et al. (2007), Banks (2012)). Based on an ABL flow reproduced in the wind tunnel, Fig. 6 shows dimensional full turbulence spectra obtained using two arbitrary mean wind speeds 10 m/s and 6 m/s at the reference height (taken as the mean roof height of a building model). It is apparent that the high frequency turbulence contents in the WOW flow is higher and lower than their full turbulence spectra counterparts obtained using 10 m/s and 6 m/s, respectively. Thus it is apparent that the high frequency portion of the WOW flow and the ABL flow will closely match only when a specific target mean wind speed is used to generate the ABL flow spectrum. The question is "What should be the target mean wind speed $U_{FS}$ corresponding to the ABL flow that will allow the high frequency portion of the corresponding ABL spectrum to match the high frequency portion of the WOW spectrum corresponding to mean wind

49

speed $U_{PS}$?" The difference between $U_{PS}$ and $U_{FS}$ is essentially the mean wind speed increment $\Delta U$ required to compensate for the missing low frequency fluctuations, i.e.,

$$\Delta U = U_{PS} - U_{FS} \tag{1}$$

It is shown in this paper that an adequate simulation of the ABL flow (with an estimated $U_{FS}$) can be achieved in the WOW by a flow with appropriate high-frequency content, thus simulating partial turbulence. Estimation of $\Delta U$ helps determine the missing low frequency content in the WOW flow. Knowing $U_{PS}$ and estimating $\Delta U$ helps in the determination of $U_{FS}$, i.e., the target mean wind speed corresponding to which the high frequency portion of the ABL flow full spectrum will match its WOW counterpart. Given a model length scale $\lambda_L$, this $U_{FS}$ can then be used to determine the velocity scale $\lambda_v$ and the time scale $\lambda_T$. Based on the run time for an aerodynamic testing at WOW and the time scale $\lambda_T$, the corresponding duration at full scale can be estimated (e.g., 10 min, 20 min, etc.). Such equivalent full scale test duration information allows the estimation of statistics of peak pressures corresponding to any specified duration (say, 30 min or 1 hr.) based on the measured WOW pressure time histories. The estimation is performed using a statistical approach proposed by Sadek and Simiu (2002). Such WOW partial turbulence simulation technique will allow the flow to have correctly simulated high frequency turbulence components deemed of significant importance for peak pressure simulation by many researchers including Banks (2012), Richards et al. (2007), and Tieleman (2003). The aerodynamic pressures results for WOW shown in this paper are based on this partial turbulence simulation technique.

To estimate $\Delta U$ by using Eq. (1) it is necessary to determine the missing low tur-bulence content in the WOW partial turbulence spectrum. This requires, in turn, to de-termine the dimensional full turbulence spectrum whose high frequency turbulence por-tion matches its counterpart in the dimensional partial turbulence spectrum. Unless the mean speed $U_{FS}$ in the expression for the target full spectrum is known, the dimensional full spectrum cannot be obtained from the corresponding non-dimensional full spectrum, since the latter depends upon $U_{FS}$ through the reduced parameter $f=nz/U_{FS}(z)$, known as the Monin coordinate, ($z$ = height above ground) or, if the von Karman spectrum is used, through the parameter $nL_u^x/U_{FS}(z)$ ($L_u^x$ = integral length scale). Thus an iterative procedure is needed to obtain $\Delta U$, as will be demonstrated in a following example.

For adequate simulation of the aerodynamic effects, it is required that the WOW flow with mean wind speed $U_{PS}$ and deficient low-frequency fluctuations satisfy the rela-tion

$$U_{PS}^{pk}(T) = U_{FS}^{pk}(T) \tag{2}$$

where $U_{PS}^{pk}(T)$ = peak wind speed in the WOW partial turbulence flow simula-tion and $U_{FS}^{pk}(T)$ = peak wind speed in the full spectrum ABL flow counterpart. By defi-nition the following relations hold:

$$U_{PS}^{pk}(T) = U_{PS} + k_{u,PS}(T)\,\sigma_{u,PS} \tag{3a}$$

$$U_{FS}^{pk}(T) = U_{FS} + k_{u,FS}(T)\,\sigma_{u,FS} \tag{3b}$$

where $k_{u,PS}$ and $\sigma_{u,PS}$ = peak factor and RMS (root-mean-square) of longitudinal velocity fluctuations, respectively, for the WOW partial turbulence flow simulation, and

$k_{u,FS}$ and $\sigma_{u,FS}$ = peak factor and RMS of longitudinal velocity fluctuations, respectively, for its full ABL flow counterpart. The WOW flows are considered stationary. Therefore the average wind speed for the test duration is considered to be the mean hourly wind speed. Thus $T$ is taken as 3600 sec for calculating the peak factors used in the above equations. From Eqs. (1)-(3) it follows that

$$\Delta U = k_{u,FS}\, \sigma_{u,FS}\ - k_{u,PS}\, \sigma_{u,PS} \tag{4}$$

The expressions for the peak factors are

$$k_{u,FS}(T) = \sqrt{2\ln\,(\gamma_{u,FS}T)} + \frac{0.577}{\sqrt{2\ln\,(\gamma_{u,FS}T)}}$$

(5a)

$$k_{u,PS}(T) = \sqrt{2\ln\,(\gamma_{u,PS}T)} + \frac{0.577}{\sqrt{2\ln\,(\gamma_{u,PS}T)}}$$

(5b)

$$\gamma_{u,FS} = \left[\frac{\int_0^{n_c} n^2 S_{FS}(n)dn}{\int_0^{n_c} S_{FS}(n)dn}\right] \tag{5c}$$

$$\gamma_{u,PS} = \left[\frac{\int_0^{n_c} n^2 S_{PS}(n)dn}{\int_0^{n_c} S_{PS}(n)dn}\right] \tag{5d}$$

In Eqs. (5c)-(5d), $n$ = dimensional frequency, $n_c$ = cut-off frequency, $S_{FS}(n)$ = dimensional full spectrum (target spectrum), and $S_{PS}(n)$ = dimensional partial spectrum (i.e., spectrum with weak or negligible low-frequency content). Non-dimensional spectrum models (such as the Kaimal, Von Karman, or Davenport models) are generally used to represent the flow fluctuations for ABL flows. For WOW flow simulation, in lieu of ABL flow characteristics, flow characteristics measured in the wind tunnel may be used, provided that those characteristics match reasonably those of ABL flows. For this paper,

suburban terrain ABL profiles were simulated in close circuit wind tunnel and open jet small-scale 12-fan WOW.

The description of the iterative procedure follows.

1. Based on Yeo and Chowdhury (2013), assume as a first approximation of $U_{FS}$ and $\Delta U$ the values

$$U_{FS,1} = \frac{U_{PS}}{1.3} \tag{6a}$$

and

$$\Delta U_1 = U_{PS} - U_{FS,1} \tag{6b}$$

The mean wind speed $U_{PS}$ is the mean wind speed used in the WOW testing. The latter is typically, though not necessarily, the largest speed obtainable in the WOW. For the small-scale 12-Fan WOW, $U_{PS} = 12.5$ m/sec (for $z_{ref} = 8.9$ cm, model mean roof height), therefore, assumed $U_{FS,1} = 12.5/1.3 = 9.6$ m/sec and $\Delta U_1 = 2.9$ m/sec.

2. Using the approximate value $U_{FS,1}$ and the specified prototype mean roof height $z_{ref}$, obtain, from the specified target non-dimensional full spectrum, the corresponding approximate dimensional full spectrum $S_{FS,1}(n)$ and the approximate RMS value $\sigma_{u,FS,1}$ corresponding to $S_{FS,1}(n)$. For this paper the target spectrum was the wind tunnel non-dimensional full spectrum based on the Von Karman model.

3. Substituting in Eq. (5c) the spectrum $S_{FS,1}(n)$ for $S_{FS}(n)$, obtain the approximation $\gamma_{u,FS,1}$ of $\gamma_{u,FS}$ and, using Eq. (5a), the corresponding approximation $k_{u,FS,1}(T)$ of $k_{u,FS}(T)$.

4. Using the WOW mean speed $U_{PS}$ at the mean roof height $z_{ref}$ obtain, from the non-dimensional partial spectrum measured in the WOW, the corresponding dimensional partial spectrum $S_{PS}(n)$ and the RMS value $\sigma_{u,PS}$.

5. From Eqs. (5b) and (5d), obtain the peak factor $k_{u,PS}(T)$.

6. Substituting in Eq. (4) the values obtained in steps 2, 3, 4 and 5, obtain the second approximation of $\Delta U_1$, denoted by $\Delta U_2$.

The procedure is repeated until the sequence $\Delta U_i$ $(i = 1, 2, ...)$ converges. For this particular case convergence was achieved after the fourth iteration with $U_{FS,4} = 8.5$ m/sec and $\Delta U_4 = 4.0$ m/sec. The dimensional target full spectrum and the WOW partial spectrum are shown in Figs. 7(a)-(b) for the first and the fourth iteration, respectively. It is to be noted that as the solution for $\Delta U$ converges the matching of the high frequency turbulence improves. Thus the target full spectrum mean wind speed $U_{FS,4} = 8.5$ m/sec results in a correct simulation of the high frequency turbulence components (see Figs. 7(b)-(c), and the corresponding mean wind speed increment $\Delta U = 4.0$ m/sec can be viewed as a flow fluctuation compensating for the missing low-frequency fluctuations in the spectrum as stated earlier. Fig. 8. Shows the wind speed time histories where the peak wind speed in the WOW partial turbulence flow simulation matches closely the peak wind speed in the full spectrum ABL flow counterpart, satisfying Eq. (2).
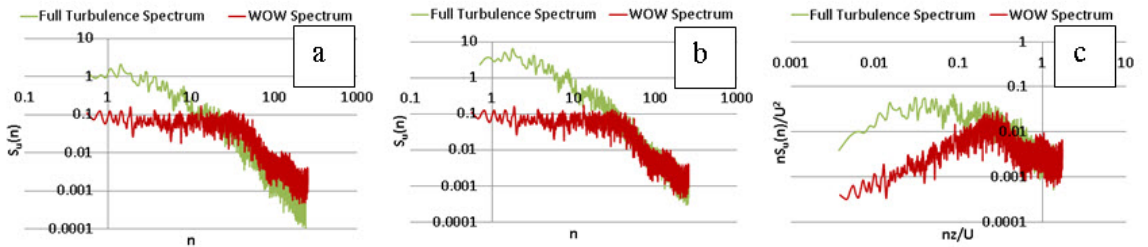
Figure 7. Target Full Turbulence Spectrum and WOW Partial Simulation Spectrum (a) Dimensional Spectra Comparison at the Beginning of Iteration, (b) Dimensional Spectra Comparison at the End of Iteration, (c) Non-Dimensional Spectra Comparison at the End of Iteration
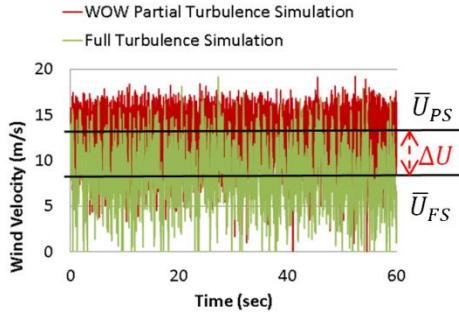


Figure 8. Wind Velocity Time Histories for WOW Partial Turbulence Flow and ABL Full Turbulence Flow

## 3.4.2    Reduced Turbulence Intensity

Irwin et al. (2008) stated that since past studies had discovered that small scale turbulence influences flow fields and aerodynamic parameters, therefore it is reasonable to match the power spectrum of turbulence only at high frequencies. For such  partial turbulence simulation the turbulence intensity will have to be lower than that for the ABL flow containing the low frequency fluctuations. Katsuchi and Yamada (2011) and Sangchuwang et al. (2013) applied Irwin's approach to create new parameter "reduced turbulence intensity" combining turbulence intensity and turbulence scale together. Using the von Karman power spectral density model, the reduced turbulence intensity for partial turbulence simulation can be obtained from the equation:

$$\left[\frac{I_u}{(L_u^x/D)^{1/3}}\right]_{PS} = \left[\frac{I_u}{(L_u^x/D)^{1/3}}\right]_{FS} \tag{7}$$

where $I_u$ is the longitudinal turbulence intensity, $L_u^x$ is the integral length scale, and $D$ is the representative length. Thus the reduced turbulence intensity for the partial turbulence simulation can be obtained from the equation:

$$[I_u]_{PS} = \left[\frac{I_u}{(L_u^x/D)^{1/3}}\right]_{FS} \left[(L_u^x/D)^{1/3}\right]_{PS} \tag{8}$$

The wind tunnel full spectrum turbulence intensity and integral length scale measured at model mean roof height were 25% and 0.7 m, respectively. The integral length measured in WOW was 0.05 m at 8.9 cm mean roof height of model. Using these values $[I_u]_{PS}$ can be estimated as about 12%. This value of suggested reduced turbulence intensity is close to the WOW turbulence intensity of 15% showing the adequacy of the turbulence intensity reduction to better match the power spectrum of turbulence only at high frequencies.

### 3.4.3    Velocity and Time Scaling

The test duration was 60 sec for each run during the building models pressure testing using the 12-Fan WOW. For Miami, the 3-second gust wind speed corresponding to open terrain and at 10 m above the ground is assumed to be 79.5 m/sec (175 mph) (Mean Recurrence Interval (MRI) 700 years, Risk Category II buildings and other structures; see ASCE 7-10). The corresponding mean hourly wind speed over suburban terrain and at 10 m above the ground is 35.5 m/sec (78.2 mph). Using the power law exponent $\alpha$ $\approx 0.25$, the corresponding wind speed is 25.5 m/sec at $z = 2.67$ m (prototype mean roof height). Thus the WOW velocity scale is $\lambda_v = 8.5/25.5 = 1{:}3$ ($U_{FS,4} = 8.5$ m/sec is used in the numerator as that is the target mean wind speed for the flow with full turbulence). The

model length scale being $\lambda_L$ = 1:30, the WOW time scale is obtained as $\lambda_T$ = 1:10. Thus the 1 min test duration at WOW represented 10 min at full scale. The velocity scaling should be based on the mean hourly wind speed $U_{FS}$, rather than on the 3-s gust wind speed. The determination of the 3-s gust speeds in the WOW must be based on the time scale $\lambda_T$. The latter is required to obtain the number of data points needed for the estimation of the wind speed averaged over 3 s, denoted by $U_{3s}$ (see Section 2.2.2). The test duration for each run in the wind tunnel was 36 sec. For the wind tunnel (simulating the full turbulence spectrum) the scales were $\lambda_L$ = 1:20, $\lambda_v$ = 1:3.3 (based on the mean hourly wind speed for the wind tunnel), and $\lambda_T$ = 1:6, thus 36 sec test duration represented 3.6 min at full scale. These equivalent full scale durations were used for peak pressure estimates given in Section 3.5.2.

### 3.5 Pressure Measurements

### 3.5.1   Tubing Correction System and Tap Locations

Scanivalve pressure acquisition systems were used in both WOW and wind tunnel facilities to capture pressure time history data with a 512 Hz sampling rate. After collecting the raw data from the Scanivalve pressure scanner, a transfer function designed for the tubing system was used to correct the raw data.  This method was developed by Irwin et al. (1979). The same tubing system was used in the wind tunnel and the WOW. In this system, 1.22 m (4 ft) PVC tubes with 1.34 mm (0.053 in) diameter connected the Scanivalve with pressure taps installed on the roof.  The transfer function was applied to the raw time history data to obtain corrected mean and minimum (peak suction) pressure coefficient $C_p$ values at 16 pressure taps. The pressure taps were located near roof corners, edges, ridge and hip lines where high suctions are anticipated. Roof pressures were inves-

tigated only as roofs are the most vulnerable elements of low buildings and are often damaged from high suction pressures induced during windstorms such as hurricanes.

### 3.5.2 Pressure Coefficients

The mean $C_p$ value calculations were obtained as follows:

$$C_{p\,mean} = \frac{p(t)_{mean}}{\frac{1}{2}\rho U_{mean}^2} \tag{9}$$

where $p(t)_{mean}$ denotes the mean pressure, $\rho$ is the air density, and $U_{mean}$ is the mean wind velocity at the reference height (for the WOW pressure coefficients $U_{mean}$ = $U_{PS}$). Peak $C_p$ coefficients were obtained by using the equation

$$C_{p\,peak} = \frac{p(t)_{peak}}{\frac{1}{2}\rho U_{3s}^2} \tag{10}$$

where $p(t)_{peak}$ is the estimated peak pressure and $U_{3s}$ is the peak 3-s gust at the reference height.

For the WOW the wind speed $U_{3s}$ was obtained by using the time scale $\lambda_T$ = 1:10, meaning that 512 x 3/10 = 154 data points were required for its determination. For the wind tunnel $U_{3s}$ was obtained by using the time scale $\lambda_T$ = 1:6, that is, 512 x 3/6 = 256 data points were required. The peak value of $U_{3s}$ was obtained in both cases by performing moving averages.

To estimate the peak pressures with 5% probability of exceedance the Sadek and Simiu (2002) method was used. This method uses the entire time history, and the estimated values it obtains are more stable than observed peaks, which vary from observation to observation. A 10 min full-scale equivalent testing duration was adopted to allow meaningful peak pressure coefficient comparisons. As mentioned earlier, based on time scaling the 1 min test duration at WOW represented 10 min at full scale and the 36 sec test dura-

tion in the wind tunnel represented 3.6 min at full scale. In using the Sadek and Simiu (2002) method duration ratios $K=3$ and $K=1$ were applied to the time history data obtained in the wind tunnel and WOW, respectively, to obtain peak pressures for a 10 min full-scale equivalent duration.

### 3.6 Comparison of Roof Cp Values Obtained in the Wind Tunnel and the Small-Scale WOW

### 3.6.1 Low-Rise Building Model Testing

For the validation of aerodynamic pressures obtained using the WOW a series of tests were conducted in both wind tunnel and the small-scale 12-fan WOW facilities on low-rise buildings with various roof types and slopes including two gable roofs (slopes: 5:12, 7:12) and two hip roofs (slopes: 3:12, 5:12). The mean roof height of each building model at WOW was approximately 8.9 cm (i.e., 2.67 m in full scale). The gable and hip roofs had 2 cm overhangs (i.e., 0.6 m in full scale) on all sides. A typical small-scale WOW testing specimen with a gable roof is shown in Fig. 9.



Figure 9. A Typical Small-Scale WOW Testing Specimen

The layout of the roof pressure taps for the models are shown in Fig. 10 and 11 for gable and hip roofs, respectively. Tests were performed for wind directions (i.e., angles of attack, or AOAs) AOA = 0° and a cornering wind angle of attack AOA = 45°.
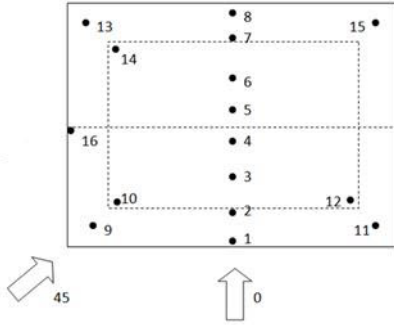
Figure 10. Tap Layout and Wind Angle of Attack (AOA) for Gable Roofs (Slope 5:12 and 7:12)
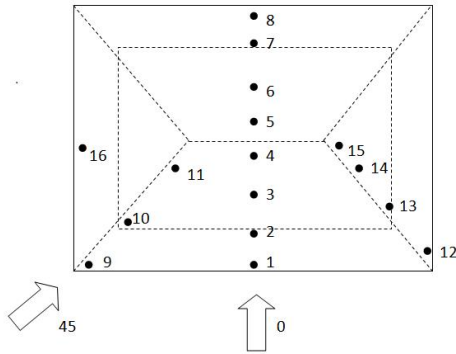


Figure 11. Tap Layout and Wind Angle of Attack (AOA) for Hip Roofs (Slope 5:12 and 7:12)

Testing was performed to investigate the mean and peak pressure coefficients at the center lines, near ridge and hip lines, and corners of the buildings models. The mean and peak pressure coefficients (see Sec. 3.5.2) obtained using the WOW open-jet testing facility flows with partial simulation of ABL spectrum were compared with their boundary-layer wind tunnel counterparts obtained using flows simulating full ABL spectrum. The test results for each roof type are discussed in the following sections.

### 3.6.2 Gable Roof Buildings Test Results

Figs. 12-13 show the comparative results for the gable roof model with roof slope 7:12. Overall, the trend of the mean and peak pressure coefficients obtained in the two facilities (wind tunnel, W.T. and Wall of Wind, WOW) compared well with each other. The mean values match well for most taps including the edge and corner pressure taps for both wind angles of attack except for tap 1 for AOA = 0°. For the critical taps under high suction pressures, the maximum difference among the $C_p$ values obtained in the two facilities was below 6%. For AOA = 0° the peak pressure coefficients for all the tap locations, including the leading edge tap 1 and the windward and leeward corner taps 9 to 15, show good agreement between the WOW and wind tunnel. The highest (in magnitude) peak suction coefficient was obtained for the leeward overhang tap 8. For AOA = 45°, the peak pressure coefficients show reasonably good agreement except for the leeward corner taps 13 and 14 for which weaker (by approximately 20%) suction was shown for WOW testing. It is to be noted that the values of the highest peak suction coefficients in most cases showed good agreement, for example, leeward overhang tap 8 coefficients for AOA = 0° being -1.5 for both WOW and wind tunnel; tap 5 coefficients for AOA = 45° being -1.95 and -2.1 for WOW and wind tunnel, respectively, showing the effect of flow separation at the ridge for a steep sloped gable roof (lower suction coefficient of -0.5 was noted for tap 4 near the windward side of the ridge); gable end tap 16 (near the ridge) coefficients for AOA = 45° being close to -2.2 for both facilities.
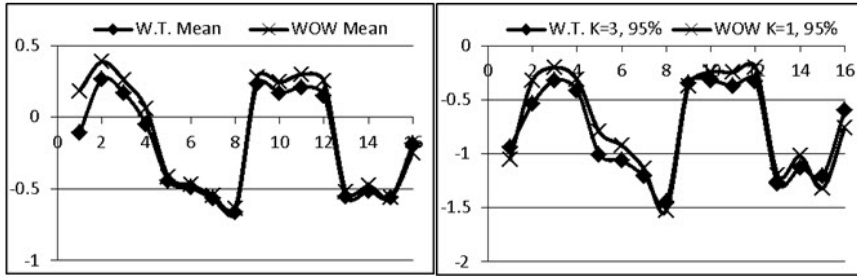
Figure 12. Gable Roof 7:12 Mean (left) and Peak (right) $C_p$ for AOA = 0°
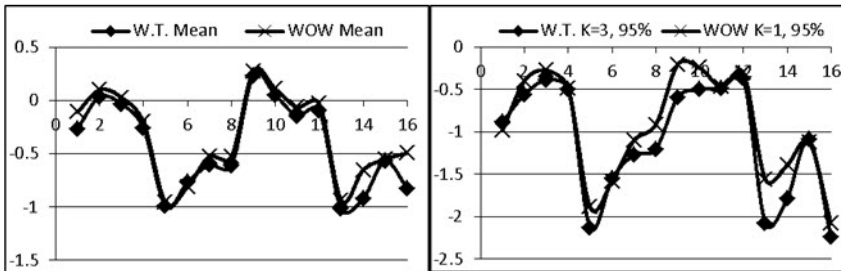


Figure 13. Gable Roof 7:12 Mean (left) and Peak (right) $C_p$ for AOA = 45°

Figs. 14-15 show the comparative results for the gable roof model with roof slope 5:12. The mean pressure coefficients obtained in the two facilities compared well with each other including those for the edge and corner pressure taps for AOA = 0°; the difference for the highest suction at tap 8 was less than 10%. The peak pressure coefficients also show similar trends for both facilities. The peak values agree well for AOA = 0° for most taps except for the leading edge taps 1 and 2 for which the WOW peak pressure coefficients were higher in magnitude than those obtained from the wind tunnel. The mean and peak pressure coefficients agree well for AOA = 45° for most taps except for the leeward taps 6 and 16 for which the WOW showed a weaker suction. For AOA = 45°, similar to the 7:12 roof model, the 5:12 roof model showed high suctions for tap 16 near the gable end ridge and tap 5 immediately downwind of the ridge.
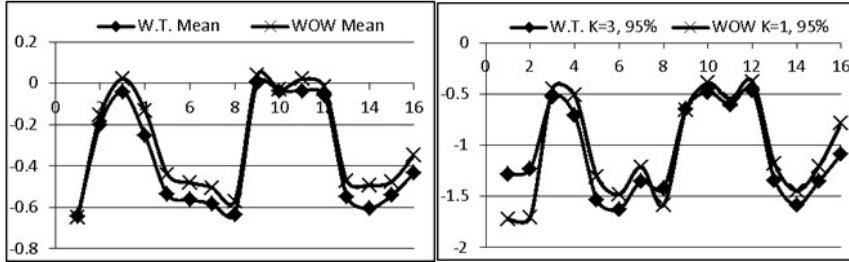
Figure 14. Gable Roof 5:12 Mean (left) and Peak (right) $C_p$ for AOA = 0°
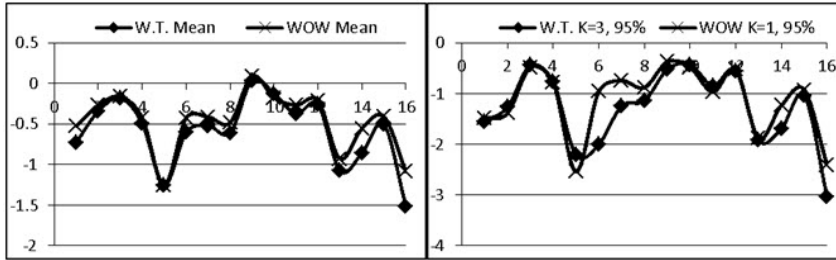


Figure 15. Gable Roof 5:12 Mean (left) and Peak (right) $C_p$ for AOA = 45°

### 3.6.3 Hip Roof Buildings Test Results

Figs. 16-17 show the comparative results for the hip roof model with roof slope 5:12. The mean pressure coefficients show reasonable agreement for the two facilities for most taps; for AOA = 0° the difference for the highest suction at tap 13 was less than 10% and for AOA = 45° the difference for the highest suction at tap 5 was about 5%. The peak pressure coefficients show similar trends for both facilities. The peak values match well for most taps except for the leading edge tap 1 for which the WOW shows a stronger and weaker suction for AOA = 0° and AOA = 45°, respectively. The values of the highest peak suction coefficients among all taps showed good agreement. For tap 13 the coefficients obtained in both facilities were close to -3.1 and -3.0 for AOA = 0° and AOA = 45°, respectively (only a difference of 2% for tap 13 was observed between the results of two facilities). It is to be noted that tap 13 peak suction, occurring downwind of the sloped hip for the 5:12 hip roof, was as high as the worst peak suction for the 5:12 gable

roof occurring near the gable end ridge at tap 16. All the taps 12, 13, 14, and 15 down-wind of the sloped hip showed high suctions for both AOAs for the 5:12 hip roof. This shows the vulnerability of roofing components near gable end ridge and downwind of sloped hip locations that can be subjected to high suctions during extreme wind events. Both the wind tunnel and the WOW produced comparable high suctions near the gable end ridge and sloped hip for the roof models tested.
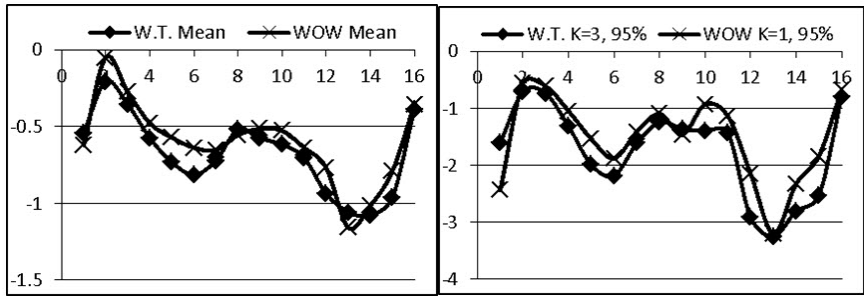


Figure 16. Hip Roof 5:12 Mean (left) and Peak (right) $C_p$ for AOA = 0°
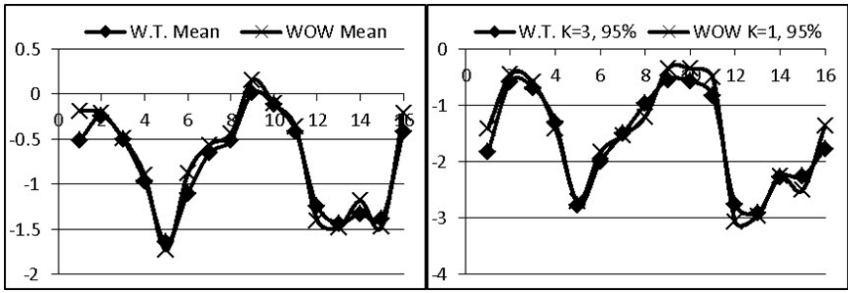


Figure 17. Hip Roof 5:12 Mean (left) and Peak (right) $C_p$ for AOA = 45°

Figs. 18-19 show the comparative results for the hip roof model with roof slope 3:12. For AOA = 0° the mean and peak pressure coefficients obtained in the two facilities compared well with each other for the taps under higher suctions. For AOA = 45° the mean values match well for most taps expect for taps 1, 13, and 14. However, for the same AOA the peak values match well for the taps with the highest suctions (taps 1, 5, 13). For tap 13, the WOW peak pressure coefficient was 15% higher than its wind tunnel

counterpart. Similar to the 5:12 hip roof, the 3:12 hip roof showed highest peak suction coefficients occurring downwind of the sloped hip for AOA = 45° (taps 12, 13, 14, 15) and downwind of the ridge for both AOAs (for tap 5 the difference was 3% between two facilities). Also, both facilities simulated the high suction effects at the leading edge of the low sloped 3:12 roof. The leading edge tap 1 peak pressure coefficients were about -2.1 and -2.3 for AOA = 0° and AOA = 45°, respectively (only a difference of 1.3% was observed between the results of two facilities).
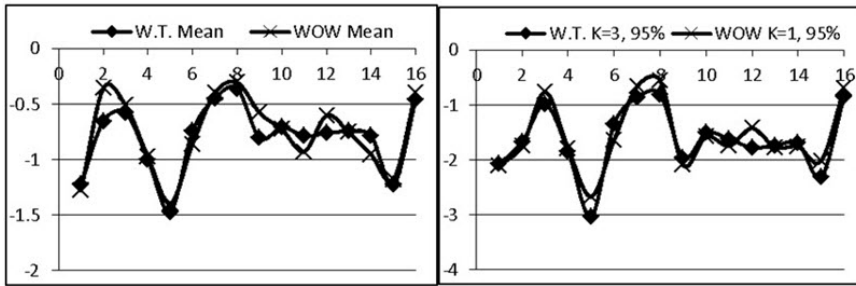


Figure 18. Hip Roof 3:12 Mean (left) and Peak (right) $C_p$ for AOA = 0°
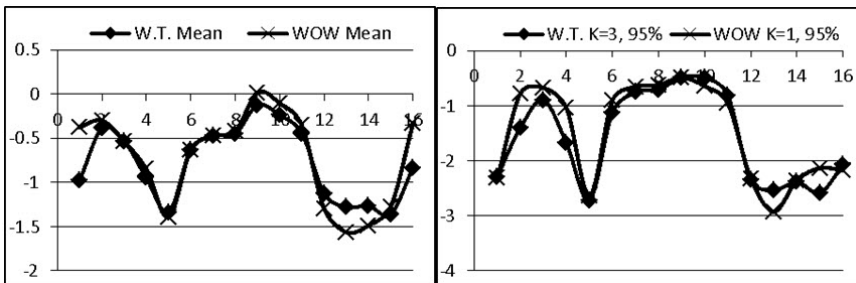


Figure 19. Hip Roof 3:12 Mean (left) and Peak (right) $C_p$ for AOA = 45°

### 3.7 Discussion and Conclusion

Both wind flow simulation and pressure field validation for the small-scale 12-Fan WOW were presented in this paper by comparing WOW flow characteristics and pressure values and their wind tunnel counterparts. A suburban exposure wind profile with a reduced longitudinal turbulence intensity was generated in the small-scale 12-fan

65

WOW to better simulate the high frequency turbulence in the ABL flow. A partial turbulence spectrum simulation was achieved in the WOW to allow the flow to have correctly simulated small scale turbulence components deemed of significant importance for peak pressure simulation by many researchers. An iteration procedure was developed to estimate the incremental wind speed DU that can be viewed to compensate for the absence of the low-frequency content in the WOW flow. The $\Delta U$ obtained at the end of the iteration allows obtaining the mean wind speed UFS for an equivalent ABL flow such that the high frequency turbulence in the WOW spectrum matches its full turbulence spectrum counterpart. The mean wind speed UFS was used to obtain scaling parameters needed to convert the actual test duration in WOW to an equivalent full scale duration to facilitate the comparison of estimated peak pressures for the WOW simulation and the wind tunnel ABL flow simulation. Pressure measurements and comparison of mean and peak pressure coefficient estimates for the partial turbulence flow in WOW and full turbulence flow in the ABL wind tunnel showed that this partial turbulence approach was effective aerodynamically. For four gable and hip roof low rise building models it was shown that both the wind tunnel and the WOW produced comparable high suctions (high peak pressure coefficients) for critical locations near the (1) leading edge for low-slope roof (e.g., tap 1 for 3:12 hip roof for AOA = 0° and AOA = 45°); (2) leeward edge (e.g., tap 8 for 7:12 and 5:12 gable roofs for AOA = 0°), (3) gable end ridge (e.g., tap 16 for 7:12 and 5:12 gable roofs for AOA = 45°), (4) downwind of ridge (e.g., tap 5 for all roofs for both AOAs), and (5) downwind of sloped hip (e.g., taps 12, 13, 14, 15 for hip roofs for both AOAs). The test results agree with the findings by Tecle et al. (2013) showing the presence of high suction at the ridge compared to the edge zones. Also, the results showed

that similar high suction can occur near the gable end ridge (tap 16) for cornering wind and the downwind side of the sloped hip (tap 13) for both cornering wind and wind perpendicular to the eave. Thus the traditional practice of considering gable roofs to be more vulnerable than hip roofs may not be applicable to the design of roofing elements, especially those at the sloped hip locations. The findings from the current tests provide an explanation to why failures initiate mostly at these ridge and hip locations, as observed in recent post damage assessments: "Aerial photos taken after Ike showed close to 90 percent of the homes near the coast toward the western part of Bolivar Peninsula had an extensive loss of hip and ridge shingles": (IBHS 2009).

### 3.8 Acknowledgements

### 3.9 Reference

American Society of Civil Engineers (2010), *Minimum design loads for buildings and other structures*, ASCE Standard, ASCE/SEI 7-10, New York City.

Aly, A. M., Bitsuamlak, G. T., & Chowdhury, A. G. (2012), "Full-scale aerodynamic testing of a loose concrete roof paver system", *Engineering Structures*, 44, 260-270.

Aly, A. M., Gan Chowdhury, A. and Bitsuamlak, G. (2011), "Wind profile management and blockage assessment of a new 12-Fan Wall of Wind facility at FIU", *Wind and Struct.*, 14(4), 285-300.

Banks, D. (2012), "Measuring peak wind loads on solar power assemblies", *CCP Wind Engineering*, Colorado, USA.

Bitsuamlak, G.T., Gan Chowdhury, A. and Sambare, D. (2009), "Application of a full-scale testing facility for assessing wind-driven-rain intrusion*", Build. Environm.*, 44(12), 2430-2441.

Fu, T.C., Aly, A. M., Gan Chowdhury, A., Bitsuamlak, G., Yeo, D., and Simiu, E. (2012), "A proposed technique for determining aerodynamic pressure on residential homes", *Wind and Struct.*, 15(1), 27.-41

Gan Chowdhury, A., Simiu, E. and Leatherman, S.P. (2009), "Destructive testing under simulated hurricane effects to promote hazard mitigation", *Nat. Hazards Review* 10(1), 1-10.

Gan Chowdhury, A., Bitsuamlak, G., Simiu, E. (2010), "Aerodynamic, hydro-aerodynamic, and destructive testing", *J. ICE Struct. Build.*, 163(2), 137-147

Huang, P., Gan Chowdhury, A., Bitsuamlak, G. and Liu, R. (2009), "Development of devices and methods for simulation of hurricane winds in a full-scale testing facility", *Wind and Struct.*, 12(2), 151-177.

Institute for Business & Hone Safety (IBHS) (2009), "*Hurricane Ike – Nature's Force vs. Structural Strength*".

Irwin, P., Cooper, K. and Girard, R. (1979), "Correction of distortion effects caused by tubing systems in measurements of fluctuating pressures", *J. Ind. Aerodyn.* 5, 93-107.

Irwin, P. (2008), "Bluff body aerodynamics in wind engineering", *J. Wind Eng. Ind. Aerodyn.*, 96, 701-712.

Katsuchi, H. and Yamada, H. (2011), "Study on turbulence partial simulation for wind-tunnel testing if bridge deck", *Proc of ICWE 12*, Amsterdam, Netherlands.

Kozmar, H. (2010), "Scale effects in wind tunnel modeling of an urban atmospheric boundary layer", *Theor. Appl. Climatol.* 100, 153-162.

Leatherman, S.P., Gan Chowdhury, A. and Robertson C.J. (2007), "Wall of Wind full-scale destructive testing of coastal houses and hurricane damage mitigation", *Journal of Coastal Research*, 23(5), 1211-1217.

Melbourne W. H. (1980), "Turbulence effects on maximum surface pressures – a mechanism and possibility of reduction", *Wind Engineering*, 1, 521-551.

Richards, P.J., Hoxey, R.P., Connell, R.P., and Lander, D.P. (2007), "Wind-tunnel modelling of the Silsoe Cube", *J. Wind Eng. Ind. Aerod.*, 95, 1384-1399.

Sangchuwong, P., Yamada, H., and Katsuchi, H. (2011), "Study on turbulence effects on flow patterns around rectangular cylinders", *Proc. of BBAA 7*, Shanghai, China.

Sangchuwang, P., Yamada, H., and Katsuchi, H. (2013), "Study on turbulence effects on flow fields around sharp-edged bluff bodies", *J. Struc. Eng.*, 59A, 627-636.

Saathoff, P. J. and Melbourne, W. H. (1997), "Effects of free-stream turbulence on surface pressure fluctuation in a separation bubble', *J Fluid Mech.,* 337, 1-24.

Sadek, F. and Simiu, E. (2002), "Peak non-Gaussian wind effects for database-assisted low-rise building design," *J. Eng. Mech.*, 128(5), 530-539.

Simiu, E., Bitsuamlak, G., Gan Chowdhury, A., Li, R., Tecle, A., Yeo, DH. (2011). "Testing of residential homes under wind loads", *ASCE Natural Hazards Review Journal*, 12(4), 166-170.

Tecle, A., Bitsuamlak, G., Suksawang N., Gan Chowdhury, A., Fuez, S. (2013). "Ridge and field tile aerodynamics for a low-rise building: a full-scale study", *Wind and Struct.,* 16(4), 301-322.

Tieleman, H. W. (2003), "Wind tunnel simulation of wind loading on low-rise structures: a review", *J. Wind Eng. Ind. Aerod.*, 91, 1627-1649.

Yamada, H. and Katsuchi, H. (2008), "Wind-tunnel study on effects of small-scale turbulence on flow patterns around rectangular cylinder", *Proceeding of the 4th International Colloquium on Bluff Bodies Aerodynamics & Applications*, Italy.

Yeo, D. and Gan Chowdhury, A. (2013), "A simplified wind flow model for the estimation of aerodynamic effects on small structures", *J. Eng. Mech.*, 139, 367-375.

**CHAPTER IV**

EXPERIMENTAL INVESTIGATION OF WIND PRESSURES ON LARGE-SCALE

BUILDING MODELS AND COMPARISONS WITH FIELD MEASUREMENTS

(A paper under review for the

*Journal of Wind Engineering and Industrial Aerodynamics*)

# CHAPTER IV

# EXPERIMENTAL INVESTIGATION OF WIND PRESSURES ON LARGE-SCALE BUILDING MODELS AND COMPARISONS WITH FIELD MEASUREMENTS

Tuan-Chun Fu[1], Arindam Gan Chowdhury[2*], Douglas Smith[3], Ioannis Zisis[4],

Peter Irwin[5], Emil Simiu[6]

[1] Doctoral Graduate Assistant, Department of Civil and Environmental Engineering, Florida International University, 10555 W. Flagler St. EC3660, Miami, FL, 33174, tfu001@fiu.edu

[2] Associate Professor, Department of Civil and Environmental Engineering, International Hurricane Research Center, Florida International University, 10555 W. Flagler St. EC3604, Miami, FL, 33174, chowdhur@fiu.edu, +1(305)3480518

[3] Associate Professor, Department of Civil and Environmental Engineering, Texas Tech University, Box 41023, Lubbock, TX, 79409, doug.smith@ttu.edu

[4] Assistant Professor, Department of Civil and Environmental Engineering, Florida International University, 10555 W. Flagler St. EC3655, Miami, FL, 33174, izisis@fiu.edu

[5] Wall of Wind Professor of Practice, Department of Civil and Environmental Engineering, Florida International University, 10555 W. Flagler St. EC3640, Miami, FL, 33174, peairwi@fiu.edu

[6] NIST Fellow, Building and Fire Research Laboratory, National Institute of Standards and Technology, 100 Bureau Dr., Gaithersburg, MD, 20899, emil.simiu@nist.gov

* Corresponding author

## 4.1 Abstract

This study describes the simulation and validation of the mean and peak aerodynamic pressures on large-scale models of the Texas Tech University (TTU) and Silsoe buildings, measured in the open-jet 12-Fan Wall of Wind (WOW) facility using a partial turbulence simulation approach; i.e. flow that reproduces only the high frequency portion of the atmospheric boundary layer (ABL) turbulence spectrum. The validation of this approach was performed through comparison of pressures on models with respect to

pressures measured on the respective prototypes in ABL flow, that is, in flow with the full content of the ABL turbulence spectrum. An iteration procedure was used and allowed the meaningful comparison of the pressures obtained in the two flows.  The pressures based on partial simulations and the full-scale pressures were in reasonable agreement for most of the pressure tap locations experiencing high suctions. This verifies that the partial turbulence flow induces aerodynamic pressures similar to those induced by an ABL flow. In fact, the tests in partial simulation are freed of integral length scale constraints, meaning that model length scales in such testing are only limited by blockage considerations. Thus the partial simulation methodology can be used to produce aerodynamic data for low-rise buildings by using large-scale models in wind tunnels and WOW-like facilities. This is a major advantage, because it allows for testing at higher Reynolds number and for greater spatial resolution of the pressure taps in high pressure zones.

## 4.2 Introduction

Building envelope damage due to high winds, such as in hurricanes and other windstorms, account for about 70% of the total insured losses (Holmes 2007). To determine wind loading on buildings and other structures, model-scale testing is performed in aerodynamic testing facilities whose flows have properties such as mean wind profile, turbulence intensity, turbulence spectrum, and integral length scale similar to those of atmospheric boundary layer (ABL) flows. Such flows are generally appropriate for small-scale models (e.g., low-rise buildings modeled at say, 1:100 scale or high-rise buildings modeled at say, 1:400 scale). However, small low-rise buildings and other small structures such as residential buildings, small warehouses, roof or ground mounted solar panel arrays need to be modeled at larger scales (of the order of, say, 1:10) to replicate the ef-

fects of architectural details, achieve adequate spatial resolution of pressures taps, and reduce Reynolds number effects. Such large-scale model testing is often constrained by the difficulty of simulating adequately the low-frequency content of the turbulence spectrum and, in particular, the integral length scale parameter. For this reason, large-scale testing may appear to be inconsistent with wind testing provisions specified by ASCE 7-10 (2010), which, among other criteria, state: "*The relevant macro- (integral) length and micro-length scales of the longitudinal component of atmospheric turbulence are modeled to approximately the same scale as that used to model the building or structure.*"

This paper describes a partial simulation approach for simulating realistic aerodynamic loads on low-rise buildings. The paper also presents comparisons of pressure coefficients obtained in the FIU 12-fan Wall of Wind facility on large-scale models of Texas Tech University (TTU) and Silsoe experimental buildings (1) by using the partial simulation approach and (2) field measurements on the prototype TTU and Silsoe buildings in ABL flows. The comparisons validate the efficacy of that approach for aerodynamic testing purposes.

Section 2.2.2 of the ASCE 49-12 Standard for wind tunnel testing considers simulations with missing content at the low frequency end of the turbulence spectrum and requires that additional interpretation of the data obtained in such simulations "shall refer to recognized literature for methods to make corrections." However, no reference to literature containing such methods is provided in the ASCE 49-12 Standard or the ASCE 7-10 Standard. It is suggested that the partial simulation approach presented in this paper can fill this gap.

### 4.3 Partial Simulation Method

### 4.3.1  Background

Consider a prototype building (a full-scale building) in ABL flow with (i) the mean wind speed profile conforms to the power or logarithmic law, and (ii) the non-dimensional spectrum of the longitudinal velocity fluctuations conforms to the ABL spectrum models, such as the modified Kaimal spectrum model, referred to for brevity as the *full spectrum.* The partial simulation produces a *laboratory flow* whose prototype counterpart has mean wind speed $U_{PS}(z)$ that satisfies the power or log law corresponding to the terrain exposure of interest ($z$ denotes height above ground; the subscript *PS* stands for "partial spectrum"). The prototype counterparts of the laboratory flow and the full-scale ABL flow have approximately similar high-frequency spectral content. However, the prototype counterpart of the laboratory flow has a *partial spectrum* with significantly weaker low-frequency content than the ABL flow's full spectrum. It is hypothesized that similar peak wind speeds in two flows, one characterized by a full spectrum and the other characterized by a partial spectrum with weak low frequency fluctuations, result in similar peak aerodynamic effects (i.e., in similar peak pressure coefficients). This hypothesis is partly based on previous studies that examined the role of small scale (high frequency) turbulence on local aerodynamic effects such as peak pressures on low-rise structures (Melbourne 1980, Saathoff and Melbourne, 1997, Suresh and Stathopoulos 1998, Tieleman 2003, Richards et al. 2007, Banks 2011, Yamada and Katsuchi 2008, Irwin 2009, Kopp et al 2013, Kopp and Banks 2013).

### 4.3.2 Description of Laboratory Flow with Partial Spectrum

The objective of the partial simulation is to test the stated hypothesis. Henceforth, quantities with and without the subscript $m$ pertain, respectively, to the laboratory model prototype. The mean wind speed of the laboratory flow and its prototype counterpart are $U_{PS,m}$ and $U_{PS}$, respectively (note that subscript $PS$ is used for a flow with "partial spectrum"). The properties of the laboratory flow must be such that the corresponding prototype peak velocity $U_{PS}^{pk}(z, T_{PS})$, where $T_{PS}$ denotes the prototype counterpart of the laboratory-flow time interval, satisfies the relation:

$$U_{PS}^{pk}(z,\ T_{PS}) = U_{FS}^{pk}(z, T_{FS}) \tag{1}$$

where $U_{FS}^{pk}(z,\ T_{FS})$ denotes the expected full spectrum peak wind speed over a time interval $T_{FS}$ in the prototype ABL flow. For the elevations $z$ of interest the mean wind speed for the flow with partial spectrum is denoted as $U_{PS}(z,\ T_{PS})$ and has the same vertical profile as the mean full spectrum wind speed $U_{FS}(z,\ T_{FS})$. The following relation holds between the two mean wind speeds:

$$U_{PS} = U_{FS} + \Delta U \tag{2}$$

The velocity $U_{FS}$ is specified based on field data or design wind speeds. The prototype mean wind speed increment $\Delta U$ may be interpreted as a flow fluctuation with zero frequency and perfect spatial coherence, which compensates -- serves as a surrogate -- for the missing low-frequency fluctuations in the laboratory flow spectrum (for additional details see Fu et al. 2012, Yeo and Gan Chowdhury 2013). As shown in Simiu et al. (2011), the use of Eq. 2 is appropriate for small structures (e.g., single residential buildings) for which spatial flow coherence over dimensions comparable to the building's

largest dimension is close to unity, unlike for large structures (e.g., large low-rise struc-

tures and high-rise buildings).

To estimate the prototype counterpart $U_{PS}$ of the mean wind speed $U_{PS,m}$

produced in the laboratory it is necessary to determine the increment $\Delta U$ that compen-

sates adequately for the missing frequencies in the partial spectrum. Given the geometric

scale $\lambda_L$ and the test duration $T_{PS,m}$ for the model test with mean speed $U_{PS,m}$, knowledge

of $U_{PS}$ allows the determination of the velocity scale $\lambda_{PS,V}$, the time scale $\lambda_{PS,T}$, the proto-

type counterpart $T_{PS}$ of $T_{PS,m}$, and the frequency scale $\lambda_{PS,n}$, using the following equations:

$$\lambda_{PS,V} = U_{PS,m}/U_{PS} \qquad (3a)$$

$$\lambda_{PS,T} = \lambda_L/\lambda_{PS,V} \qquad (3b)$$

$$T_{PS} = T_{PS,m}/\lambda_{PS,T.} \qquad (3c)$$

$$\lambda_{PS,n} = 1/\lambda_{PS,T} \qquad (3d)$$

By definition

$$U_{PS}{}^{pk}(T_{PS}) = U_{PS} + k_{u,PS}(T_{PS})\,\sigma_{u,PS} \qquad (4a)$$

$$U_{FS}{}^{pk}(T_{FS}) = U_{FS} + k_{u,FS}(T_{FS})\,\sigma_{u,FS} \qquad (4b)$$

where $k_{u,PS}$ and $\sigma_{u,PS}$ = peak factor and rms (root mean square) of the longitudinal

velocity fluctuations, respectively, for the prototype counterpart of the partial flow simu-

lation, and $k_{u,FS}$ and $\sigma_{u,FS}$ = peak factor and rms of longitudinal velocity fluctuations, re-

spectively, for the prototype ABL (full spectrum) flow. From Eqs. 1, 2, 4a and 4b it fol-

lows that:

$$\Delta U = k_{u,FS}\,\sigma_{u,FS} - k_{u,PS}\,\sigma_{u,PS}. \qquad (5)$$

The expressions for the peak factors in Eqs. 4 and 5 are

$$k_{u,FS}(T_{FS}) = \sqrt{2\ln\left(\gamma_{u,FS}T_{FS}\right)} + \frac{0.577}{\sqrt{2\ln\left(\gamma_{u,FS}T_{FS}\right)}}$$

(6a)

$$k_{u,PS}(T_{PS}) = \sqrt{2\ln\left(\gamma_{u,PS}T_{PS}\right)} + \frac{0.577}{\sqrt{2\ln\left(\gamma_{u,PS}T_{PS}\right)}}$$

(6b)

$$\gamma_{u,FS} = \left[\frac{\int_0^{n_c} n^2 S_{FS}(n)dn}{\int_0^{n_c} S_{FS}(n)dn}\right]^{\frac{1}{2}} \qquad (7a)$$

$$\gamma_{u,PS} = \left[\frac{\int_0^{n_c} n^2 S_{PS}(n)dn}{\int_0^{n_c} S_{PS}(n)dn}\right]^{\frac{1}{2}} \qquad (7b)$$

In Eqs. 7a, 7b, $n_c$ = prototype cut-off frequency (considered as 15 Hz at full scale for the current work), $S_{PS}$ $(n)$ = prototype counterpart of the dimensional partial spectrum $S_{PS,m}(n_m)$ produced in the laboratory, and $S_{FS}$ $(n)$ = prototype dimensional ABL spectrum.

The wind speed increment $\Delta U$ depends upon the dimensional spectra $S_{FS}$ $(n)$ and $S_{PS}$ $(n)$ (see Eqs. 5, 6 and 7). $S_{FS}$ $(n)$ can be obtained from field measurements of wind data obtained using anemometers with adequate frequency response to capture high frequency turbulence fluctuations (Yahaya and Frangi, 2004). If field data is unavailable or in case the anemometers have low frequency responses, meaning that fast gusts cannot be captured without error (Subramanian et al. 2012), $S_{FS}$ $(n)$ can be estimated using ABL non-dimensional spectrum models such as (a) the modified Kaimal spectrum by using reference height $z_{ref}$, the mean speed $U_{FS}(z_{ref})$, and the surface roughness length $z_0$ in Eq. 8a, or (b) the Von Karman spectrum model by using $U_{FS}$, longitudinal turbulence intensity $I_u$, and integral length scale $^xL_u$ at the reference height in Eq. 8b.

$$S_u(n) = \frac{1}{n}\left[\frac{U_{FS}(z_{ref})}{2.5\ln\left(\frac{z_{ref}}{z_0}\right)}\right]^2 \frac{200f}{(1+50f)^{\frac{5}{3}}}$$

(8a)

where $f = \dfrac{nz_{ref}}{U_{FS}(z_{ref})}$.

$$S_u(n) = \frac{1}{n}\left(I_u U_{FS}\right)^2 \frac{4f'}{(1+70.8f'^2)^{\frac{5}{6}}}$$ 　　　　(8b)

where $f' = \dfrac{n^x L_u}{U_{FS}}$

The prototype counterpart of the partial spectrum $S_{PS,m}(n_m)$ measured in the laboratory can be obtained using the equation:

$$S_{PS}(n) = S_{PS,m}(n_{,m}).\ [1/(\lambda^2_{PS,V}\ \lambda_{PS,T})]$$ 　　　　(9)

The increment $\Delta U$ is obtained iteratively. Initially the following are given: (i) specified ABL flow velocity $U_{FS}$ obtained either (a) from field wind speed data when validating flow and pressures against field measurements (such as the TTU and Silsoe measurements), or (b) from wind maps in standards (such as ASCE 7-10) if estimating pressures on buildings for design purposes, (ii) dimensional ABL full spectrum from the field wind speed data when available or using Eq. 8a or 8b, (iii) wind velocity $U_{PS,m}$ and test duration $T_{PS,m}$ in the laboratory partial simulation, which depend upon the capabilities of the laboratory facilities and considerations of economy in conducting the tests, respectively, and (iv) dimensional partial spectrum $S_{PS,m}(n_m)$ obtained using the laboratory flow data. The peak factor $k_{u,FS}$ is obtained using Eqs. 6a and 7a and the rms $\sigma_{u,FS}$ is obtained

from the ABL full spectrum assuming a prototype cut-off frequency $n_c$. The prototype counterpart $U_{PS}$ of $U_{PS,m}$ is obtained by successive iterations as follows.

1. As a first approximation assume

$$U_{PS,1} = 1.2\ U_{FS} \tag{10}$$

Using $U_{PS,1}$ obtain the first approximation to the: velocity scale, $\lambda_{PS,V,1} = U_{PS,m}/U_{PS,1}$ (Eq. 3a); time scale, $\lambda_{PS,T,1} = \lambda_L/\lambda_{PS,V,1}$ (Eq. 3b); $T_{PS\,1} = T_{PS,m}/\lambda_{PS,T,1}$ (Eq. 3c); frequency scale $\lambda_{PS,n,1} = 1/\lambda_{PS,T,1}$ (Eq. 3d); dimensional spectrum $S_{PS,1}\ (n)$ (Eq. 9) and rms $\sigma_{u,PS,1}$; radius of gyration of the spectral area, $\gamma_{u,PS,1}$ (Eq. 7b); peak factor, $k_{u,PS,1}$ ($T_{PS,1}$) (Eq. 6b); and mean speed increment

$$\Delta U_1 = k_{u,FS}\ \sigma_{u,FS} - k_{u,PS,1}\sigma_{uPS,1} \tag{11}$$

2. Substitution in Eq. 2 yields a second approximation of $U_{PS}$ as,

$$U_{PS,2} = U_{FS} + \Delta U_1 \tag{12}$$

Using $U_{PS,2}$ repeat the above procedure to obtain the second approximation of $\Delta U$, denoted by $\Delta U_2$. The procedure is repeated until the sequence $\Delta U_i$ ($i = 1, 2, \ldots n$) converges.

The iterations result in an estimate of $U_{PS}$ for which the high frequency portion of the prototype partial spectrum should match approximately the high frequency portion of the prototype ABL full spectrum. Such agreement of the high frequency turbulence components should be also observed if the two spectra are plotted in the non-dimensional format using $nS(n)/U^2$ as functions of the Monin parameter $nz/U$, where $n$ is the frequency and $U$ is the mean wind speed at the reference height $z$ (Richards et al. 2007, Banks 2012). This simulation will ensure the approximate reproduction of the small scale (high

frequency) turbulence in the incident flow and, therefore, of the thickness of the separated shear layers (estimated for low-rise structures by Melbourne (1980) as 1/10 of their height). This will in turn ensure the adequate simulation of mean and peak pressures. $U_{PS}$ is also used to determine $T_{PS}$ (the prototype counterpart of $T_{PS,m}$), required to obtain statistical estimates of peak pressure coefficients for comparisons with those obtained for a particular time duration (say 15 min., 1 hr., etc.) for the prototype buildings in ABL flow. The following sections describe partial simulation in the FIU 12-fan Wall of Wind facility and show comparisons of pressure coefficients obtained in the facility using large-scale models of TTU and Silsoe buildings with those obtained from field measurements in ABL flows on the respective prototype buildings.

**4.4 12-Fan Wall of Wind Partial Simulation and Pressure Measurement Results**

Jones et al. (1995) noted that although most wind engineering research is conducted for tall buildings and long bridges, experience shows that it is the more common structures – e.g., residential homes, schools, low-rise commercial and industrial structures – that are most vulnerable. Therefore, there is a need to develop innovative methods for accurate large- or full-scale wind testing of low-rise structures to make a significant impact in mitigating hurricane damage by enhancing building codes and validating mitigation technologies. To address windstorm-induced economic losses wind engineering research is currently undergoing dramatic changes, with new large- and full-scale testing facilities being built worldwide. Some of these facilities are: The "Insurance Research Lab for Better Homes" (Kopp et al. 2010) and the Wind Engineering, Energy and Environment Dome (Natarajan and Hangan, 2010) at the University of Western Ontario; the wind generator at the University of Florida (Mensah et al. 2011), the new multi-peril fa-

cility of the Institute of Business and Home Safety (Liu et al. 2011), and the Wall of Wind at Florida International University (Aly et al. 2011).

The 12-fan Wall of Wind (WOW) facility at FIU (Fig. 1) is an open jet facility built for testing of structures in hurricane-level flow speeds. The 12 electric fans are arranged in a two-row by six-column pattern to generate a wind field corresponding to a 6 m wide and 4.3 m high test section. This test section size allows aerodynamic testing of large-scale models of low-rise buildings and other structures. A contraction section was used downwind of the fan array to attain uniform flow field with high wind velocity. A set of vertical flow directing vanes at the exit of the contraction section guides the air flow in the longitudinal direction. Figure 1b shows the WOW exit side without any flow management devices. To simulate ABL and turbulence characteristics a set of flow management devices – comprising a long rectangular box, spires, and floor roughness elements – was installed as shown in Fig. 1c. The 9.75 m long box is located downwind of the contraction section. The rectangular box provides the required fetch length and contains the spires and floor roughness elements for ABL flow development. The optimal shape and size of the spires and floor roughness were designed through a rigorous trial-and-error procedure of wind profile measurements in the 1:15 small-scale 12-fan WOW (Aly et al. 2011). Figure 2a shows an open terrain ABL mean wind speed profile generated for the prototype 12-fan WOW using four triangular-shape spires and floor roughness elements. Figures 2b and 2c show the turbulence intensity profile and longitudinal partial turbulence spectrum at mean roof height of typical models (about 1.2 m), respectively. The test section (corresponding to the center of the turntable for testing model buildings) was located at 6.1 m from the rectangular box exit. This distance was optimized based on

several experiments performed by Aly et al. (2011). For comparison purposes, Figs. 2a, 2b, and 2c also show the profiles and spectrum without using the flow management devices (for this case the test section was located at 6.1 m from the contraction exit). Note that without the flow management devices the flow had a uniform vertical mean wind speed profile with low turbulence intensities. Also, the spectrum without flow management devices did not conform to the slopes associated with the high frequency fluctuations in typical ABL models (Irwin 2009). The difference in the cut-off frequencies in Fig. 1c was due to the use of different sampling rates (100 Hz versus 512 Hz) in measuring wind data due to limitation of instrumentation during the early stages of WOW development.



Figure 1. a. 12-Fan WOW Intake Side, b. WOW Exit Side Without Flow Management Devices, c. WOW Exit Side With Flow Management Devices
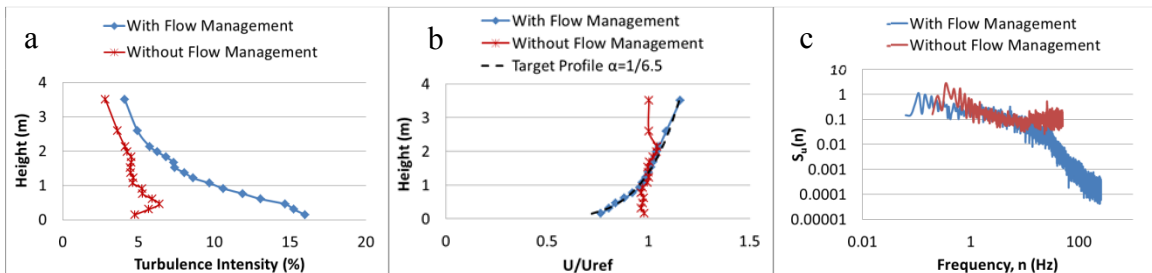
Figure 2. WOW Open Terrain ABL Flow Characteristics at Test Section With and Without Flow Management Devices: a. Non-dimensional Mean Wind Speed Profile, b. Turbulence Intensity Profile, c. Longitudinal Velocity Spectrum

### 4.5 TTU Results

### 4.5.1 Flow Simulation

For the TTU prototype building the mean wind speed $U_{FS}$ at mean roof height of 3.97 m was considered as 8.3 m/s based on measurements performed at the TTU site. The dimensional full turbulence spectrum was obtained using the Kaimal spectrum model (see Eq. 8a) using reference height $z_{ref}$ = 3.97 m, $U_{FS}$ = 8.3 m/s at $z_{ref}$, and surface roughness length $z_0$ = 0.02 m for open terrain exposure (typical value of $z_0$ in ASCE 7-10 for exposure category C corresponding to open terrain). Based on the dimensional full spectrum and using $T_{FS}$ = 15 min. (i.e., the full scale test duration) and cut-off frequency $n_{c\,FS}$ = 15 Hz, the peak factor $k_{u,FS}(T_{FS})$ and the rms $\sigma_{u,FS}$ were estimated as 3.32 and 1.8 m/s, corresponding to a longitudinal turbulence intensity $I_u$ = 21.7% (slightly lower than 25.4% as given by Eq. 26.9-7 in ASCE 7-10).

The TTU building model was tested in WOW using $\lambda_L$ = 1:6. For the WOW simulation $T_{PS,m}$ = 3 min. and $U_{PS,m}$ = 15.7 m/s at the 0.66 m model mean roof height. The iterative procedure described in Section 2.2 was performed based on the WOW mean wind speed $U_{PS,m}$ and spectrum $S_{PS,m}(n_m)$ for open terrain simulation. Convergence was achieved after the third iteration, with final values as $\Delta U$ = 1.51 m/s, $U_{PS} = U_{FS} + \Delta U$ = 8.3 + 1.51 = 9.81 m/s, $\lambda_{PS,V}$ = 15.7: 9.81 = 1.6:1, $\lambda_{PS,T} \approx$ 1:10, $T_{PS} \approx$ 30 min. and $\sigma_{u,PS}$ = 1.15 m/s. The turbulence intensity was 11.7% for WOW as compared to 21.7% obtained using the ABL spectrum. Given the final values of $\lambda_{PS,V}$ and $\lambda_{PS,T}$, the dimensional partial

spectrum $S_{PS}$ $(n)$ is obtained and compared with the dimensional full spectrum $S_{FS}$ $(n)$.

Figure 3 shows the comparisons between the ABL full spectrum for TTU and the WOW prototype partial spectrum at the end of iteration. The ABL full spectrum and the WOW prototype high frequency spectrum match for frequencies higher than 0.2 Hz. For non-dimensional Monin parameter values $f > 0.2$ the turbulence is approximately isotropic (Simiu and Scanlan 1996, p. 57). This value corresponds to $n = 0.2U_{PS}/h = 0.2$ x 9.81/4.0 = 0.49 Hz. By virtue of Taylor's hypothesis the wavelength corresponding to this frequency is $\Lambda = 9.81/0.49 = 20.0$ m at full scale. According to Melbourne (1980) turbulence eddies with dimensions roughly one-tenth those of the building height and smaller are critical to obtaining the correct simulation of pressures in zones of flow separation. For the TTU building with a height of 4 m, this implies that prototype wavelengths of 0.4 m and smaller need to be well simulated. Clearly the WOW's ability to cover the range up to 20 m in the current experiments more than satisfied this requirement.

Recall that the flow simulation was based on the requirement that Eq. 1 be satisfied, that is, that the expected peak wind speed in partial simulation be equal to the expected peak wind speed in the ABL flow. At the end of the iteration the peak wind speeds in the two flows matched closely ($U_{PS}^{pk}(T_{PS}) = 14.4$ m/s versus $U_{FS}^{pk}(T_{FS}) = 14.3$ m/s). The hypothesis that two flows with similar peak wind speeds and with matching high frequency portions of the spectrum will induce similar wind effects (e.g., mean and peak pressure coefficients) is demonstrated in the next section.
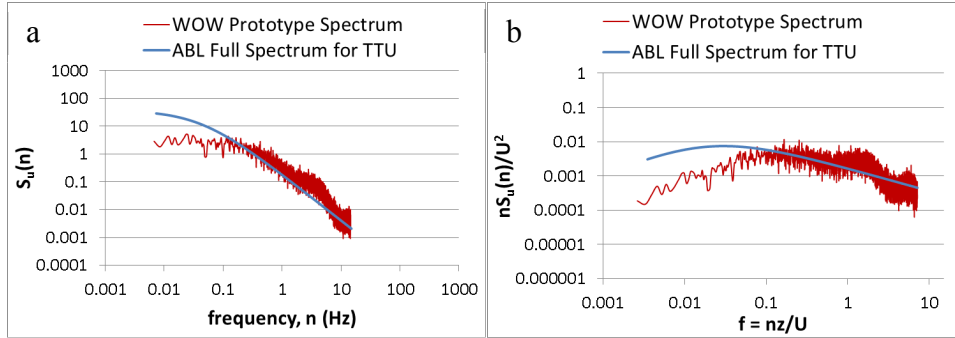
Figure 3. Comparisons of the ABL and Partial Spectrum: a. Dimensional Spectra, b. Non-Dimensional Spectra

## 4.5.2    Pressure Coefficients Comparison

A Scanivalve pressure acquisition system was used in the WOW to capture pressure time history data with a 512 Hz sampling rate. After collecting the raw data from the Scanivalve pressure scanners, a transfer function designed for the tubing system was used to correct the raw data. This correction method was developed by Irwin et al. (1979). The provided TTU pressure data were sampled at 30 Hz for 15 min. and low pass filtered at 10 Hz. Based on the frequency scale $\lambda_{PS,n}$ = 10:1, 100 Hz was used for low pass filtering of WOW pressure data. Figure 4 shows the 1:6 scale TTU building model and pressure tap locations at the centerline and corners of the roof. Only roof pressures were investigated in the current paper as roofs are considered the most vulnerable elements of low buildings and are often damaged from high suction pressures induced during windstorms.

85
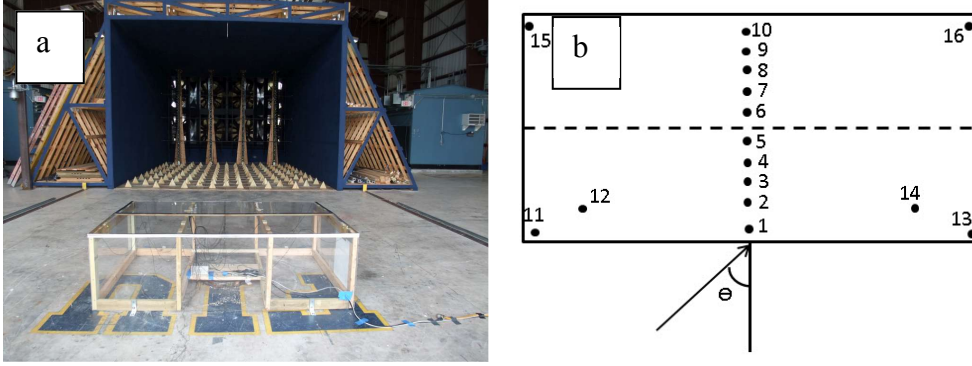
Figure 4. a. TTU Building Model Tested in WOW, b. Tap Locations on TTU Model

The mean $C_p$ value calculations were defined as follows:

$$C_{p\,mean} = \frac{p_{mean}}{\frac{1}{2}\rho U_{mean}^2} \qquad (13)$$

where $p_{mean}$ denotes the mean pressure, $\rho$ is the air density, and $U_{mean}$ is the mean wind velocity at the reference height. Peak $C_p$ coefficients were obtained by using the equation

$$C_{p\,peak} = \frac{p_{peak}}{\frac{1}{2}\rho U_{3s}^2} \qquad (14)$$

where $p_{peak}$ is the estimated peak pressure and $U_{3s}$ is the peak 3-s gust at the reference height. Note for the TTU pressure coefficients, $U_{mean} = U_{FS} = 8.3$ m/s and $U_{3s} = U_{FS\_3s} = 13.78$ m/s were used as provided for the mean roof height. For WOW pressure coefficients, we used $U_{mean} = U_{PS\,m} = 15.7$ m/s and $U_{PS,m\_3s}$ was obtained by using the time scale $\lambda_T = 1{:}10$, meaning that 512 Hz x 3/10 sec = 154 data points were required for its determination. The peak value of $U_{3s}$ was obtained by performing moving averages. The Reynolds numbers corresponding to the reference height were estimated as $2.1\times10^6$ and $1.3\times10^6$ for TTU site and WOW, respectively.

The Sadek and Simiu (2002) method was used to estimate the peak pressures with probability of non-exceedance of 95% (i.e., 95% fractile) for both WOW and TTU data.

This method uses entire time histories; for this reason the estimates are more stable than observed peaks, which vary from observation to observation. To facilitate meaningful comparison of pressure coefficients the WOW pressure data for 3 min. was divided into two 1.5 min. segments so that the prototype duration of 15 min. matched the TTU field measurement duration. The pressure coefficients presented for WOW are the averages of those obtained from the two segments. The duration ratio applied to both the WOW and TTU pressure time history data to obtain peak pressure coefficients for a 15 min full-scale equivalent duration was $K=1$. It was observed that the differences between peak pressure coefficients obtained based on segment 1 (1.5 min.) data, on segment 2 (1.5 min.) data, on the entire 3 min. record, and by averaging results based on segments 1 and 2, were minimal (maximum difference was about 3% when using 1.5 min. versus 3 min. data segments). This justifies the use of relatively small duration tests in operationally expensive large-scale facilities using partial simulation, which can achieve significant reduction in time and resources when various model configurations and several wind directions are to be considered. In this example 1.5 min., 3 min., and 6 min. runs would represent 15 min., 30 min., and 1 hr. prototype durations, respectively.

For this study the TTU pressure data used for comparison purposes were based on field measurements corresponding to the following wind directions (WDs): 7°, 13°, 44°, 59°, 74°, 83°, and 96°. Field measured pressure time histories were available for all these WDs expect WD = 59°. Thus Sadek and Simiu (2002) method was used for peak pressure estimation for all WDs other than WD = 59° for which pressure coefficients were based on observed peak pressures. In addition, peak pressure coefficients based on TTU

field data for two wind directions, WD = 0° and 30°, were available from Endo et al. (2006).

Figures 5 to 11 show comparisons of mean ($C_{p\,mean}$) and peak ($C_{p\,peak}$) pressure coefficient values for WD = 7°, 13°, 44°, 59°, 74°, 83°, and 96° obtained from the field measurements for the full-scale TTU building and the 1:6 scale TTU building model tested in the WOW using partial simulation. Overall, the trend of the mean and peak pressure coefficients obtained from field data and WOW experimentation matches reasonably well. The mean and peak values match well for most taps for all wind directions, except for taps 15 and 16 for WD = 7°, taps 3 to 5 for WD = 13°, and taps 9 and 10 for WD = 96°; however, these were not critical locations as the suctions were low in magnitude. For critical corner zones with high suction pressures (see results for taps 11 and 13 for WD = 7°, taps 11 and 12 for WD = 13°, tap 11 for WD = 44°, tap 11 and 15 for WD = 74° and 83°), the mean and peak values were in good agreement, the maximum differences among the peak values obtained in the field and in the WOW being approximately 5% to 10%. For WD = 59°, the peak pressure coefficient from field measurement was 14% higher than its WOW counterpart. Taps 12 and 14 were 0.92 m (full-scale dimension) away from the windward eave for WD = 7° and the mean and peak values matched well. However, higher differences were noted for tap 12 for WD = 83° and 96°. This is ascribed to earlier flow reattachment for the WOW flow because of its somewhat higher high frequency turbulence content (see Fig. 3a). This could result in pressure recovery and lower suction when tap 12 was further away from the roof edge (1.53 m in full scale) for these two wind directions. Similar phenomenon was observed for taps 3 to 5 WD = 13°. Figure 12 shows the $C_{p\,peak}$ comparisons for WD = 0° and 30° for the TTU model in

WOW and full-scale TTU measurements (Endo et al. 2006). For corner taps 11 and 12 the TTU field and WOW results are in good agreement. Note that for the cornering wind angle with WD = 30°, the WOW simulation generated high suction peak coefficient $C_p$ $_{peak}$ = -7 at leading corner tap 11 which matched the coefficient based on the field data. Some differences in results were noted for the leeward taps 7 and 8 experiencing low suctions.



Figure 5. $C_p$ Values Comparison for WD = 7°: a. Mean $C_p$ Comparison, b. Peak $C_p$ Comparison



Figure 6. $C_p$ Values Comparison for WD = 13°: a. Mean $C_p$ Comparison, b. Peak $C_p$ Comparison
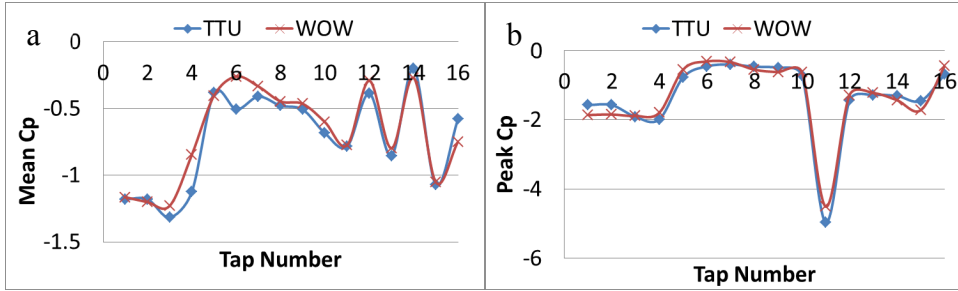
Figure 7. $C_p$ Values Comparison for WD = 44°: a. Mean $C_p$ Comparison, b. Peak $C_p$ Comparison
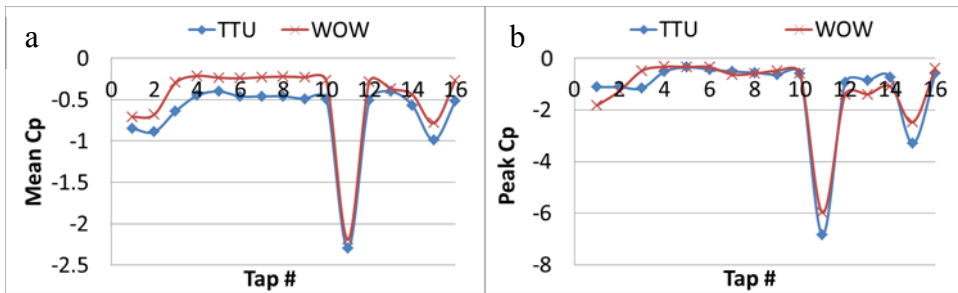


Figure 8. $C_p$ Values Comparison for WD = 59°: a. Mean $C_p$ Comparison, b. Peak $C_p$ Comparison
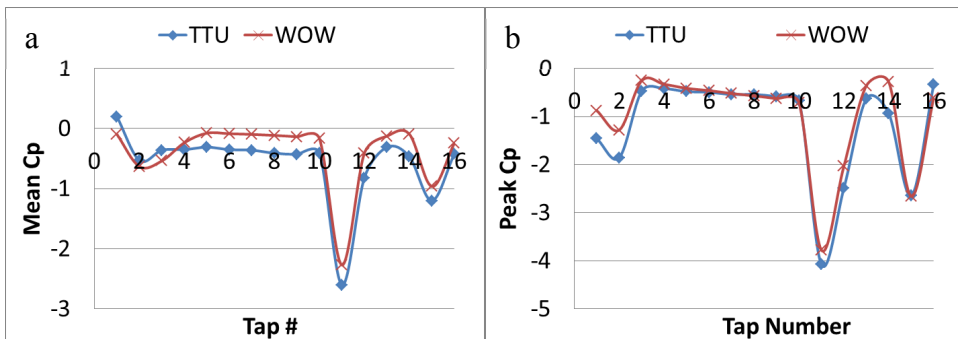


Figure 9. $C_p$ Values Comparison for WD = 74°: a. Mean $C_p$ Comparison, b. Peak $C_p$ Comparison
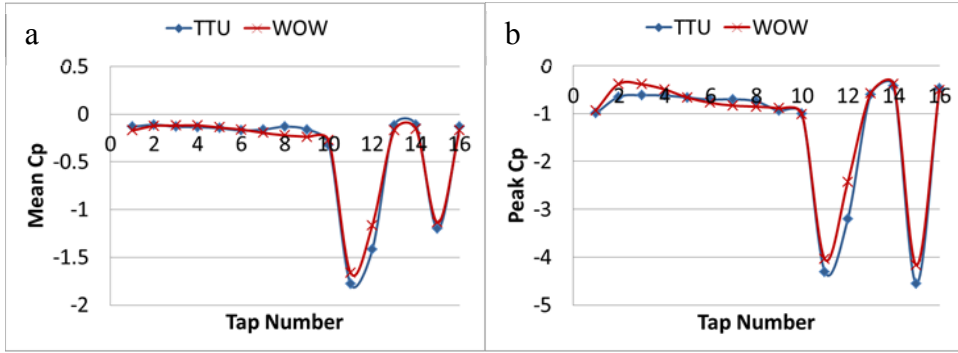
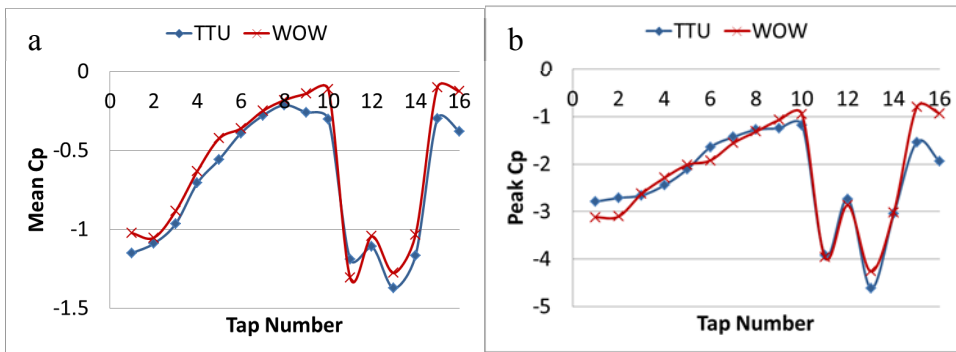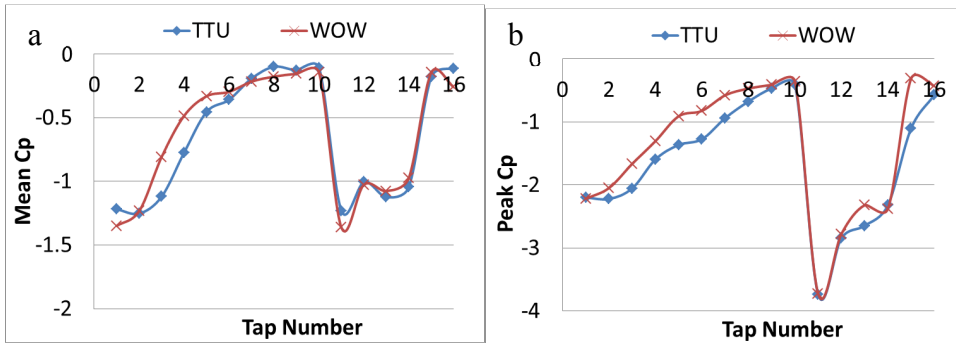Figure 10. $C_p$ Values Comparison for WD = 83°: a. Mean $C_p$ Comparison, b. Peak $C_p$ Comparison
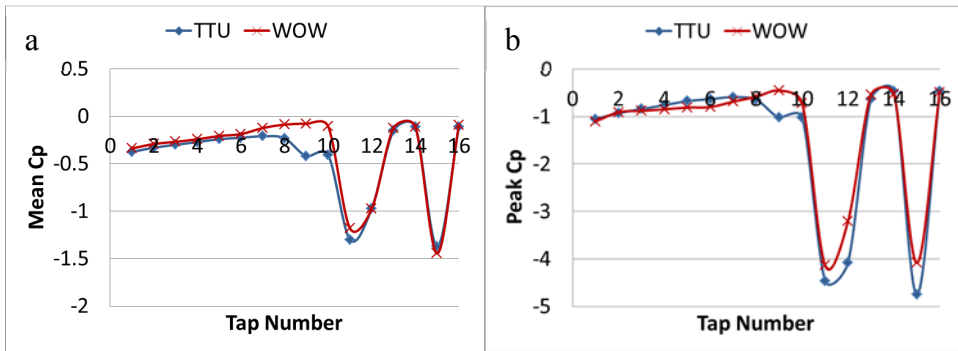


Figure 11. $C_p$ Values Comparison for WD = 96°: a. Mean $C_p$ Comparison, b. Peak $C_p$ Comparison
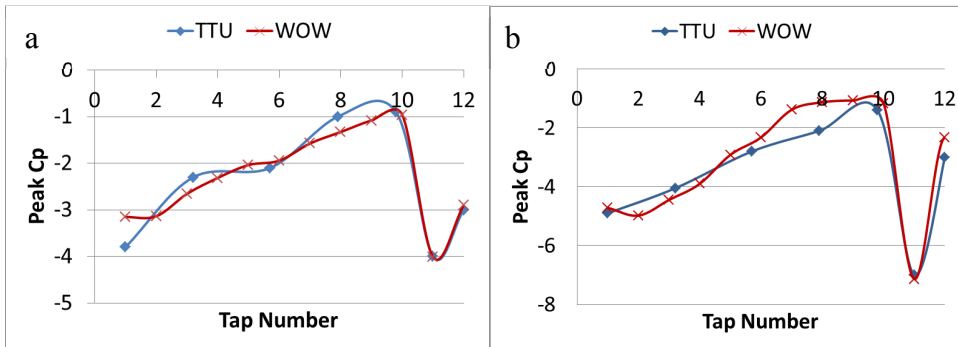


Figure 12. Peak $C_p$ Values Comparison Based on Data from Endo et al. (2006): a. WD = 0°, b. WD = 30°

### 4.6 Silsoe Results

#### 4.6.1 Flow Simulation

The most recent measurements of the velocity profile at the Silsoe Research Institute site, with southwest to west winds, resulted in longitudinal turbulence intensity $I_u$ values of 19–20% at Silsoe cube roof height and roughness length $z_0 = 0.006$–$0.01$ m (Richards and Hoxey, 2012). The dimensional full turbulence spectrum, needed for flow simulation approach presented in this paper, was obtained using the Kaimal spectrum model (Eq. 8a) using reference height $z_{ref} = 6$ m, $U_{FS} = 9.52$ m/s at $z_{ref}$, and surface roughness length $z_0 = 0.01$ m (Richards et al., 2001, Richards and Hoxey, 2012). Based on the dimensional full spectrum, using the test duration $T_{FS} = 12$ min., and cut-off frequency $n_{c\ FS} = 15$ Hz, the peak factor $k_{uFS}(T_{FS})$ and the rms $\sigma_{uFS}$ were estimated as 3.96 and 1.84 m/s, respectively.

The Silsoe building model was tested in WOW using $\lambda_L = 1{:}5$. The iterative procedure was performed based on the WOW mean wind speed $U_{PS,m} = 17.6$ m/s at the 1.2 m Silsoe cube model mean roof height, $T_{PS,m} = 3$ min., and spectrum $S_{PS,m}(n_m)$ for open terrain simulation. Convergence was achieved after the fifth iteration, with final values $\Delta U = 2.63$ m/s, $U_{PS} = U_{FS} + \Delta U = 9.52 + 2.63 = 12.15$ m/s, $\lambda_{PS,V} = 17.6{:}12.15 = 1.45{:}1$, $\lambda_{PS,T} \approx 1{:}7.3$, $T_{PS} \approx 22$ min. and $\sigma_{u,PS} = 1.04$. The turbulence intensity was 8.6% for WOW as compared to 19–20% for the Silsoe site. At the end of the iteration the peak wind speeds in the two flows matched closely ($U_{PS}^{pk}(T_{PS}) = 16.77$ m/s versus $U_{FS}^{pk}(T_{FS}) = 16.80$ m/s), so Eq. 1 was satisfied.

Given the final values of $\lambda_{PS,V}$ and $\lambda_{PS,T}$, the dimensional partial spectrum $S_{PS}(n)$ is obtained and compared with the dimensional full spectrum $S_{FS}(n)$. Figure 13a shows

the comparisons of the dimensional ABL full spectrum for Silsoe and the WOW proto-

type partial spectrum at the end of iteration. For comparison purposes, we also plotted the

estimated dimensional full turbulence spectrum based on the von Karman spectrum mod-

el (see Eq. 9b) in conjunction with $U_{FS} = 9.52$ m/s, longitudinal turbulence intensity $I_u =$

19.3%, and integral length scale $^xL_u = 53$ m (Richards et al., 2001). Compared to the

Kaimal model the von Karman model resulted in slightly lower spectral values for the

higher frequencies. Figure 13b shows the non-dimensional spectra comparisons where all

spectra were plotted in terms of turbulence-independent normalizing parameters as

$nS(n)/U^2$ and $nz/U$, as recommended by Richards et al. (2007). The ABL full spectrum

based on the Kaimal model and the WOW prototype high frequency spectrum approxi-

mately match for frequencies higher than 0.3 Hz. As was the case for TTU, it follows that

the relevant turbulent eddy dimensions were larger than one-tenth of the building height

(0.6 m), i.e., the approximate thickness of the shear layer (Melbourne, 1980).
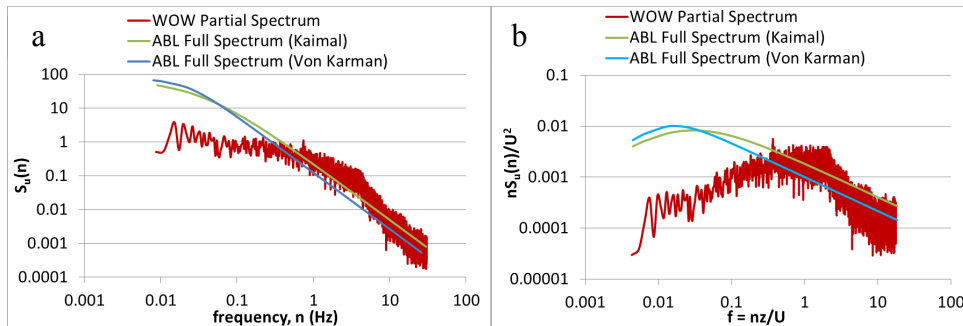


Figure 13. Comparisons of the ABL and Partial Spectrum: a. Dimensional Spectra, b. Non-Dimensional Spectra

Based on the von Karman power spectral density model, Katsuchi and Yamada

(2011) and Sangchuwang et al. (2013) suggested that the reduced turbulence intensity for

the partial turbulence simulation can be obtained from the equation:

$$[I_u]_{PS} = \left[\frac{I_u}{(^xL_u/D)^{1/3}}\right]_{FS} \left[(^xL_u/D)^{1/3}\right]_{PS} \tag{15}$$

where $I_u$ is the longitudinal turbulence intensity, $^xL_u$ is the integral length scale, and $D$ is the representative length. As noted earlier, at the Silsoe roof height the turbulence intensity estimated was 19.3%; the integral length scale was 53 m (Richards et al., 2001). The integral length measured in WOW was 0.4 m at the Silsoe model roof height. Using these values Eq. 15 yields $[I_u]_{PS} \approx 6.5\%$, i.e., somewhat lower the 8.6% turbulence intensity measured in the WOW partial spectrum simulation.

### 4.6.2 *Pressure Coefficient Comparisons*

The pressure coefficient comparisons shown in this section are based on full-scale Silsoe measurement results given in Richards and Hoxey (2012), available only for roof centerline pressure tap locations. Figure 14 shows the 1:5 scale Silsoe building model at WOW and pressure tap locations at the centerline of the roof matching the full-scale tap locations. For comparison purposes mean and peak pressure coefficient values for the roof centerline taps measured in the field were obtained from Appendix A in Richards and Hoxey (2012). The wind directions considered were WD = 0° to 90° at 15° intervals.
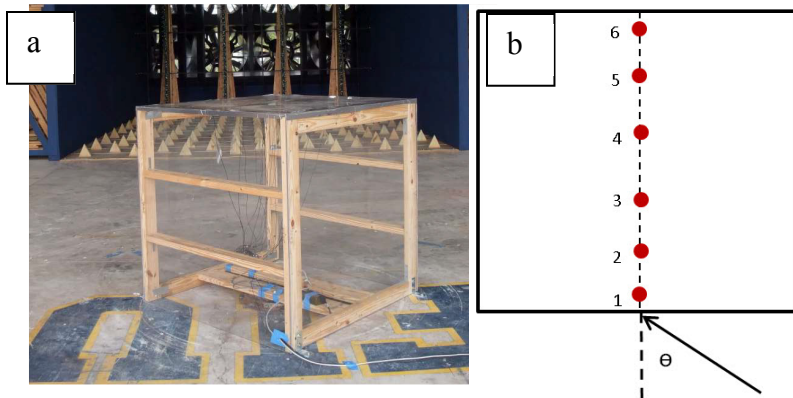
Figure 14. a. Silsoe Cube Building Model Tested in WOW, b. Tap Locations on Silsoe
Model

Richards and Hoxey (2012) defined the pressure coefficients in terms of the mean
dynamic pressure $q_{mean}$ as follows:

$$C_{mean} = \frac{p_{mean}}{q_{mean}} \tag{16}$$

$$C_{peak} = \frac{p_{peak}}{(3q_{mean})} \tag{17}$$

where $p_{mean}$ is the mean surface pressure, and $p_{peak}$ is the highest positive or low-
est negative pressure observed during the test duration at the Silsoe site. The Silsoe pres-
sure data provided by Richards and Hoxey (2012) were sampled at 4.165 Hz for 12 min.
segments.

WOW pressure data were obtained using the method described in Sec. 3.2.2. For
comparison purposes, the mean and peak pressure coefficients for the Silsoe model tested
in WOW were obtained by using Eqs. 16 and 17, where $q_{mean}$ was taken as $0.5\rho(U_{PS,m})^2$
($\rho$ = air density), $p_{mean}$ were the mean pressures obtained in WOW testing, and $p_{peak}$ were
the estimated peak pressures obtained from WOW pressure time histories using the Sadek
and Simiu method. Since the pressure measurement duration at the full-scale Silsoe site
was 12 min. and $T_{PS}$ = 22 min., only 100 sec of the 3 min. WOW pressure data was used
to estimate the peak pressures (duration ratio $K$=1 was applied). Averaging of results ob-
tained from multiple 100 sec test segments was not necessary, as it was observed from
the TTU model testing that results obtained from a single segment were close to those
obtained from multiple segments or longer segments. This small variability is a conse-

quence of the absence of low frequency content in the spectra measured in the laboratory flow.

The results of mean and peak $C_p$ values obtained from Silsoe field measurements and WOW test data are shown in Figures 15 to 21. The trends of the mean $C_p$ values match well between the WOW and Silsoe full-scale cases for all seven WDs. The mean pressure coefficients were in good agreement for most of the taps including the leading edge taps experiencing high suction. Some of the highest (in magnitude) mean coefficients matched very closely for WOW and Silsoe full-scale cases (for example, -1.0 for leading edge taps 2 and 3 for WD = 0° and -1.5 for leading edge tap 1 under oblique winds with WD = 45°). The peak $C_p$ values show very good agreement for most taps for all the WDs, especially for the taps experiencing critical uplift pressures (-1.9 and -1.8 for leading edge tap 1 for WD = 45° and 60°, respectively, and -1.5 for tap 2 for WD = 30°). A difference of about 17% was observed for tap 1 for WD = 30°.
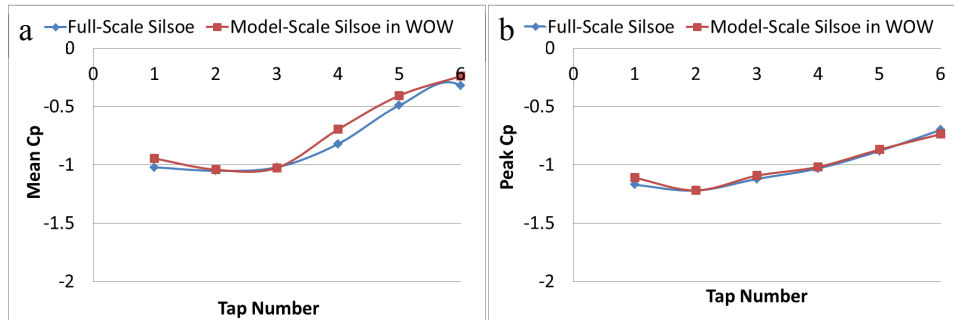


Figure 15. $C_p$ Values Comparison for WD = 0°: a. Mean $C_p$ Comparison, b. Peak $C_p$ Comparison

96
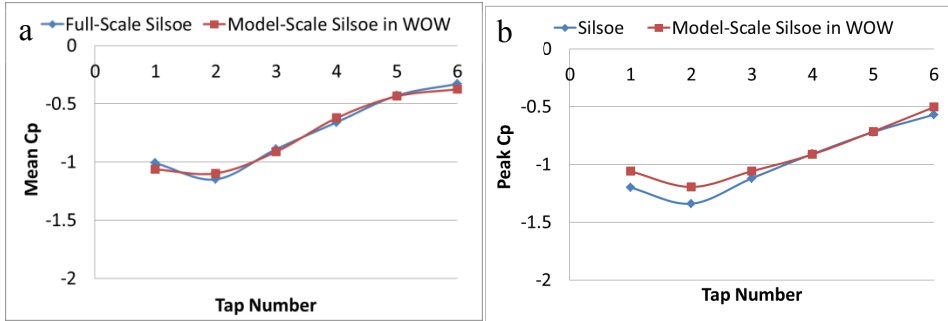
Figure 16. $C_p$ Values Comparison for WD = 15°: a. Mean $C_p$ Comparison, b. Peak $C_p$
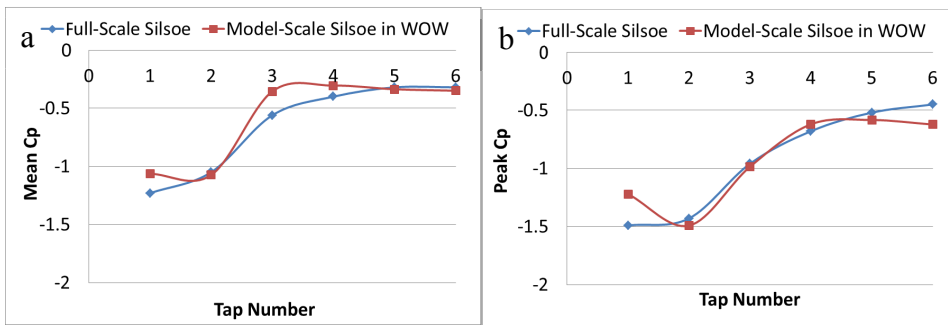
Comparison



Figure 17. $C_p$ Values Comparison for WD = 30°: a. Mean $C_p$ Comparison, b. Peak $C_p$
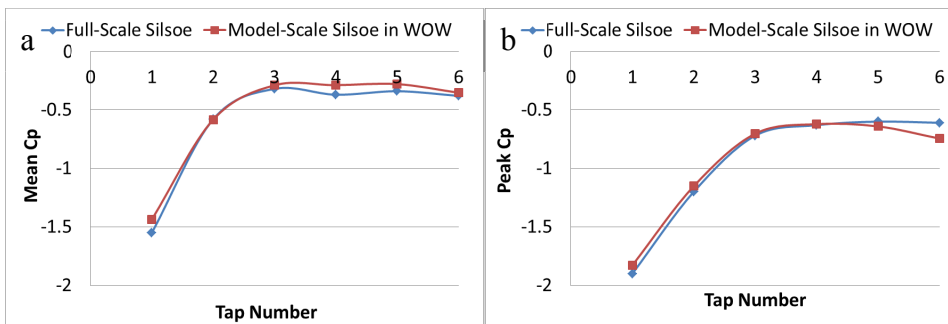
Comparison



Figure 18. $C_p$ Values Comparison for WD = 45°: a. Mean $C_p$ Comparison, b. Peak $C_p$
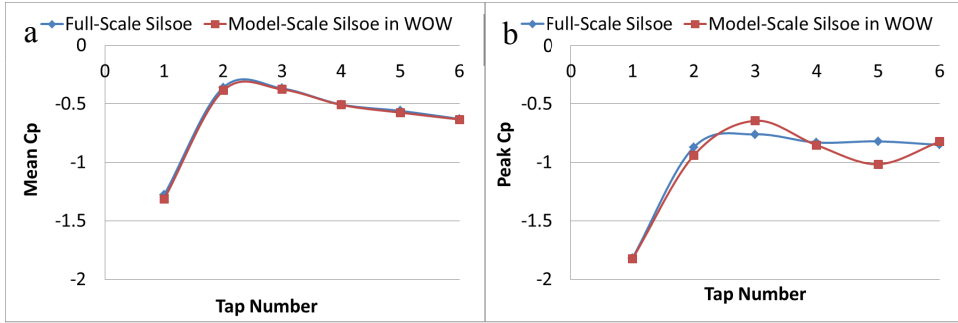
Comparison

Figure 19. $C_p$ Values Comparison for WD = 60°: a. Mean $C_p$ Comparison, b. Peak $C_p$
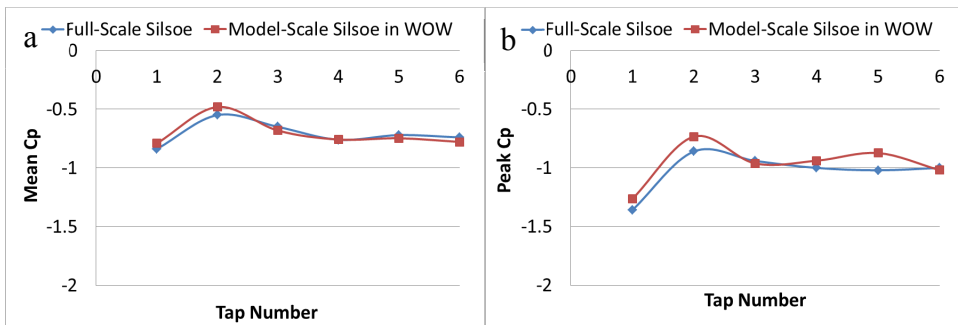
Comparison



Figure 20. $C_p$ Values Comparison for WD = 75°: a. Mean $C_p$ Comparison, b. Peak $C_p$
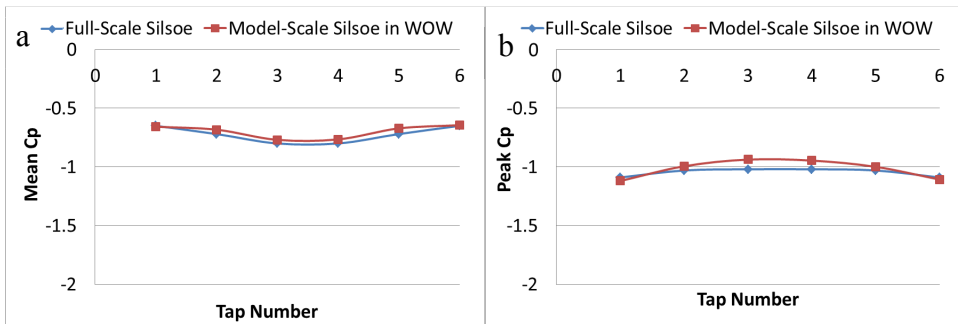
Comparison



Figure 21. $C_p$ Values Comparison for WD = 90°: a. Mean $C_p$ Comparison, b. Peak $C_p$

Comparison

**4.7 Conclusions**

A partial turbulence simulation methodology using an iterative procedure was presented in this paper. The simulation was shown to be appropriate for testing of large-scale models in aerodynamic facilities. The methodology was applied successfully in the 12-fan WOW open-jet wind testing facility and partial simulation results were presented. For the wind field simulation, flow management devices were used to generate high frequency turbulence. A numerical iteration procedure was shown to yield good agreement of the high frequency portion of the partial spectrum obtained in the laboratory on the one hand and the ABL spectrum model on the other. Pressure results obtained using large-scale models at the WOW facility compared well to the full-scale TTU and Silsoe building measurements. For most cases, the pressure results obtained from WOW partial simulation for taps experiencing high mean and peak suctions were in reasonable agreement with their full-scale counterparts. This validated the hypothesis that two flows with similar peak wind speeds and with matching high frequency portion of the full spectrum will induce similar mean and peak pressures on low-rise buildings with dimensions not exceeding those of typical residential homes.

The partial simulation methodology developed for low-rise buildings used in wind tunnels and WOW-like facilities was shown to produce aerodynamic pressure coefficients on large-scale models that matched well their measured full-scale counterparts. This capability is not reflected in current ASCE 7-10 provisions, which are based on integral length scale similarity requirements. Some of the advantages of the partial turbulence simulation for aerodynamic testing of small low-rise buildings and other structures are listed below:

(1) Small scale or high frequency turbulence is adequately modeled for proper simulation of aerodynamic effects on low-rise structures.

(2) In the absence of significant low-frequency content of the longitudinal turbulence spectra, the turbulence intensity of the longitudinal velocities is considerably smaller than is the case for ABL flows. Relaxing the turbulence intensity generation requirement will result in simpler and more economical design and construction of flow management devices.

(3) In ABL flow the bulk of the integral longitudinal turbulence scale $^xL_u$ is contributed by the low-frequency velocity fluctuations. In the partial spectrum flow these fluctuations are weak, and their contribution to the integral turbulence scale becomes negligible. Recall the interpretation of the mean velocity increment $\Delta U$ as a flow fluctuation with zero frequency and perfect spatial coherence. The aerodynamic effect of that increment approximates slightly conservatively the effect of the ABL flow low-frequency fluctuations, which are highly but imperfectly coherent. It follows that tests in simulation with deficient low-frequency spectral content are freed of integral length scale constraints related to the ratio $^xL_u/D,$ where $D$ is a characteristic length of the structure. This means that model length scales in such testing are only limited by blockage considerations. This is a major advantage, both because it allows for testing at higher Reynolds number (Re) (high Re testing was shown to be very effective by Cheung et al., 1997 when testing 1:10 model of TTU building) and for greater spatial resolution of the pressure taps in high pressure zones.

Section 2.2.2 of the ASCE 49-12 Standard for wind tunnel testing considers simulations with missing content at the low frequency end of the turbulence spectrum and

requires that additional interpretation of the data obtained in such simulations "shall refer to recognized literature for methods to make corrections." However, no reference to literature containing such methods is provided in the ASCE 49-12 Standard or the ASCE 7-10 Standard. It is suggested that the partial simulation approach presented in this paper can fill this gap.

## 4.8 Acknowledgments

## 4.9 Reference

American Society of Civil Engineers (2010), *Minimum design loads for buildings and other structures*, ASCE Standard, ASCE/SEI 7-10, New York City.

Aly, A. M., Bitsuamlak, G. T., & Chowdhury, A. G. (2012), "Full-scale aerodynamic testing of a loose concrete roof paver system", *Engineering Structures*, 44, 260-270.

Aly, A. M., Gan Chowdhury, A. and Bitsuamlak, G. (2011), "Wind Profile Management and Blockage Assessment of a New 12-Fan Wall of Wind Facility at FIU", *Wind and Struct.*, 14(4), 285-300.

Banks D. (2011), "Measuring peak wind loads on solar power assemblies", *The 13th International Conference on Wind Engineering*, Amsterdam, Netherlands.

Banks, D. (2012), "Measuring peak wind loads on solar power assemblies", *CCP Wind Engineering*, Colorado, USA.

Bitsuamlak, G.T., Gan Chowdhury, A. and Sambare, D. (2009), "Application of a full-scale testing facility for assessing wind-driven-rain intrusion", *Build. Environm.*, 44(12), 2430-2441.

Cheung, J. C. K., Holmes, J. D., Melbourne, W. H., Lakshmanan, N. and Bowditch, P. (1997), "Pressure on a 1:10 scale model of the Texas Tech Building", *J. Wind Eng. Ind. Aerodyn.*, 69-71, 529-538.

Endo, M., Bienkiewicz, B. and Ham, H. J. (2006). "Wind-tunnel investigation of point pressure on TTU test buildings", *J. Wind Eng. Ind. Aerodyn.*, 94, 553-578.

Fu, T.C., Aly, A. M., Gan Chowdhury, A., Bitsuamlak, G., Yeo, D., and Simiu, E. (2012), "A proposed technique for determining aerodynamic pressure on residential homes", *Wind and Struct.*, 15(1), 27.-41

Gan Chowdhury, A., Simiu, E. and Leatherman, S.P. (2009), "Destructive testing under simulated hurricane effects to promote hazard mitigation", *Nat. Hazards Review* 10(1), 1-10.

Gan Chowdhury, A., Bitsuamlak, G., Simiu, E. (2010), "Aerodynamic, hydro-aerodynamic, and destructive testing", *J. ICE Struct. Build.*, 163(2), 137-147

Huang, P., Gan Chowdhury, A., Bitsuamlak, G. and Liu, R. (2009), "Development of devices and methods for simulation of hurricane winds in a full-scale testing facility", *Wind and Struct.*, 12(2), 151-177.

Holmes, J.D. (2007), "Wind Loading of Structures, 2nd Edition", Taylor and Francis, London.

Irwin, P., Cooper, K. and Girard, R. (1979), "Correction of distortion effects caused by tubing systems in measurements of fluctuating pressures", *J. Ind. Aerodyn.*, 5, 93-107.

Irwin, P. (2008), "Bluff body aerodynamics in wind engineering", *J. Wind Eng. Ind. Aerodyn.*, 96, 701-712.

Irwin, P. (2009), "Wind engineering research needs, building codes and project specific studies", *11th Americas Conference on Wind Engineering,* San Juan, Puerto Rico.

Jones, N.P., Reed, D.A. and Cermak, J.E. (1995), "National wind-hazards reduction program", *ASCE Journal of Professional Issues in Engineering Education and Practice*, 121(1), 41–46.

Katsuchi, H. and Yamada, H. (2011), "Study on turbulence partial simulation for wind-tunnel testing if bridge deck", *Proc of ICWE 12*, Amsterdam, Netherlands.

Kopp, G. A. and Banks, D. (2013), "Use of the wind tunnel test method for obtaining de-

sign wind loads on roof-mounted solar arrays", *J. Struct. Eng.*, 139, 284-287.

Kopp, G. A., Morrison, M. J., Gavanski, E., Henderson, D. J. and Hong, H. P. (2010), "The 'Three Little Pigs' project: hurricane risk mitigation by integrated wind tunnel and fullscale laboratory tests", *Nat. Haz. Rev.*, 11, 151–161.

Kozmar, H. (2010), "Scale effects in wind tunnel modeling of an urban atmospheric boundary layer", *Theor. Appl. Climatol.*, 100, 153-162.

Leatherman, S.P., Gan Chowdhury, A. and Robertson C.J. (2007), "Wall of wind full-scale destructive testing of coastal houses and hurricane damage mitigation", *Journal of Coastal Research*, 23(5), 1211-1217.

Liu, Z., Brown, T.M., Cope, A.D., Reinhold, T.A. (2011), "Commissioning of the wind test capabilities of the IBHS Research Center", *Proc. 13th Int. Conf. Wind Eng.*, Amsterdam, Netherlands.

Melbourne W. H. (1980), "Turbulence effects on maximum surface pressures – a mechanism and possibility of reduction", *Wind Engineering*, 1, 521-551.

Mensah A. F., Datin, P. L., Prevatt, D., Gupta, R. and van de Lindt, J. W. (2011), "Database-assisted design methodology to predict wind – induced structural behavior of a light-framed wood building", *J. Eng. Struct.*, 33, 674-684.

Natarajan, D. and Hangan, H. (2010), "Preliminary numerical simulation of axi-symmetric flows in WindEEE dome facility", *Proc., 5th Int. Symp. on Computational Wind Engineering (CWE2010)*, *International Association for Wind Engineering (IAWE)*, Kanagawa, Japan.

Richards, P.J. and Hoxey, R.P., (2012), "Pressures on a cubic building – Part 1: Full-scale results", *J. Wind Eng. Ind. Aerod.*, 102, 72-86.

Richards, P.J., Hoxey, R.P., Connell, R.P., and Lander, D.P. (2007), "Wind-tunnel modelling of the Silsoe Cube", *J. Wind Eng. Ind. Aerod.*, 95, 1384-1399.

Saathoff, P. J. and Melbourne, W. H. (1997). "Effects of free-stream turbulence on surface pressure fluctuation in a separation bubble', *J Fluid Mech.,* 337, 1-24.

Sadek, F. and Simiu, E. (2002), "Peak non-Gaussian wind effects for database-assisted low-rise building design," *J. Eng. Mech.*, 128(5), 530-539 http://www.itl.nist.gov/div898/winds/pdf_files/b02030.pdf (last accessed Sept. 11, 2013).

Sangchuwong, P., Yamada, H., and Katsuchi, H. (2011). "Study on turbulence effects on flow patterns around rectangular cylinders", *Proc. of BBAA 7*, Shanghai, China.

Sangchuwang, P., Yamada, H., and Katsuchi, H. (2013), "Study in turbulence effects on

flow fields around sharp-edged bluff bodies", *J. Struct. Eng.*, 59A, 627-636.

Simiu, E., Bitsuamlak, G., Gan Chowdhury, A., Li, R., Tecle, A., Yeo, D. (2011). "Testing of residential homes under wind loads", *ASCE Natural Hazards Review Journal*, 12(4), 166-170.

Subramanian C., Pinelli, J.-P., Kostanic I. and Lapilli, G. (2012). "Analysis and Characterization of hurricane winds", *J. Eng. Mech.*, 139, 325-338.

Suresh Kumar, K. and Stathopoulos, T. (1998), "Spectral Density Functions of Wind Pressures on Various Low Building Roof Geometries", *Wind and Structures*, 1(3), 203-223.

Tecle, A., Bitsuamlak, G., Suksawang N., Gan Chowdhury, A., Fuez, S. (2013). "Ridge and field tile aerodynamics for a low-rise building: a full-scale study", *Wind and Struct.,* 16(4), 301-322.

Tieleman, H. W. (2003), "Wind tunnel simulation of wind loading on low-rise structures: a review", *J. Wind Eng. Ind. Aerod.*, 91, 1627-1649.

Yahaya, S. and Frangi, J. P. (2004), "Cup anemometer response to the wind turbulence – measurement of the horizontal wind varinance", *Annales Geophysicae*, 22, 3363-3374.

Yamada, H. and Katsuchi, H. (2008), "Wind-tunnel study on effects of small-scale turbulence on flow patterns around rectangular cylinder", *Proceeding of the 4th International Colloquium on Bluff Bodies Aerodynamics & Applications*, Italy.

Yeo, D. and Gan Chowdhury, A. (2013), "A simplified wind flow model for the estimation of aerodynamic effects on small structures", *J. Eng. Mech.*, 139, 367-375.

# CHAPTER V

## LARGE-SCALE TESTING OF RESIDENTIAL BUILDINGS AND

## REDUCTION OF ROOF UPLIFT USING PERFORATED PARAPETS

(A paper under review for the *Engineering Structures*)

# CHAPTER V

# LARGE-SCALE TESTING OF RESIDENTIAL BUILDINGS AND

# REDUCTION OF ROOF UPLIFT USING PERFORATED PARAPETS

Tuan-Chun Fu[1], Arindam Gan Chowdhury[2*], Ioannis Zisis[3], Peter Irwin[4]

[1] Doctoral Graduate Assistant, Department of Civil and Environmental Engineering, Florida International University, 10555 W. Flagler St. EC3660, Miami, FL, 33174, tfu001@fiu.edu

[2] Associate Professor, Department of Civil and Environmental Engineering, International Hurricane Research Center, Florida International University, 10555 W. Flagler St. EC3604, Miami, FL, 33174, chowdhur@fiu.edu, +1(305)3480518

[3] Assistant Professor, Department of Civil and Environmental Engineering, Florida International University, 10555 W. Flagler St. EC3655, Miami, FL, 33174, izisis@fiu.edu

[4] Wall of Wind Professor of Practice, Department of Civil and Environmental Engineering, Florida International University, 10555 W. Flagler St. EC3640, Miami, FL, 33174, peairwi@fiu.edu

* Corresponding author

## 5.1 Abstract

Building roofs are subjected to high uplift forces during strong wind events such as hurricanes which often lead to severe roofing component damage as well as water intrusion. It is therefore important to estimate peak uplift pressures (suctions) for design purposes and develop mitigation techniques to enhance roof performance and reduce losses. This paper presents an experimental study conducted to investigate the uplift pressures on two two-story low-rise buildings. The experiments were carried out in both an atmospheric boundary layer (ABL) wind tunnel using a model scale 1:50 and the open-jet 12-Fan Wall-of-Wind (WOW) facility using a model scale of 1:6. A flow with the full ABL turbulence spectrum was simulated in the wind tunnel. In the WOW the turbulence spectrum's low frequency content was weaker than in ABL flows, while the high frequency content correctly reproduced its ABL counterpart; therefore the non-

dimensionalized integral turbulence length was smaller than in the ABL. Mean and peak pressure coefficients obtained from both facilities were compared and the results showed reasonable agreement, thus validating the pressures obtained in the WOW. The large-scale models were then retrofitted with discontinuous perforated parapets at critical locations and tested in the WOW to assess the parapets' effectiveness in mitigating the roof pressures. Pressure comparisons showed that peak pressure coefficients in zones with high suctions were significantly lower in models with parapets. This demonstrates the potential of such aerodynamic add-on devices to reduce uplift forces. In addition, the validation of the WOW simulation methodology enables testing of larger models than those that may be used in laboratories with simulated ABL flows, as long as the high frequency turbulence spectrum is correctly modeled. This allows testing at larger scales, with higher Reynolds numbers and better spatial resolution of the pressure taps, incorporation of architectural details, and assessment of aerodynamic add-on devices to reduce wind effects.

## 5.2 Introduction

Windstorm insured losses are estimated about 70% of the total amount due to natural catastrophes (Holmes 2007). About 39% of the United States population lives in the counties directly on the shorelines prone to hurricanes (National Oceanic and Atmospheric Administration (NOAA. 2013). Although wind forces may not damage the building structure significantly, they inflict severe effects on the building envelope, especially the roofing components on low-rise buildings (MDC-BCCO, 2006). Many wind-induced damages are due to strong corner suction on the roofs and associated high local wind velocities. Therefore, shingles, tiles, or pavers placed on roofs are vulnerable to being dislodged and become wind-borne debris (Aly et al. 2012, Tecle et al. 2013). In addition,

losing roofing components could lead to rain water intrusion and losses to interior appliances and building contents (Bitsuamlak et al. 2009). Therefore, the need to reduce roof damages due to wind effects has recently become one of the most important challenges for designers, building component manufacturers, and building code officials. Understanding the relationship between strong winds and wind-induced uplift on roofs is required for developing passive mitigation devices that reduce suctions.

Wind tunnel research has been conducted on the modification of roof aerodynamics by using parapets and passive aerodynamic edges shapes that suppress vortex generation. To eliminate the straight sharp edges that create the vortices, methods for disturbing the vortices using different roof mounted edges or screens have been studied by Cochran and English (1997) and Lin and Surry (1993). Also Baskaran and Stathopoulos (1988) showed that the thickness of roof parapets does not affect the uplift pressure on the roof, whereas the height of the parapets does so. Stathopoulos et al. (1999) conducted wind tunnel and field studies on the effects of parapets on flat roofs by measuring the mean pressure coefficients on roof corners. They concluded that high parapets generally reduce the high suction on roof corners while low parapets may increase the roof suction at the edges and corners, and showed that only for ratios of parapet height to building maximum horizontal dimension ($h_p$ /$L$) between 0.01 and 0.02 did the mean suctions increase significantly for corner taps. Surry and Lin (1995) used various parapet configurations on a 1:50 Texas Tech University (TTU) building model, including saw-tooth partial parapets, semi-cylindrical parapets, solid and porous roof corner splitters and isolated porous parapets. The ratio of the height of the parapets to the roof eave height varied between 0.064 and 0.192. The isolated porous parapets resulted in the highest reduction in suc-

tions near the roof corner. Kopp et al. (2005) reported the effects of various parapets, including spoilers, in decreasing area-averaged loads associated with corner vortices. The ratio of parapet height to total building height ($h_p/(H_{eave} + h_p)$) was 0.17. The spoilers and porous continuous parapets performed best and maximum reductions of peak pressure coefficients near roof corner were 44% and 56%, respectively.

Most studies on roof wind load mitigation have been based on small scale models (between 1:50 and 1:200) for which scaling limitations make it difficult to replicate detailed flow phenomena occurring around individual components on the building envelope. Large-scale testing is especially advantageous for assessing the effectiveness of aerodynamic devices in roof suction mitigation for at least two reasons: (1) some devices involve curved surfaces with significant Reynolds number effects that can only be captured reliably in large-scale tests under high wind speeds, (2) some devices contain perforations of critical functionality that are too small in size to be reproduced in small scale tests. For this reason large- and full-scale tests have been performed recently for roof suction mitigation. Suaris and Irwin (2010) studied the effect of porous parapets on a 1:20 model of a single story 3:12 gable roof tested in an atmospheric boundary layer (ABL) wind tunnel. For individual pressure taps at the roof corner zones, the highest reduction in peak pressure coefficients was about 60% after installing the parapets. Blessing et al. (2009) performed both roof gravel scour testing and pressure testing in a 6-fan Wall of Wind (WOW), and determined that approximately 55% reduction in area-average peak uplift pressure can be achieved by installing curved-shaped aerodynamic devices on flat roof edges. However, for the 6-fan system the higher frequency spectral ordinates were higher than those in the atmosphere, and the flow was deemed appropriate only for com-

parisons of peak uplift pressures with and without modified aerodynamic edge shapes. More recently, Bitsuamlak et al. (2013) also used the 6-fan WOW to investigate the effectiveness of simple architectural elements including trellis, gable end and ridgeline extensions, and wall extensions for the reduction of roof and wall corner suctions. The highest reductions recorded for individual taps at the gable end corners and the roof ridge were 65% and 60%, respectively.

However, large-scale models testing is often constrained by the difficulty of simulating adequately the low-frequency content of the turbulence spectrum and the integral length scale which, in flows with weak low-frequency content, is considerably smaller than its scaled ABL counterpart. For this reason, large-scale testing may appear to be inconsistent with wind testing provisions specified by ASCE 7-10 (2010), which require, among other criteria, "*The relevant macro- (integral) length and micro-length scales of the longitudinal component of atmospheric turbulence are modeled to approximately the same scale as that used to model the building or structure.*" The recently published ASCE 49-12 Standard for wind tunnel testing acknowledges that there will be situations where it is desirable, for scaling reasons, to relax the requirement to scale the macro-(integral) length scale as long as appropriate analysis methods are used to account for missing low frequency turbulence. However, no reference to literature containing such methods is provided in the ASCE 49-12 Standard or the ASCE 7-10 Standard. A *partial turbulence simulation* approach has been developed that will fill this gap. This approach is freed from the integral length constraint stated above and can be used to perform aerodynamic testing on large-scale building models and mitigation devices in wind tunnels and WOW-like facilities as long as the blockage is acceptable (Aly et al. 2011). This pa-

110

per presents comparisons of pressure coefficients obtained by using (1) the partial simulation approach in the FIU 12-fan WOW facility on 1:6 models of prototype two-story residential buildings, and (2) wind tunnel measurements on 1:50 models of those prototype buildings in ABL flows. The comparisons validated the efficacy of the partial simulation approach for large-scale aerodynamic testing purposes. Following this validation the 1:6 models were retrofitted with discontinuous perforated parapets at critical roof locations and tested in the WOW to assess their effectiveness in attenuating roof pressures.

Section 2 describes the FIU 12-fan WOW facility. Section 3 provides details on the WOW partial and wind tunnel ABL simulation and shows comparisons of model roof pressures measured in the WOW and ABL wind tunnel. Section 4 shows the results of WOW measurements for using discontinuous perforated parapets for mitigating the uplift pressures effectively to reduce the risk of wind induced damages. Finally, section 5 presents the summary and conclusions.

### 5.3 12-Fan Wall of Wind (WOW) Facility

Most wind tunnel tests are performed for high-rise buildings, large structures such as long span roofs, and bridges; however, common low-rise residential or commercial buildings are the ones that are most vulnerable to strong winds (Jones et al., 1995). To address the vulnerability of such low rise structures, several large-scale or full-scale wind testing facilities are being developed: "Insurance Research Lab for Better Homes" (Kopp et al. 2010); the Wind Engineering, Energy and Environment Dome at the University of Western Ontario (Natarajan and Hangan 2010); the wind generator at the University of Florida (Mensah et al. 2011); the facility of the Institute of Business and Home Safety (Liu et al. 2011). Moreover, a large-scale 12-fan Wall of Wind (WOW) testing facility at

Florida International University (FIU) has been developed to conduct large-scale testing of low-rise buildings for improving their design and developing mitigation techniques to reduce wind damage. Figure 1 shows the schematic for the 12-fan WOW design. Figure 2 shows the intake and exit sides of the WOW. The 12 fans are mounted on a steel frame and arranged in a two-row by six-column pattern to accommodate a wind field corresponding to a test section of 6 m wide and 4.3 m high. Each fan has a maximum flow rate of 113.3 cubic meter/second (240,000 cubic foot/minute (cfm)) with a total pressure head of 3736 Pa (15 in. $H_2O$). Each fan is driven by a motor that has a power rating of 522 kilowatt (700hp). The fan rotation speeds are controlled by variable frequency drives (VFD). A contraction section helps attain uniform flow field with high wind velocity while a set of vertical flow directing vanes at the exit of the contraction section guides the air flow in the longitudinal direction. The contraction section boosts the mean wind speed up to about 72 m/s at about 2.6 m above the ground. The open jet test section allows large-scale aerodynamic testing for low-rise buildings and even full-scale accessories (e.g., solar panels, roof top equipment) on low-rise structures. However, such large-scale model testing is often constrained by the difficulty of simulating adequately the low-frequency content of the turbulence spectrum and, in particular, the integral length scale parameter (ASCE 7-10, 2010). A partial turbulence simulation method is adopted for the WOW to circumvent this constraint.
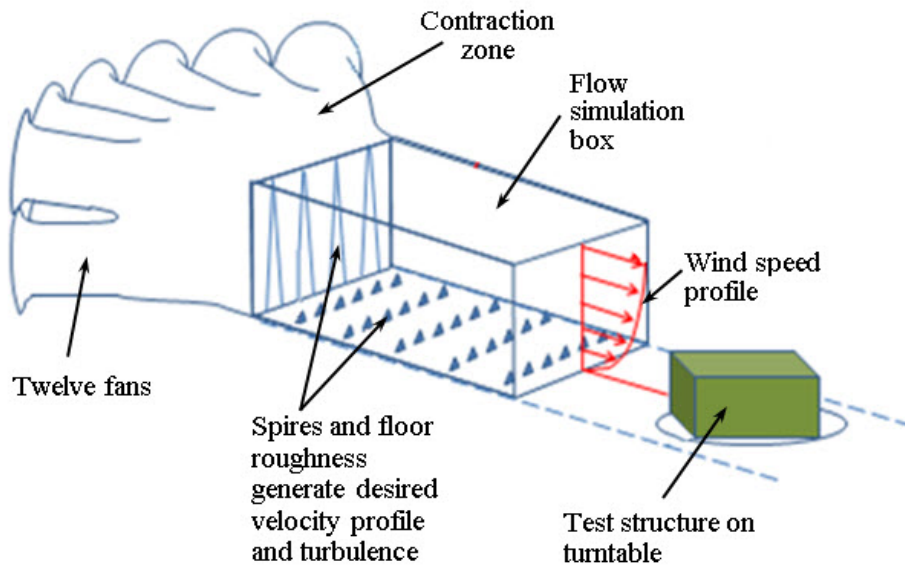
Figure 1. Schematic Diagram of 12-fan Wall of Wind (WOW)
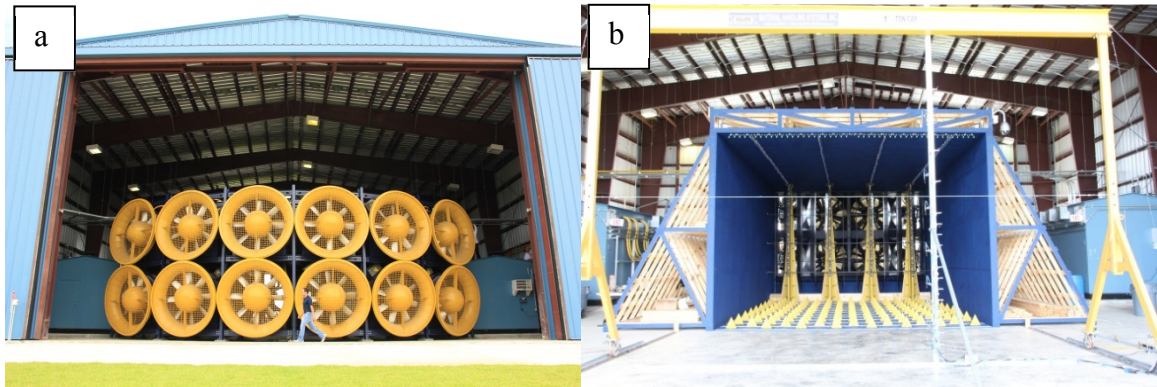


Figure 2. a. WOW Intake Side, b. WOW Exit Side with Flow Management Devices

The findings of Melbourne (1980), Saathoff and Melbourne (1997), Suresh and Stathopoulos (1998), (Tieleman et al. 1998), Tieleman (2003), Richards et al. (2007), Banks (2011), Yamada and Katsuchi (2008), Irwin (2009), Kopp and Banks (2013), and others established that the high frequency or small scale turbulence generation is important for aerodynamic testing of low-rise structures. The small scale turbulence affects critical aerodynamic phenomena causing high suctions, such as (1) flow separation from

sharp edges creating shear layers and separation bubbles, and (2) conical vortices originating at corners from cornering winds. For the WOW, a partial turbulence generation method was developed to ensure that the high frequency portion of the WOW turbulence spectrum matches its counterpart in the atmospheric boundary layer (ABL) spectrum, whereas the low frequency content is much lower in the WOW than in the ABL. To ensure that the 12-fan WOW is capable of replicating the ABL vertical mean wind speed profile and the high frequency portion of the ABL spectrum, flow management devices, including a 9.75m long box, four triangular spires, and floor roughness elements, were designed and installed. The optimized dimensions of the flow management devices were designed using the procedure described by Irwin (1981) supplemented by trial-and-error refinements in a 1:15 small-scale 12-Fan WOW (Aly et al., 2011).

The low frequency spectrum is a measure of the large scale turbulence components that can be depicted by slowly fluctuating gusts. Unlike small-scale turbulence, large-scale turbulence does not affect significantly local vortex formation or flow reattachment, except insofar as it augments the sustained wind speed. For practical purposes, therefore, the atmospheric flow, containing as it does slowly varying flow fluctuations due to large-scale turbulence, can be represented approximately by a WOW flow with weak or no low-frequency fluctuations, provided that the respective sustained speeds are approximately equal. Thus for the WOW simulation and testing of large-scale models, it was proposed to compensate for the missing low-frequency content by increasing the mean wind speed $U$ by an incremental wind speed $\Delta U$ (Simiu et al., 2011, Yeo and Gan Chowdhury, 2013). The mean wind speed increment $\Delta U$ may be viewed as a flow fluctuation with zero frequency and perfect spatial coherence and, therefore, as a reasonable

114

approximation of the missing low-frequency fluctuations in the spectrum (for more details see Fu et al. 2012, Yeo and Gan Chowdhury, 2013). These assumptions are valid for small structures (such as single residential buildings and their components) for which, unlike for high-rise and large low-rise buildings, the coherence of the oncoming flow turbulence is close to unity over distances comparable to the dimensions of the structure. This approach is also hypothesized to be appropriate for testing on local aerodynamic effects, such as local pressures on roof components and cladding, over which high spatial coherence of low frequency turbulence is expected. To validate the WOW partial turbulence simulation approach (i.e., the approach in which only the high frequency part of the ABL turbulent fluctuations spectrum is replicated), a series of tests were conducted in an ABL wind tunnel and in the 12-fan WOW facility. The models used in both studies included two two-story low-rise buildings with different roof configurations. The flow simulation and pressure comparisons results are presented in the following section.

### 5.4 12-Fan WOW and ABL Wind Tunnel Results Comparison

### 5.4.1    Flow Simulation Results Comparison

Flow simulations in both an ABL wind tunnel (RWDI wind tunnel in Miramar, Florida) and the 12-Fan WOW were performed in order to validate the partial turbulence simulation methodology used in the WOW. In both facilities spires as well as floor roughness elements were used to reproduce suburban wind profiles. A rake system having Pitot tubes mounted at various heights was used for the mean wind speed measurements. The mean wind speeds at reference height (mean roof height of building models) were approximately 8.6 m/s and 16.7 m/s for wind tunnel and WOW, respectively. Figure 3a shows the target suburban terrain mean wind speed profile (with power law exponent

α ≈ 0.25) and the non-dimensional profiles for the wind tunnel and the 12-fan WOW plotted against the prototype height above ground. The prototype (full-scale) building is shown as well.

The full longitudinal turbulence spectrum was reproduced in the wind tunnel, whereas in the WOW only a partial longitudinal turbulence spectrum with weaker low frequency fluctuations was simulated. Cobra probes were used for the measurements of fluctuating wind speeds at various heights. Figure 3b shows the turbulence intensity profiles in the two facilities. Note that the turbulence intensities in the WOW simulation were lower than those in the wind tunnel. These lower turbulence intensities in the WOW were due to partial turbulence simulation (see also Richards et al. 2007, Banks 2011, Yamada and Katsuchi 2008, Irwin 2009, and Kopp and Banks 2013). This section describes the partial turbulence simulation method as developed and applied for the WOW facility. In this paper the subscripts *FS* and *PS*, used in the subsequent equations stand for "full spectrum" and "partial spectrum," respectively. Henceforth, quantities with the subscripts *m* and *p* pertain, respectively, to laboratory model (wind tunnel or WOW model) and the prototype (full-scale).
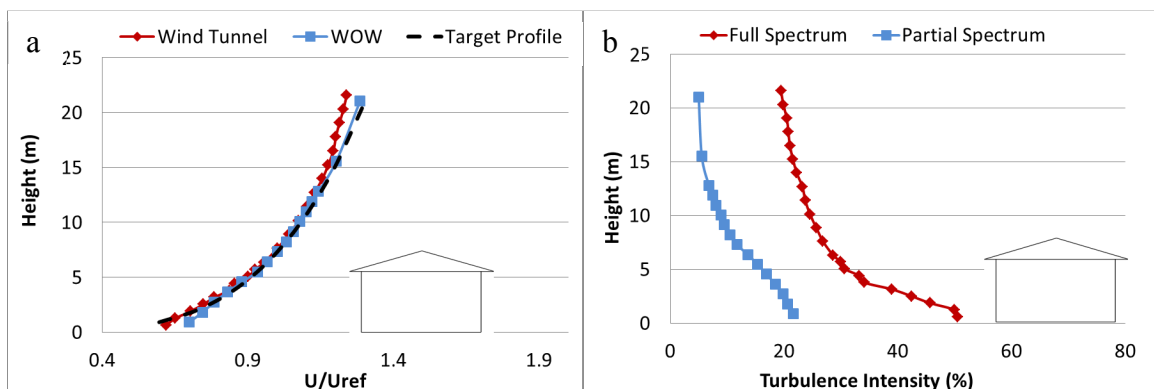
Figure 3. a. Non-Dimensional Mean Wind Profiles b. Turbulence Intensity Profiles (the y-axis represents prototype height)

A 79.5 m/sec prototype (full-scale) 3-second gust wind speed corresponding to open terrain and at 10 m above ground is considered for Miami, FL (Mean Recurrence Interval (MRI) 700 years, Risk Category II buildings and other structures; see ASCE 7-10). The corresponding mean hourly wind speed over suburban terrain and at 10 m above the ground is 35.5 m/sec. Considering the mean roof height of a prototype two-story building to be $h = 7.28$ m and using the power law exponent $\alpha \approx 0.25$, the corresponding wind speed is 32.9 m/sec at the prototype mean roof height. This wind speed is designated as $U_{FS,p}$. Thus the wind tunnel velocity scale is $\lambda_{v,W.T.} = U_{FS,m} / U_{FS,p} = 8.6/32.9 = 1:3.8$ ($U_{FS,m} = 8.6$ m/sec was measured in the wind tunnel). The model length scale being $\lambda_{l,W.T.} = 1:50$, the wind tunnel time scale was obtained as $\lambda_{t,W.T.} = 1:50/1:3.8 = 1:13$. Thus the 2 min test duration in wind tunnel was equivalent to 26 min in full scale. The WOW model length scale was $\lambda_{l,WOW} = 1:6$. To obtain the WOW velocity scale, it is necessary to determine the mean wind speed increment $\Delta U$ which compensates for the missing low-frequency fluctuations in the WOW flow spectrum. A numerical iteration procedure was developed to obtain $\Delta U$ as presented below.

We consider two prototype flows with approximately similar high-frequency spectral content but of which one is characterized by weak low frequency fluctuations (i.e., with a partial spectrum) while the other has a full-spectrum. It is hypothesized that similar peak wind speeds in these two flows result in similar peak aerodynamic effects (i.e., in similar peak pressure coefficients) for small structures. The peak wind speeds thus need to satisfy the relation:

$$U_{PS,p}{}^{pk}(z,\ T_{PS,p}) = U_{FS,p}{}^{pk}(z, T_{FS,p}) \tag{1}$$

where $U_{PS,p}{}^{pk}(z,\ T_{PS,p})$ and $U_{FS,p}{}^{pk}(z,\ T_{FS,p})$ denote the expected peak wind speeds over a time interval $T_p$ for the prototype full turbulence (ABL-like) flow and partial turbulence flow, respectively. The non-dimensional mean wind speed profile for the flow with partial spectrum matches that of the flow with full spectrum (as shown in Fig. 3a). The following relation holds for the two mean wind speeds:

$$U_{PS,p} = U_{FS,p} + \Delta U \tag{2}$$

Equation 2 is justified as follows. The rms (root mean square) of the velocity fluctuations is smaller in the partial turbulence flow than in the ABL flow. On the other hand, Eq. 1 requires that respective peaks be the same. This is only possible if the mean wind speed $U_{PS,p}$ is *larger* than $U_{FS,p}$.

By definition

$$U_{PS,p}{}^{pk}(T_{PS,p}) = U_{PS,p} + k_{uPS,p}(T_{PS,p})\ \sigma_{uPS,p} \tag{3a}$$

$$U_{FS,p}{}^{pk}(T_{FS,p}) = U_{FS,p} + k_{uFS,p}(T_{FS,p})\ \sigma_{uFS,p} \tag{3b}$$

where $k_{uPS,p}$ and $\sigma_{uPS,p}$ = peak factor and rms of the longitudinal velocity fluctuations, respectively, for the partial spectrum prototype, and $k_{uFS,p}$ and $\sigma_{u,FS,p}$ = peak factor and rms of longitudinal velocity fluctuations, respectively, for the full-spectrum prototype flow. From Eqs. 1, 2, 3a and 3b it follows that:

$$\Delta U = k_{uFS}\ \sigma_{uFS} - k_{uPS}\ \sigma_{uPS} \tag{4}$$

The expressions for the expectations of the peak factors in Eqs. 3 and 4 are

$$k_{uFS,p} \qquad (T_{FS,p}) \qquad = \qquad \sqrt{2\ln{(\gamma_{u,FS,p}T_{FS,p})}} + \frac{0.577}{\sqrt{2\ln{(\gamma_{u,FS,p}T_{FS,p})}}}$$

(5a)

$$k_{uFS,p} \quad\quad (T_{PS,p}) \quad\quad = \quad\quad \sqrt{2\ln(\gamma_{u,PS,p}T_{PS,p})} + \frac{0.577}{\sqrt{2\ln(\gamma_{u,PS,p}T_{PS,p})}}$$

(5b)

$$\gamma_{uFS,p} = \left[\frac{\int_0^{n_c} n^2 S_{FS,p}(n)dn}{\int_0^{n_c} S_{FS,p}(n)dn}\right]^{\frac{1}{2}} \tag{6a}$$

$$\gamma_{uPS,p} = \left[\frac{\int_0^{n_c} n^2 S_{PS,p}(n)dn}{\int_0^{n_c} S_{PS,p}(n)dn}\right]^{\frac{1}{2}} \tag{6b}$$

In Eqs. 6a, 6b, $n_c$ = prototype cut-off frequency, $S_{PS,p}$ *(n)* = prototype dimensional partial spectrum, and $S_{FS,p}$ *(n)* = prototype dimensional full spectrum.

The increment *ΔU* given in Eq. 2 is obtained iteratively. Initially the following are given: (i) specified ABL flow velocity $U_{FS,p}$ = 32.9 m/sec at the prototype mean roof height of *h* = 7.28 m (based on ASCE 7-10), (ii) prototype full spectrum, which can be estimated from the ABL wind tunnel full spectrum using scaling laws, that is: $S_{FS,p}(n_p)$ = $S_{FS,WT}(n_{WT})$. $[1/(\lambda^2{}_{V,WT}\ \lambda_{T,WT})]$, (iii) prototype time duration and cut-off frequency, assumed to be $T_{FS,p}$ = 26 min and $n_{c,p}$ = 12 Hz, respectively. As a first approximation we assume that for the prototype counterpart of the WOW partial turbulence flow the mean wind speed is $U_{PS,p,\ 1}$ = 1.1 $U_{FS,p}$ = 36.2 m/sec. The WOW mean wind speed at the model mean roof height $h_{WOW}$ = 1.22 m (WOW length scale $\lambda_{l,WOW}$ = 1:6) was $U_{PS\ m}$ = 16.7 m/s. Thus we get, $\lambda_{v,WOW,\ 1}$ = 1:2.2 and $\lambda_{t,WOW,\ 1}$ = 1:2.7, and the $T_{PS\ m}$ = 3 min test duration in WOW was equivalent to $T_{PS,p,1} \approx$ 8 min in full scale. The prototype counterpart of the WOW partial spectrum can be estimated as $S_{PS,p}(n_p)$ = $S_{FS,WOW}(n_{WOW})$. $[1/(\lambda^2{}_{v,WOW}\ \lambda_{t,WOW})]$. The rms can be obtained from the spectra and peak factors can be obtained using Eqs. 5 and 6. Using Eq. 4, we obtain the first approximation of $\Delta U_1$ = $k_{uFS,p}\ \sigma_{uFS,p}$ − $k_{u,PS,p,\ 1}\sigma_{uPS,p,\ 1}$ = 22.0 m/sec. Substitution in Eq. 2 yields a second approximation of $U_{PS}$

as, $U_{PS,p,2} = U_{FS,p} + \Delta U_1 = 54.9$ m/s. Using $U_{PS,p,2}$ we repeat the above procedure to obtain the second approximation of $\Delta U$, denoted by $\Delta U_2$. The procedure is repeated until the sequence $\Delta U_i$ ($i = 1, 2, \ldots$) converges. The iterations result in an estimate of $U_{PS,p}$ for which the high frequency portion of the prototype counterpart of the WOW partial spectrum should match approximately the high frequency portion of the prototype ABL full spectrum.

A MATLAB program was developed for this iterative procedure and, for the current simulation, convergence was achieved after 12 iterations giving: $\Delta U = 16.4$ m/sec, $U_{PS,p} = U_{FS,p} + \Delta U = 32.9 + 16.4 = 49.3$ m/sec, $\lambda_{v,WOW} = U_{PS,m} / U_{PS,p} = 16.7/49.3 \approx 1{:}3$, and $\lambda_{t,WOW} = 1{:}2$. Thus, the 3 min test duration in WOW represented 6 min duration in full scale. The wind tunnel and WOW scales along with the Reynolds number, turbulence intensities, and non-dimensional integral length scales corresponding to the model mean roof heights are summarized in Table 1. Note that the turbulence intensity and the non-dimensionalized integral turbulence length for the WOW partial turbulence simulation flow are significantly lower than those for the wind tunnel full turbulence simulation flow. Figures 4a show the spectra of the two flows. Using surface roughness length $z_0 = 0.3$ m (typical $z_0$ value for Exposure Category B, Table C26.7-1, ASCE 7-10) and $U_{FS,p} = 32.9$ m/sec at the prototype mean roof height of $h = 7.28$ m, the modified Kaimal spectrum was also plotted in Fig. 4a. Note that the high frequency portions of the WOW and wind tunnel spectra match satisfactorily and show good agreement with the -5/3 slope corresponding to the inertial subrange of the dimensionalized Kaimal spectrum. As noted by Melbourne (1980), this is necessary for an adequate simulation of the separated flows.

Recall that the flow simulation was based on the requirement that Eq. 1 be satisfied, that is, that the expected peak wind speed in partial simulation be equal to the expected peak wind speed in the ABL flow. At the end of the iteration the peak wind speeds in the two flows matched closely ($U_{PS,p}{}^{pk}(T_{PS}) = U_{FS,p}{}^{pk}(T_{FS}) = 70.4$ m/s). Figure 4b shows the wind tunnel and WOW wind speed time histories scaled to the prototype wind speeds and plotted for duration of 6 min. Note that the peak wind speed for the partial turbulence flow matches closely the peak wind speed in the full turbulence ABL flow, satisfying Eq. 1.

Table 1. Summary of Wind Tunnel and WOW Parameters

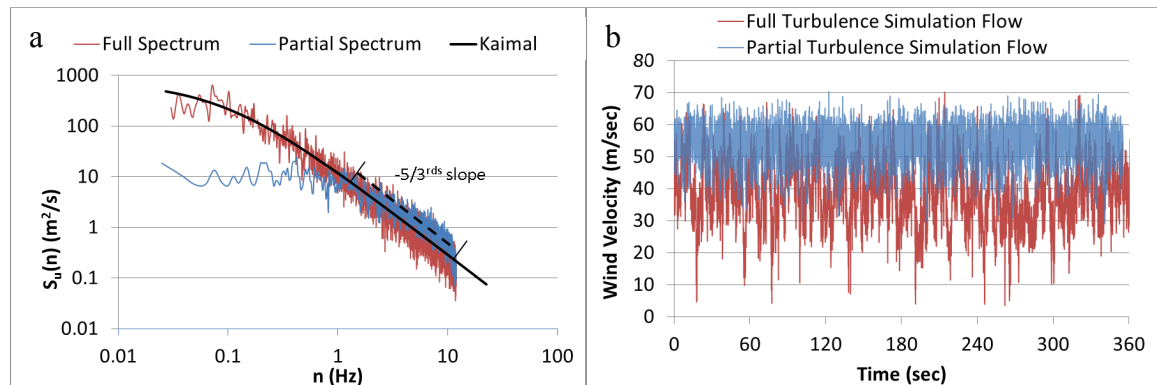| Facility | $\lambda_l$ | $\lambda_v$ | $\lambda_t$ | $\lambda_n$ | $U_{mean}$ (m/sec) | Re | T.I. (%) | ${}^{x}L_u/h$ (m) |
|---|---|---|---|---|---|---|---|---|
| Wind Tunnel | 1:50 | 1:4 | 1:12.5 | 1:0.08 | 8.6 | $8.4 \times 10^4$ | 26.8 | 2.60 |
| WOW | 1:6 | 1:3 | 1:2 | 1:0.5 | 16.7 | $1.34 \times 10^6$ | 11.7 | 0.48 |



Figure 4. a. Comparison of Full and Partial Turbulence Spectra, b. Comparison of Wind Speed Time Histories of Prototype Flows.

## 5.4.2  Pressure Coefficient Results Comparison

Two two-story residential buildings models, one with 3:12 gable roof and the other with 3:12 hip roof, were tested in each of the ABL wind tunnel and WOW facilities. The prototype builing dimensions were: length = 13.7 m, width = 9.2 m, eave height = 6.7 m, mean roof height = 7.3 m, roof overhang on all sides = 0.6 m. Scaling information for the wind tunnel and the WOW can be found in Table 1. The objective of the testing was to compare pressure coefficients obtained in the two facilities to validate the hypothesis stated earlier that two flows with similar peak wind speeds and with matching high frequency portions of the spectrum will induce similar wind effects (e.g., mean and peak pressure coefficients).

Figure 5 shows the pressure tap layout for the models' roofs and the wind direction (WD) convention. The pressure taps were mostly located near roof corners, edges, ridges, and sloped hip lines where high suctions are anticipated. Based on model symmetry, the wind directions tested were WD = 0°, 45°, and 90° and the test durations were 2 min and 3 min for wind tunnel and WOW, respectively. Scanivalve pressure acquisition systems were used in both facilities to capture pressure time history data with a 512 Hz sampling rate. PVC tubes with 1.22 m length and 1.34 mm diameter were used to connect pressure taps installed on the roof to the Scanivalve pressure scanner. In order to obtain accurate peak pressure coefficients, a transfer function designed for the tubing system was applied to raw data captured from the Scanivalve pressure (Irwin 1979). Considering the prototype cut-off frequency for wind induced pressures to be 12 Hz, digital low-pass filtering at 156 Hz and 24 Hz were applied for the wind tunnel and WOW pressure data,

a                                              b

122

respectively (Note: frequency scales were $\lambda_{n,W.T.} = 13:1$ and $\lambda_{n,WOW} = 2:1$).
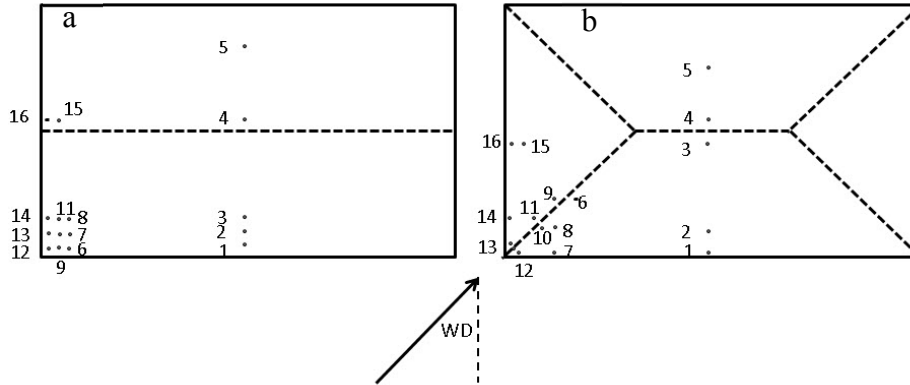


Figure 5. Pressure Tap Numbering and Wind Direction (WD): a. Gable Roof Building Model, b. Hip Roof Building Model

The mean pressure coefficients are defined as follows:

$$C_{p\,mean} = \frac{p_{mean}}{\frac{1}{2}\rho U_{mean}^2} \tag{7}$$

where $p_{mean}$ denotes the mean pressure, $\rho$ is the air density, and $U_{mean}$ is the mean wind velocity at the model mean roof height. Peak pressure coefficients are obtained using the equation

$$C_{p\,peak} = \frac{p_{peak}}{\frac{1}{2}\rho U_{3s}^2} \tag{8a}$$

where $p_{peak}$ is the estimated peak pressure, obtained from the pressure time history $p(t)$ using Sadek and Simiu (2002) method and 95% fractile, and $U_{3s}$ is the peak 3-s (prototype averaging time) gust at the model mean roof height. Area averaged peak pressure coefficients were calculated using tributary areas of the pressure taps using the equation

$$C_{p\,avg\,peak} = \frac{\sum p_i A_i / \sum A_i}{\frac{1}{2}\rho U_{3s}^2} \tag{8b}$$

123

where $p_i$ and $A_i$ denote the pressure data and tributary area for tap $i$, respectively. Instantaneous area averaging of the pressures was performed for all relevant taps using the pressure data supported by interpolation using MATLAB program and then area averaged peak pressure coefficients were obtained using Eq. 8b.

For the pressure coefficients corresponding to the wind tunnel full spectrum flow, we considered $U_{mean} = U_{FS,m} = 8.6$ m/s and $U_{3s} = U_{FS,m\_3s} = 13.1$ m/s; the latter was obtained using the time scale $\lambda_{t,W.T.} = 1{:}13$, meaning that 512 Hz x 3/13 sec $\approx$ 118 data points were required for its estimation. For the pressure coefficients corresponding to the WOW partial spectrum flow, $U_{mean} = U_{PS,m} = 16.7$ m/s and $U_{3s} = U_{PS,m\_3s} = 17.9$ m/s; the latter was obtained using $\lambda_{t,WOW} = 1{:}2$, meaning that 512 Hz x 3/2 sec = 768 data points were used for $U_{3s}$. The peak value of $U_{3s}$ was obtained by performing moving averages in both cases. Since the test durations in the wind tunnel and WOW were 2 min and 3 min respectively, the corresponding prototype test durations were 26 min and 6 min respectively. For peak pressure estimates, a prototype duration of 26 min was assumed and thus the duration ratios applied for the Sadek and Simiu method were $K = 1$ and $K = 26/6 \approx 4$ for the wind tunnel and WOW, respectively.

### 5.4.2.1 Pressure Coefficient Comparisons for Gable Roof Building Models

Figure 6 shows the 3:12 gable roof building models tested in wind tunnel and WOW, respectively. Figures 7 to 9 show the $C_{p\,mean}$ and $C_{p\,peak}$ results from the wind tunnel (abbreviated as W.T. in the plots) and WOW. For all three wind directions, the $C_{p\,mean}$ values for most of the taps matched well between the two facilities. For a few taps, such as close-to-ridge tap 15 for WD = 0° and corner tap 9 for WD = 90°, the $C_{p\,mean}$ values were higher in the WOW testing. For WD = 0°, although reasonable agreement for $C_{p\,peak}$

values was found between the wind tunnel and WOW for the corner taps 6, 9, and 12, the

WOW $C_{p\,peak}$ values were higher by about 22% to 33% for the leading edge taps 1 to 3.

Very good agreement for the $C_{p\,peak}$ values was achieved for most taps including those at

the windward corner for WD = 45° and 90°. For few taps near the corner and the gable

end ridge areas, such as taps 9 and 16 for WD = 45° and tap 15 for WD = 90°, the $C_{p\,peak}$

values were higher in magnitude in the WOW.
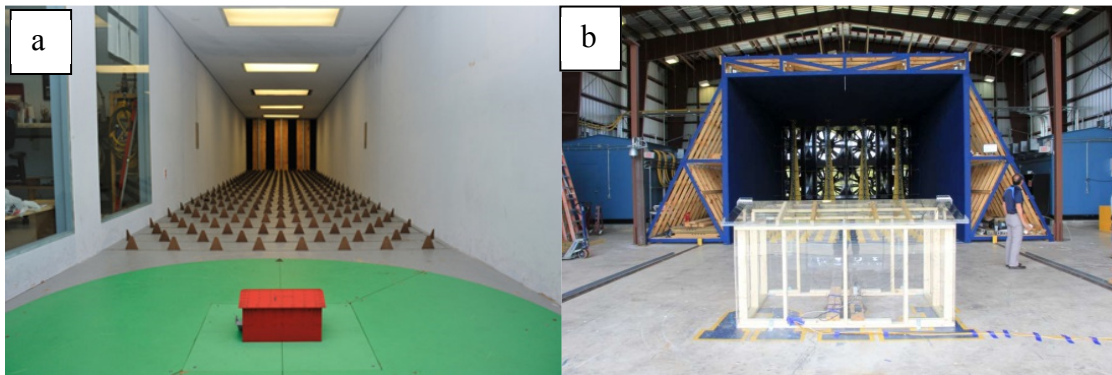


Figure 6. a. 1:50 Gable Roof Building Model Tested in Wind Tunnel, b. 1:6 Gable Roof
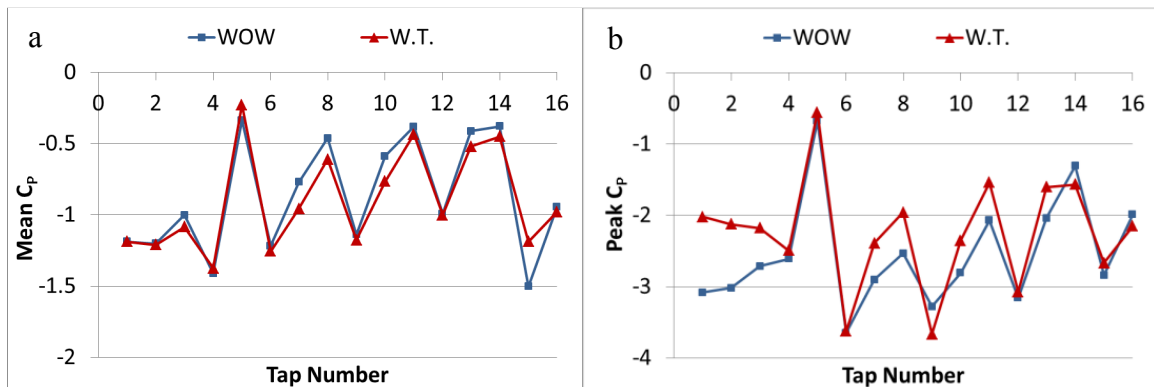
Building Model Tested in WOW



Figure 7. Comparisons of Wind Tunnel and WOW $C_p$ Values for Gable Roof Model for

WD = 0°: a. $C_{p\,mean}$ Comparison, b. $C_{p\,peak}$ Comparison
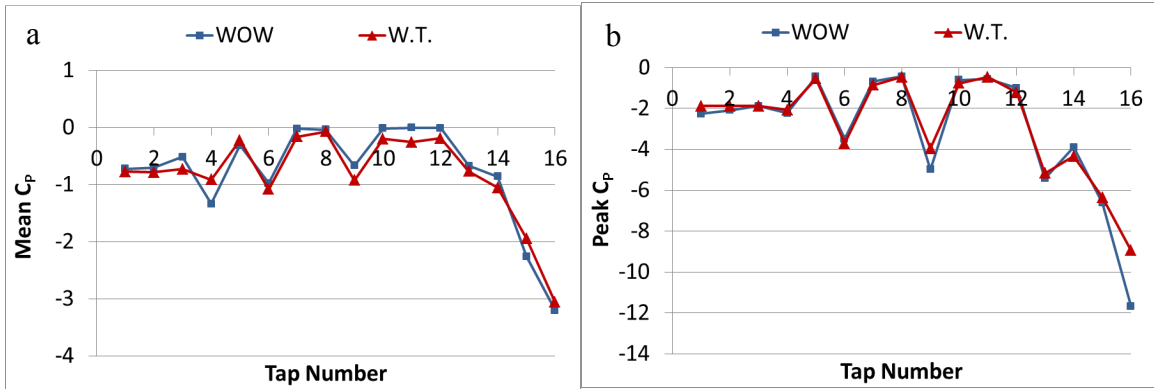
Figure 8. Comparisons of Wind Tunnel and WOW $C_p$ Values for Gable Roof Model for WD = 45°: a. $C_{p\,mean}$ Comparison, b. $C_{p\,peak}$ Comparison
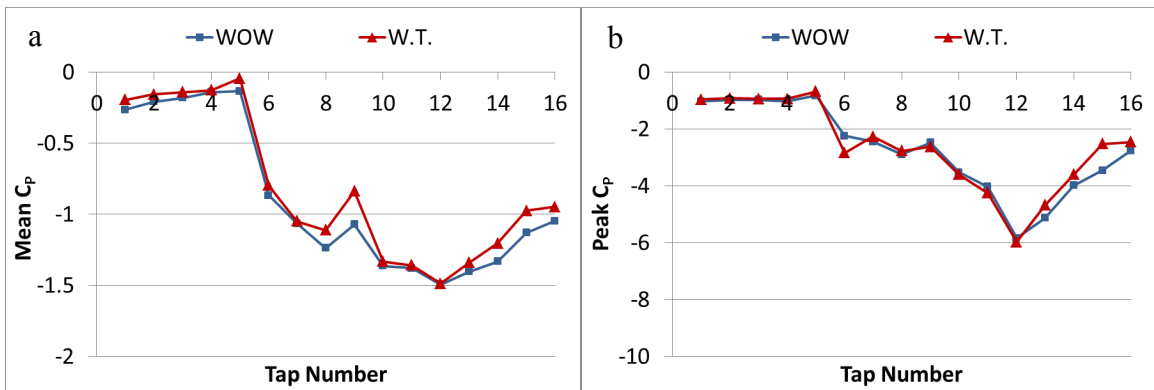


Figure 9. Comparisons of Wind Tunnel and WOW $C_p$ Values for Gable Roof Model for WD = 90°: a. $C_{p\,mean}$ Comparison, b. $C_{p\,peak}$ Comparison

**5.4.2.2 Pressure Coefficient Comparisons of Hip Roof Building**

Figure 10 shows the 3:12 hip roof building models tested in the wind tunnel and WOW, respectively. Figures 11 to 13 show the comparative results of $C_{p\,mean}$ and $C_{p\,peak}$ for WD = 0°, 45°, and 90°. For all WDs, the trends of the $C_{p\,mean}$ and $C_{p\,peak}$ obtained in the two facilities compared well. For WD = 0°, there was very good agreement between the two facilities, except that the WOW estimates for $C_{p\,peak}$ values for windward leading edge taps 1 and 2 were about 10% higher in magnitude compared to the wind tunnel val-

ues. This was similar to the gable roof case for which WOW produced higher peak pressure coefficients for the leading edge taps. For WD = 45°, most of the values were in agreement except for taps 4, 12, and 14. The highest percentage difference was obtained for tap 12 located at the windward corner near the sloped ridge for which the $C_{p\,peak}$ values were -5.0 and -6.5 for the wind tunnel and WOW, respectively. This indicates that the peak suction coefficient in WOW was 23% higher than the wind tunnel value. For the WD = 90°, the $C_{p\,mean}$ values matched well between the two facilities while the $C_{p\,peak}$ values matched better for the taps subjected to stronger suctions such as taps 12 and 13 near the windward corner of the sloped ridge. A difference of about 14% was obtained for tap 14 in which case the wind tunnel estimated value was higher in magnitude.
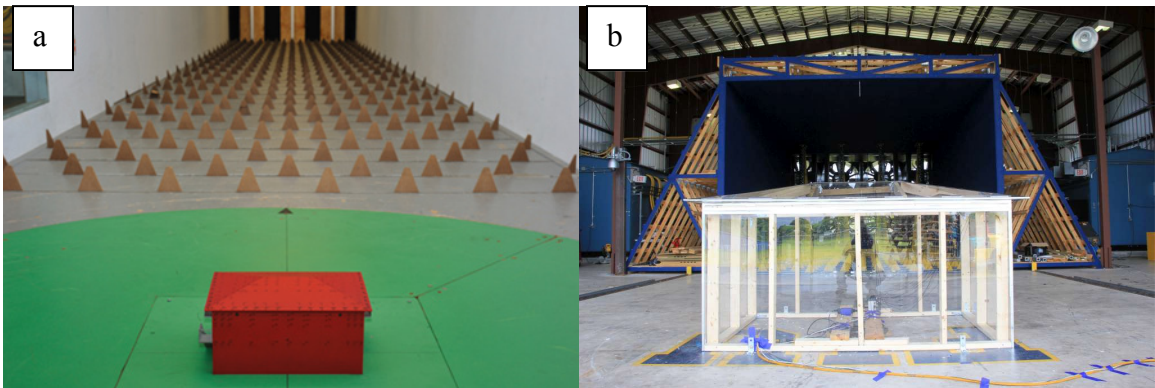


Figure 10. a. 1:50 Hip Roof Building Model Tested in Wind Tunnel, b. 1:6 Hip Roof Building Model Tested in WOW
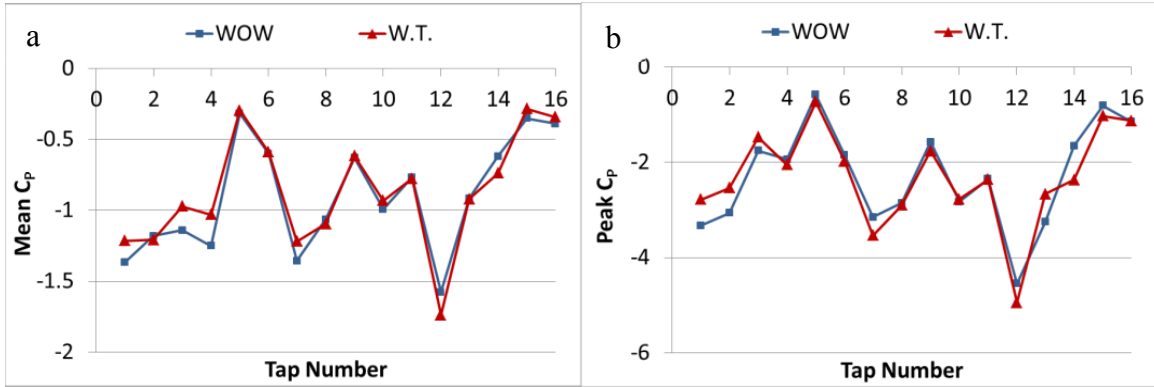
Figure 11. Comparison of Wind Tunnel and WOW $C_p$ Values for Hip Roof Model for WD = 0°: a. $C_{p\,mean}$ Comparison, b. $C_{p\,peak}$ Comparison



Figure 12. Comparison of Wind Tunnel and WOW $C_p$ Values for Hip Roof Model for WD = 45°: a. $C_{p\,mean}$ Comparison, b. $C_{p\,peak}$ Comparison



Figure 13. Comparison of Wind Tunnel and WOW $C_p$ Values for Hip Roof Model for WD = 90°: a. $C_{p\,mean}$ Comparison, b. $C_{p\,peak}$ Comparison
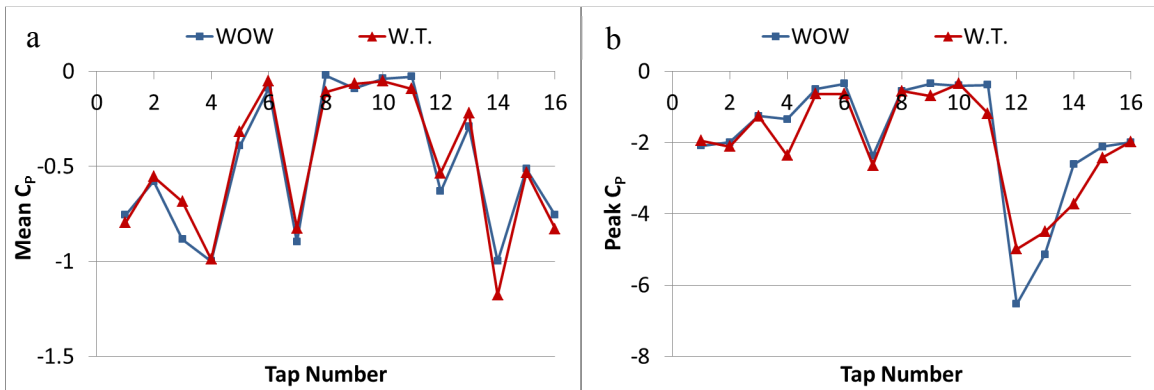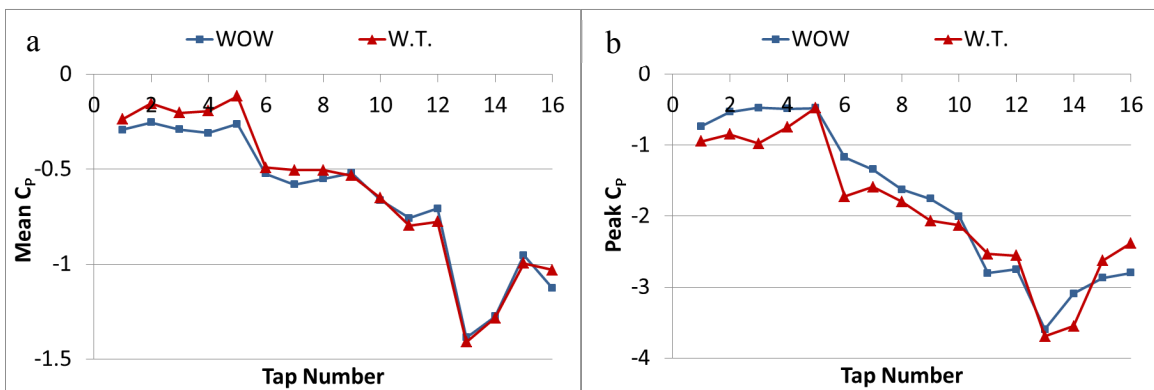
**5.4.2.3 Summary of Wind Tunnel and WOW Results Comparison**

Pressure coefficients obtained using the two facilities were in reasonable agreement for most cases where high suctions were experienced. This validated the efficacy of partial turbulnece flow simulation to induce realistic mean and peak pressures on low-rise buildings with dimensions not exceeding those of typical residential homes. For some critical locations, where roofing components are often damaged due to high suctions during windstorms, such as the roof leading edge (for WD = 0°), gable end ridge (for WD = 45°), and windward corner near sloped hip (for WD = 45°), the WOW estimated peak pressure coefficients were higher in magnitude than their wind tunnel counterparts. In the literature it was hypothesized that some of these differences can be due to Reynolds number (Re) effect, as suggested for Silsoe Building by Hoxey et al. (1998) and Texas Tech Building by Cheung et al. (1997). Additional research will be performed in future to closely investigate Re effects by testing models under a wide range of wind speeds in the WOW.

**5.5 Discontinuous Perforated Parapets for Mitigating Roof Negative Pressures**

**5.5.1   Test Models**

After validating the partial turbulence flow simulation methodology for testing large-scale models, WOW experimentation was performed to study the effectiveness of discontinuous perforated parapets in alleviating high suctions (in magnitude) at critical locations on the roof of low-rise buildings. The 1:6 large-scale models of the two story gable and hip buildings with 3:12 roof slope were tested with and without parapets. The large scale modeling allowed accurate fabrication and installation of 33% porous discontinuous parapets. For the gable roof building model the parapets were installed close to

four roof corners and also at the two gable end ridge intersections (see Fig. 14). For the hip roof building model the parapets were installed close to four roof corners near the sloped ridge and eave intersections (see Fig. 15). The length of each parapet was 15.2 cm, that is, 10% of the shorter horizontal dimension of the test building as was proposed by Suaris and Irwin (2010). The height of the parapet was 3.8 cm, thus its ratio to the roof eave height of the building was about $h_p/H_{eave} = 0.034$. In this study, a shorter parapet height ratio was used than those used in past studies. This was done to facilitate installation and lower the cost of construction of parapets on prototype buildings. All the tests were conducted in the 12-Fan WOW facility using the partial turbulence simulation technique. Each building model was tested for seven wind directions -- WD = 0° to 90°, with 15° increments. The duration of each test was 3 min and pressure data collection method was similar to that described in Section 5.4.2.
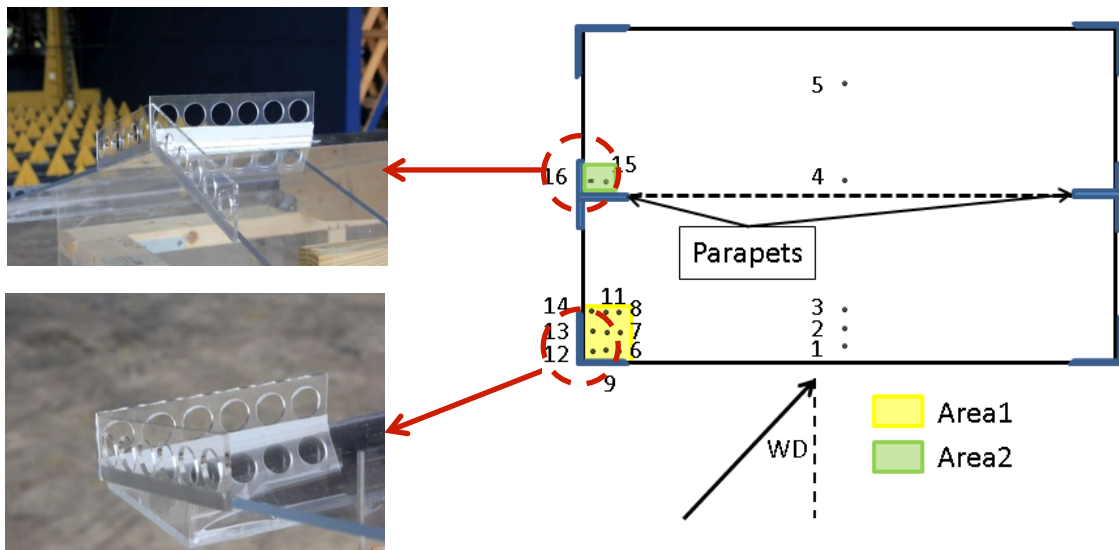


Figure 14. Discontinuous Perforated Parapets Installed on Gable Roof Building Model
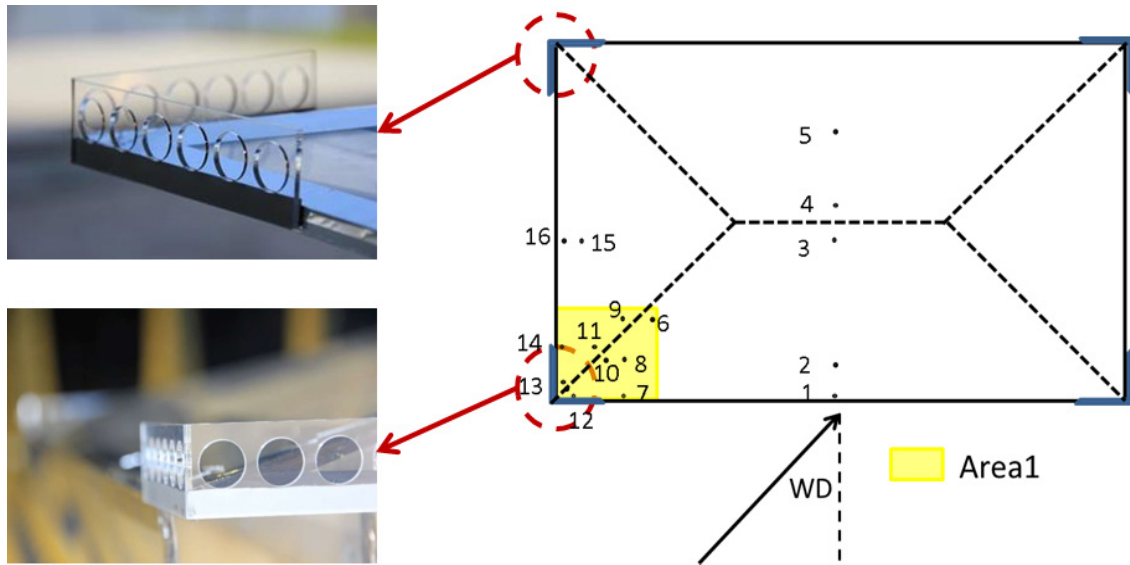
130

Figure 15. Discontinuous Perforated Parapets Installed on Hip Roof Building Model

## 5.5.2 Results for Gable Roof Building Model

Figures 16 to 22 show the comparisons of mean ($C_{p\,mean}$) and peak ($C_{p\,peak}$) pressure coefficients without and with the discontinuous perforated parapets for the gable roof model. The results show the efficacy of the parapets in significantly reducing the uplift pressures near the roof corners and gable end ridge intersections. The highest reductions in $C_{p\,mean}$ values were noted for gable end ridge tap 15 for WD = 0° (~33% reduction, see Fig. 16a) and roof corner tap 13 for WD = 60° (~60% reduction, see Fig. 20a). The highest reductions in $C_{p\,peak}$ values were noted for several taps at critical locations with high suctions, for example, edge tap 6 for WD = 15° (~40%, see Fig. 16b), gable end ridge tap 16 for WD = 45° (~72% reduction, see Fig. 19b), and corner tap 13 for WD = 60° (~55% reduction, see Fig. 20b). In the work performed by Suaris and Irwin (2010), the highest reduction in peak pressure coefficients was about 60% while using perforated parapets of similar configurations as used in this study.

The reductions in area-averaged peak pressure coefficients were estimated for Area 1 (corner area with taps 6 to 14) and Area 2 (gable end ridge intersection area with taps 15 and 16) (see Fig. 14 for Area 1 and Area 2). Significant reductions in area averaged peak pressures were obtained, e.g.: 20% reduction for Area 1 for WD = 45°; 48% and 31% reductions for Area 2 for WD = 45° and 90°, respectively. Figure 23 compares the without- and with-parapet cases by showing the instantaneous pressure coefficient surfaces for Area 1 for WD = 45° for the instant of time when the peak area-average uplift pressure attained the highest magnitude in each case. In Fig. 23, three-dimensional contours are plotted to visualize the spatial distributions of recorded instantaneous pressure coefficients of 9 taps close to roof corner region (Area 1) without- and with- parapet cases for WD = 45°. The contours show instantaneous pressure coefficients $C_p = \frac{p(t)}{\frac{1}{2}\rho U_{3s}^2}$ corresponding to time $t$ when the area-averaged peak pressure coefficient reached the highest magnitude (largest suctions occurred at $t$ = 90.3 s and 31.0 s for without- and with-parapet cases, respectively). The without-parapet contour (Fig. 23b) shows that the worst uplift pressures occurred at taps 13 and 14 located close to the roof edge in a region susceptible to strong conical vortices generated for cornering winds at WD = 45°. Significant reductions of suction pressures were observed on taps 13 and 14 after the discontinuous perforated parapets were installed (see Fig. 23c). The overall results demonstrated that the extreme uplift pressures were alleviated by installing discontinuous perforated parapets near critical roof locations where damage initiation commonly occurs during severe windstorms. The discontinuous parapets had minimal effects on pressures on roof areas farther away from the corners and ridges. Results showed that the parapets did not

132

have any unwanted effect (such as increase in uplift magnitude) at the center taps (i.e. taps 1-5). For comparison purposes limited tests were also performed in the wind tunnel with and without the porous parapets. Figures 23d and 23e show the contours obtained from wind tunnel for Area 1 and a 20% reduction was observed which is same as the WOW result. However, for Area 2 the reductions were 25% and 10% for WD = 45° and 90°, respectively. These reductions estimated in the wind tunnel were lower than the reductions estimated in the WOW testing which were 48% and 31% for WD = 45° and 90°, respectively.
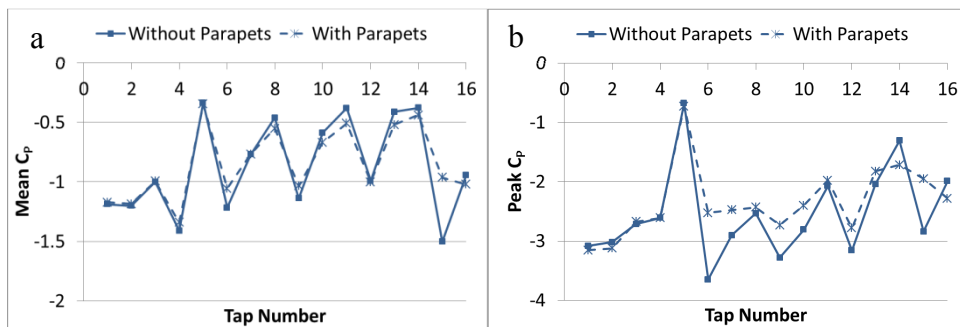


Figure 16. Comparisons of $C_p$ Values Without and With Parapets on Gable Roof Model for WD = 0°: a. $C_{p\,mean}$ Comparison, b. $C_{p\,peak}$ Comparison



Figure 17. Comparisons of $C_p$ Values Without and With Parapets on Gable Roof Model for WD = 15°:, a. $C_{p\,mean}$ Comparison, b. $C_{p\,peak}$ Comparison

Figure 18. Comparisons of $C_p$ Values Without and With Parapets on Gable Roof Model for WD = 30°: a. $C_{p\,mean}$ Comparison, b. $C_{p\,peak}$ Comparison



Figure 19. Comparisons of $C_p$ Values Without and With Parapets on Gable Roof Model for WD = 45°: a. $C_{p\,mean}$ Comparison, b. $C_{p\,peak}$ Comparison



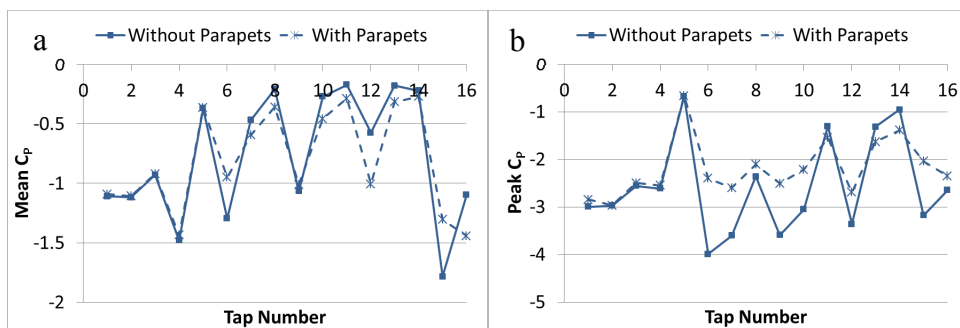Figure 20. Comparisons of $C_p$ Values Without and With Parapets on Gable Roof Model for WD =60°: a. $C_{p\,mean}$ Comparison, b. $C_{p\,peak}$ Comparison

Figure 21. Comparisons of $C_p$ Values Without and With Parapets on Gable Roof Model

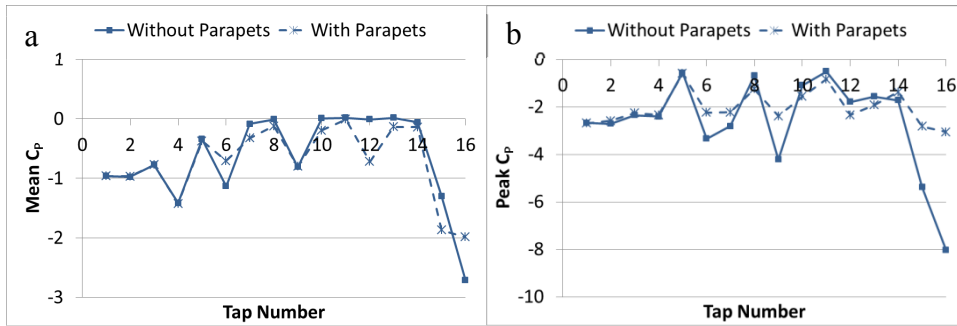for WD = 75°: a. $C_{p\,mean}$ Comparison, b. $C_{p\,peak}$ Comparison



Figure 22. Comparisons of $C_p$ Values Without and With Parapets on Gable Roof Model

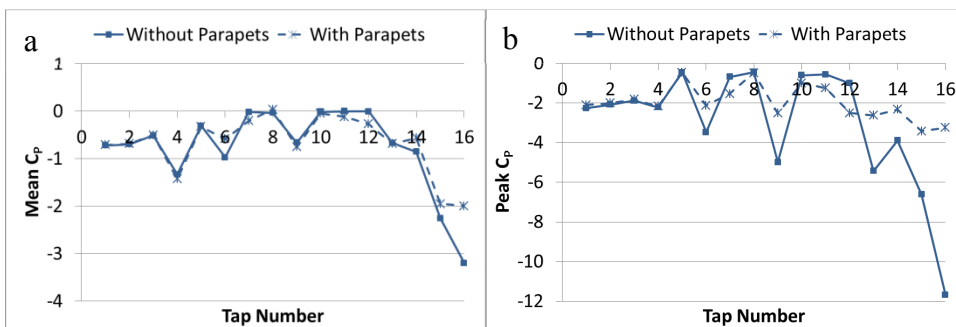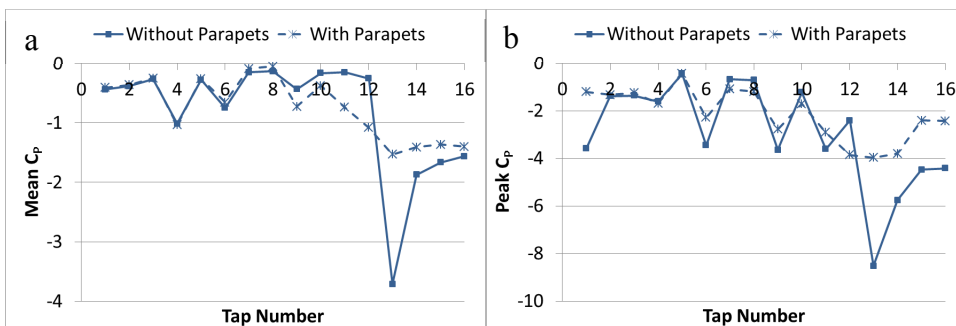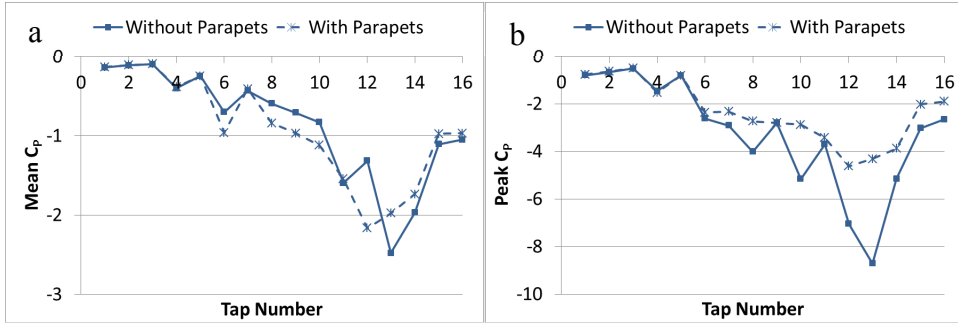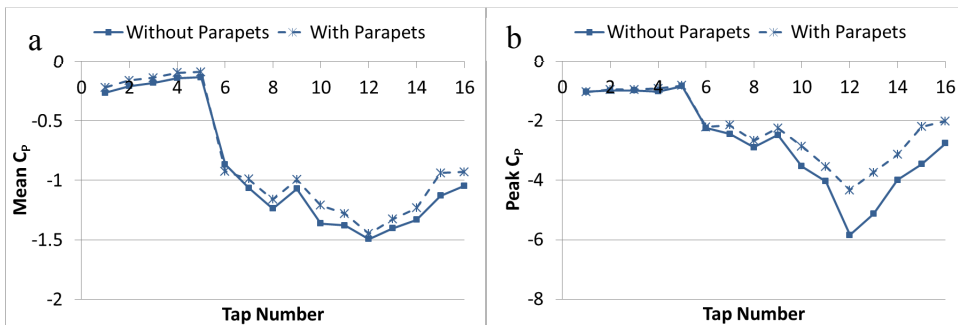for WD = 90°: a. $C_{p\,mean}$ Comparison, b. $C_{p\,peak}$ Comparison



135
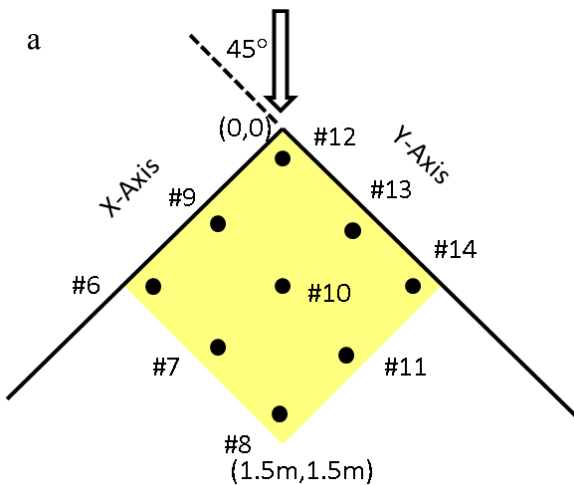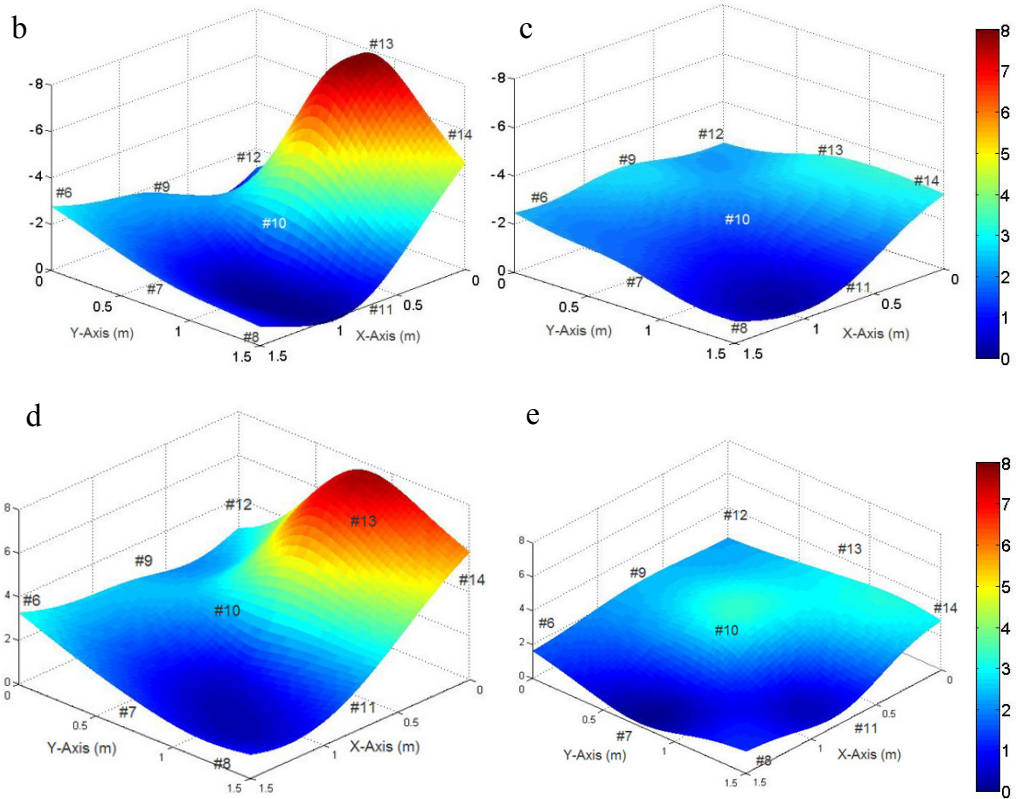
Figure 23. Comparison of Instantaneous 3-D Pressure Coefficient Contours Without and With Parapets for Gable Roof Corner (Area 1) for WD = 45°: a. Tap Locations for Area 1 (Prototype Dimension), b. Pressure Coefficient Contours Without Parapets for WOW, c. Pressure Coefficient Contours With Parapets for WOW, d. Pressure Coefficient Contours Without Parapets for Wind Tunnel, e. Pressure Coefficient Contours With Parapets for Wind Tunnel.

### 5.5.3. Results for Hip Roof Building Model

Figures 24 to 30 show the comparisons of pressure coefficients without and with the discontinuous parapets for the hip roof model. The parapets did not have significant effects on $C_{p\,mean}$ values. The highest reductions in $C_{p\,peak}$ values were noted for corner

taps near the sloped ridge line, for example, 57% and 54% reductions for taps 12 and 13, respectively, for WD = 45° (see Fig. 27b) and 54% reduction for tap 13 for WD = 60° (see Fig. 28b). The reduction in area averaged peak pressure coefficient was estimated for corner Area 1. Similar to the gable roof case, the highest reduction (38%) was achieved for diagonal wind direction WD = 45°. In Fig. 31, three-dimensional pressure coefficient contours are plotted for Area 1 for WD = 45°. The contours correspond to the time when the area-averaged suction reached the highest magnitude (largest suctions occurred at $t$ = 16.8 sec and $t$ = 62.9 sec for without- and with- parapet case, respectively). The without-parapet contour (Fig. 31b) shows that the large suctions occurred at taps 12 and 13 near the corner and the suctions were significantly mitigated after installing the perforated parapets (Fig. 31c). Thus the parapets were effective in alleviating high suctions for corner zones on both sides of the sloped ridge line where damage initiation often occurs. About 18% reduction was estimated by analyzing the wind tunnel results (Figs. 31d and 31e), which was lower than the 38% reduction obtained in the WOW. The differences could due to Reynolds number effects as the Reynolds number in WOW was about 15 times greater than that in the wind tunnel.



Figure 24. Comparisons of $C_p$ Values Without and With Parapets on Hip Roof Model for WD = 0°: a. $C_{p\ mean}$ Comparison, b. $C_{p\ peak}$ Comparison

Figure 25. Comparisons of $C_p$ Values Without and With Parapets on Hip Roof Model for

WD = 15°: a. $C_{p\,mean}$ Comparison, b. $C_{p\,peak}$ Comparison



Figure 26. Comparisons of $C_p$ Values Without and With Parapets on Hip Roof Model for

WD = 30°: a. $C_{p\,mean}$ Comparison, b. $C_{p\,peak}$ Comparison



Figure 27. Comparisons of $C_p$ Values Without and With Parapets on Hip Roof Model for

WD = 45°: a. $C_{p\,mean}$ Comparison, b. $C_{p\,peak}$ Comparison

138

Figure 28. Comparisons of $C_p$ Values Without and With Parapets on Hip Roof Model for

WD = 60°: a. $C_{p\,mean}$ Comparison, b. $C_{p\,peak}$ Comparison



Figure 29. Comparisons of $C_p$ Values Without and With Parapets on Hip Roof Model for

WD = 75°: a. $C_{p\,mean}$ Comparison, b. $C_{p\,peak}$ Comparison
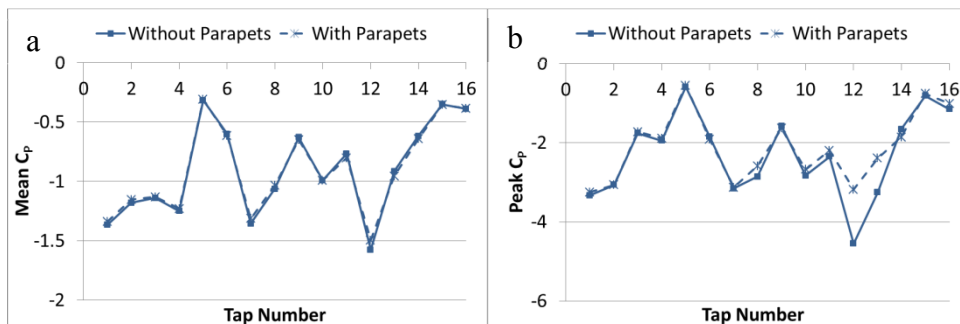


Figure 30. Comparisons of $C_p$ Values Without and With Parapets on Hip Roof Model for

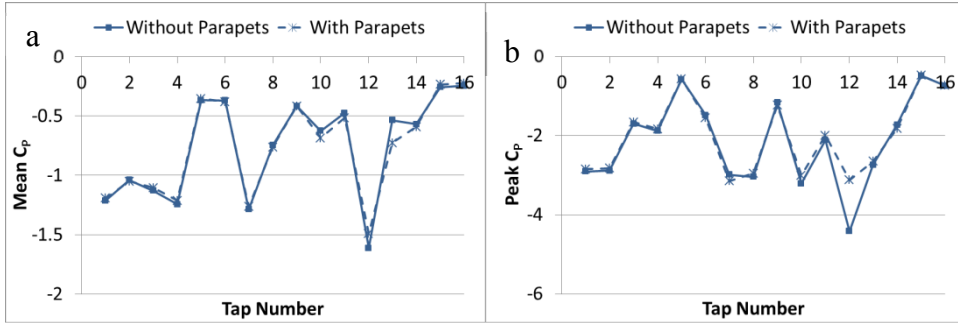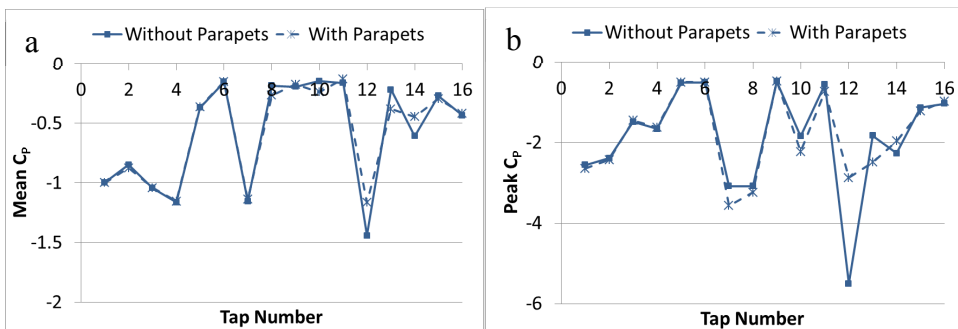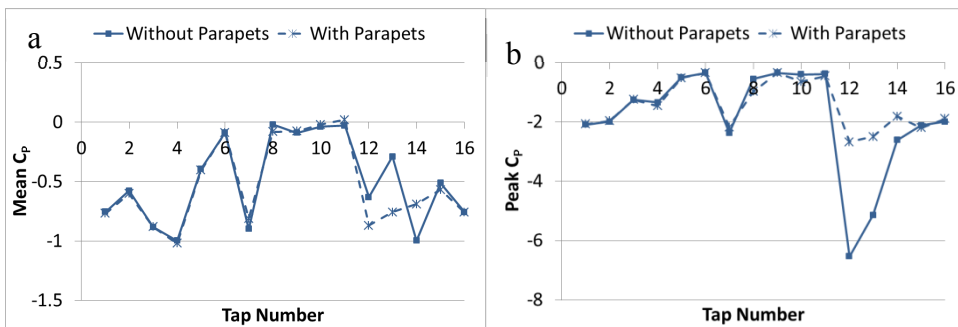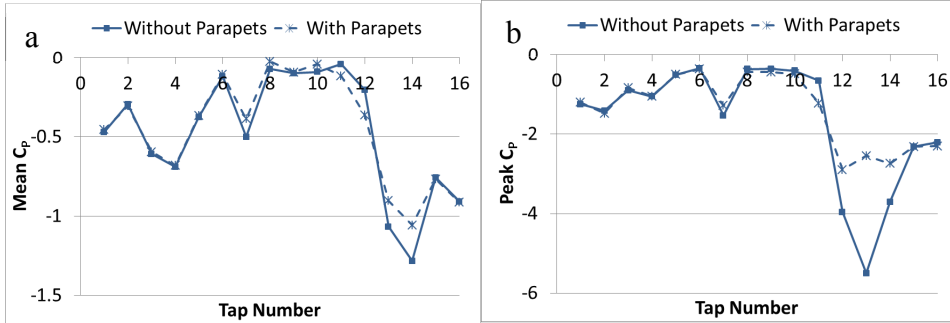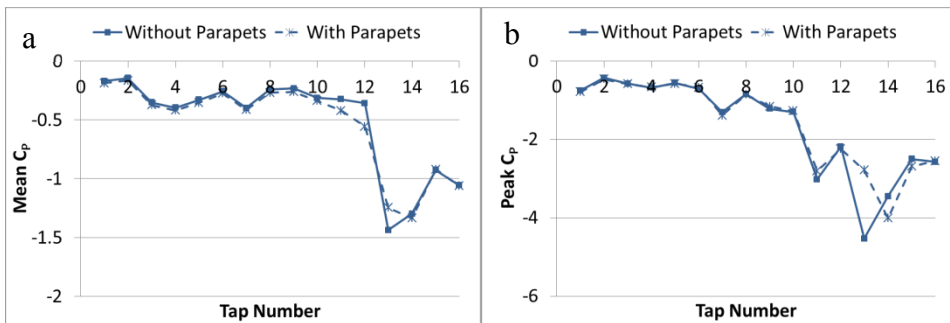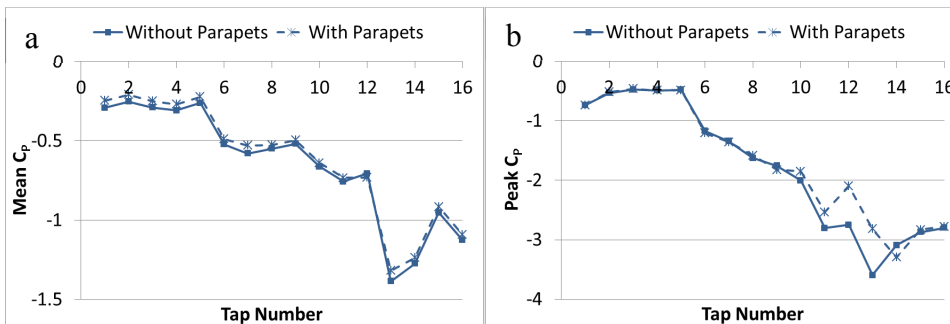WD = 90°: a. $C_{p\,mean}$ Comparison, b. $C_{p\,peak}$ Comparison
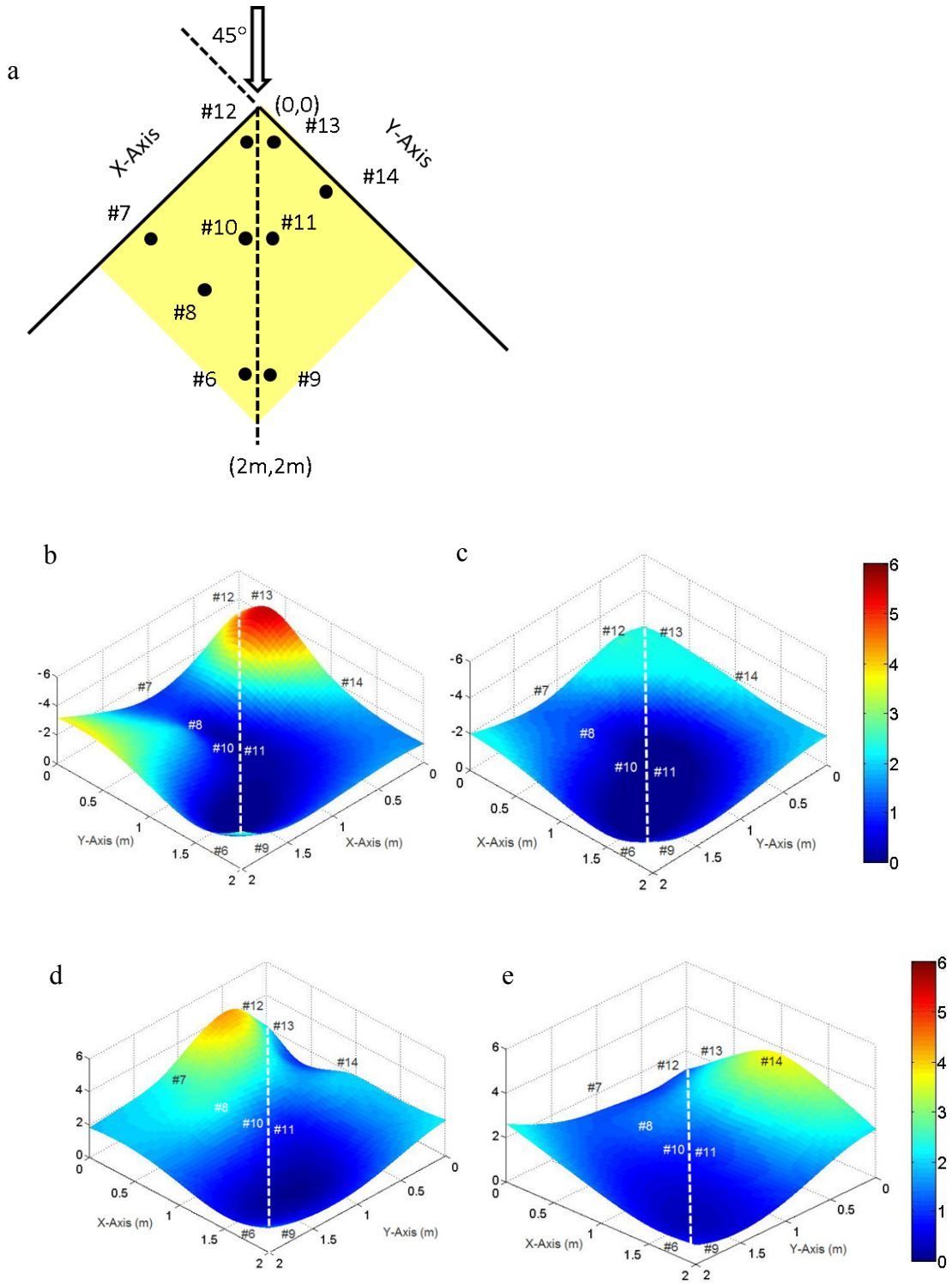
Figure 31. Comparison of Instantaneous 3-D Pressure Coefficient Contours Without and

With Parapets for Hip Roof Corner (Area 1) for WD = 45°: a. Tap Locations for Area 1

(Prototype Dimension), b. Pressure Coefficient Contours Without Parapets for WOW, c. Pressure Coefficient Contours With Parapets for WOW, d. Pressure Coefficient Contours Without Parapets for Wind Tunnel, e. Pressure Coefficient Contours With Parapets for Wind Tunnel.

### 5.6 Summary and Conclusions

A methodology was presented for testing large-scale models of low-rise buildings in flows that replicate only the high frequency fluctuations of the longitudinal wind velocity. Flow management devices were used in an open-jet 12-fan WOW facility to generate a turbulence spectrum with high frequency turbulence components similar to those of ABL flows. It was hypothesized that two flows – characterized, respectively, by a full turbulence spectrum (achieved in an ABL wind tunnel flow) and by a partial turbulence spectrum with missing low frequency fluctuations (achieved in the WOW flow) – will induce similar wind effects (e.g., pressure coefficients) if both flows have (1) similar high frequency content, and (2) the mean wind speed $U$ in the flow with weak low frequency fluctuations is augmented by an increment $\Delta U$ to compensate for the missing fluctuations. A numerical iteration procedure, developed for estimating $\Delta U$, was shown to yield good agreement of the high frequency portions of the prototype counterparts of the partial spectrum obtained in the WOW on the one hand and the ABL wind tunnel full spectrum on the other. The hypothesis was validated by comparing pressures measured on 3:12 gable and hip roof building models tested in a full turbulence spectrum flow in the ABL wind tunnel and a partial turbulence spectrum flow in the WOW. Mean and peak pressure coefficients obtained in the two facilities were in reasonable agreement for most cases. For some tap locations in high suction zones on the roof, the WOW estimated peak pres-

141

sure coefficients were higher in magnitude than their wind tunnel counterparts. Further research will be conducted to evaluate if these differences are due to Reynolds number effects and/or slightly higher spectral content in the WOW. After validating the partial turbulence flow simulation methodology for testing large-scale models, WOW experimentation was performed to study the effectiveness of discontinuous perforated parapets in alleviating high suction pressure at critical roof locations. For the gable roof, a maximum reduction of 72% in peak pressure coefficient was observed for a gable end ridge tap when using the parapet (a maximum reduction of 60% was observed in a wind tunnel study by Suaris and Irwin (2010) while using similar perforated parapets on a 3:12 gable roof). For the hip roof, a maximum reduction of 57% was observed for a corner tap near the sloped ridge line. Significant reductions in area averaged peak pressures for high suction zones were obtained for both roofs when using discontinuous parapets (up to 48% and 38% for gable and hip roofs, respectively). Overall, the discontinuous porous parapets, which can be also used as architectural features, performed well in reducing high suctions at critical roof locations and did not have any unwanted effect on the remaining roof area. These simple architectural features can be retrofitted in existing buildings or constructed on new low-rise buildings to improve roof performance. Limited comparisons showed that the percentage reductions in area-averaged pressures were in most cases higher in the WOW large-scale testing than those obtained in the wind tunnel small-scale testing. This study demonstrated that the partial simulation methodology can be effective in validating mitigation techniques to reduce wind damage on low-rise buildings. Such simulations with deficient low-frequency spectral content are freed of integral length scale constraints so that model length scales are only limited by blockage considerations.

This is a major advantage, because it allows for both testing at higher Reynolds number and better spatial resolution of the pressure taps in high pressure zones.

### 5.7 Acknowledgements

### 5.8 Reference

ASCE. (2010). "Minimum design loads for buildings and other structures." ASCE/SEI 7-10, Reston, VA.

ASCE. (2012). "Wind tunnel testing for buildings and other structures." ASCE/SEI 49-12, Reston, VA.

Aly, A. M., Bitsuamlak, G. T., and Gan Chowdhury, A. (2012). "Full-scale aerodynamic testing of a loose concrete roof paver system." *J. Eng. Struct.*, 44, 260-270.

Aly, A. M., Gan Chowdhury, A., and Bitsuamlak, G. (2011). "Wind Profile Management and Blockage Assessment of a New 12-Fan Wall of Wind Facility at FIU." *J. Wind Struct.*, 14(4), 285-300.

Banks D. (2011). "Measuring peak wind loads on solar power assemblies." *The 13th International Conference on Wind Engineering*, Amsterdam, Netherlands.

Baskaran A., and Stathopoulos, T. (1998). "Roof corner pressure loads and parapet configurations." *J. Wind Eng. Ind. Aerodyn.*, 29, 79-88.

Bitsuamlak, G.T., Gan Chowdhury, A., and Sambare, D. (2009). "Application of a full-scale testing facility for assessing wind-driven-rain intrusion." *J. Building Environm.*, 44(12), 2430-2441.

Bitsuamlak, G. T., Warsido, W., Ledesma E., and Gan Chowdhury, A. (2013). "Aerodynamic Mitigation of Roof and Wall Corner Suctions Using Simple Architectural Elements." *J. Eng. Mech.*, 139, 396-408.

Blessing, C., Gan Chowdhury, A., Lin, J., and Huang, P. (2009). "Full-scale validation of vortex suppression techniques for mitigation of roof uplift." *J. Eng. Struct.*, 31(12), 2936–2946.

Cheung, J. C. K., Holmes, J. D., Melbourne, W. H., Lakshmanan, N., and Bowditch, P. (1997). "Pressure on a 1:10 scale model of the Texas Tech Building." *J. Wind Eng. Ind. Aerodyn.*, 69-71, 529-538.

Cochran, J. S. and English, E. (1997), "Reduction of roof wind loads by architectural features", *Architectural Science Review*, 40, 79-87.

Fu, T.C., Aly, A. M., Gan Chowdhury, A., Bitsuamlak, G., Yeo, D., and Simiu, E. (2012). "A proposed technique for determining aerodynamic pressure on residential homes." *J. Wind Struct.*, 15(1), 27.-41

Huang, P., Gan Chowdhury, A., Bitsuamlak, G., and Liu, R. (2009). "Development of devices and methods for simulation of hurricane winds in a full-scale testing facility." *J. Wind Struct.*, 12(2), 151-177.

Holmes, J.D. (2007). *Wind Loading of Structures,* 2nd Ed. Taylor & Francis, London.

Hoxey, R. P., Reynolds, A. M., Richardson, G. M., Robertson, A. P., and Short, J. L. (1998). "Observations of Reynolds number sensitivity in the separated flow region on a bluff body." *J. Wind Eng. Ind. Aerodyn.*, 73, 231-249.

Irwin, P. (1981). "The design of spires for wind simulation." *J. Wind Eng. Ind. Aerodyn.*, 7, 361-366.

Irwin, P. (2009). "Wind engineering research needs, building codes and project specific studies." 11th Americas Conference on Wind Engineering, San Juan, Puerto Rico.

Irwin, P., Cooper, K., and Girard, R. (1979). "Correction of distortion effects caused by tubing systems in measurements of fluctuating pressures." *J. Wind Eng. Ind. Aerodyn.*, 5, 93-107.

Jones, N.P., Reed, D.A., and Cermak, J.E. (1995). "National wind-hazards reduction program." *J. Prof. Issues Eng. Educ. Pract.*, 121(1), 41–46.

Kopp, G. A., and Banks, D. (2013). "Use of the wind tunnel test method for obtaining

design wind loads on roof-mounted solar arrays." *J. Struct. Eng.*, 139, 284-287.

Kopp, G.A., Mans, C., and Surry, D. (2005). "Wind effects of parapets on low buildings: Part 4. Mitigation of corner loads with alternative geometry." *J. Wind Eng. Ind. Aerodyn.*, 93, 873-888.

Kopp, G. A., Morrison, M. J., Gavanski, E., Henderson, D. J., and Hong, H. P. (2010). "The 'Three Little Pigs' project: hurricane risk mitigation by integrated wind tunnel and fullscale laboratory tests." *Nat. Haz. Rev.*, 11, 151–161.

Lin, J.X., and Surry, D. (1993). "Suppressing extreme suction on low buildings by modifying the roof corner geometry." *Proc. 7th US National Conf. on Wind Eng.*, Univ. of Calif., USA, Session 3A.

Liu, Z., Brown, T.M., Cope, A.D., and Reinhold, T.A. (2011). "Commissioning of the wind test capabilities of the IBHS Research Center." *Proc. 13th Int. Conf. Wind Eng.*, Amsterdam, Netherlands.

MDC-BCCO. Post hurricane Wilma progress assessment. Miami-Dade County Building Code Compliance Office, Miami, FL, 2006:1-22.

Melbourne W. H. (1980). "Turbulence effects on maximum surface pressures – a mechanism and possibility of reduction." *J. Wind Eng.*, 1, 521-551.

Mensah A. F., Datin, P. L., Prevatt, D., Gupta, R., and van de Lindt, J. W. (2011). "Database-assisted design methodology to predict wind – induced structural behavior of a light-framed wood building." *J. Eng. Struct.*, 33, 674-684.

Natarajan, D., and Hangan, H. (2010). "Preliminary numerical simulation of axi-symmetric flows in WindEEE dome facility." *Proc. 5th Int. Symp. on Computational Wind Engineering (CWE2010)*, *International Association for Wind Engineering (IAWE)*, Kanagawa, Japan.

National Oceanic and Atmospheric Administration (2013). Population trends from 1970 to 2020. National Costal Population Report.

Richards, P.J., Hoxey, R.P., Connell, R.P., and Lander, D.P. (2007). "Wind-tunnel modelling of the Silsoe Cube." *J. Wind Eng. Ind. Aerod.*, 95, 1384-1399.

Sadek, F., and Simiu, E. (2002). "Peak non-Gaussian wind effects for database-assisted low-rise building design." *J. Eng. Mech.*, 128(5), 530-539.

Simiu, E. (2011), *Design of Buildings for Wind¸* Wiley, Hoboken.

Simiu, E., Bitsuamlak, G., Gan Chowdhury, A., Li, R., Tecle, A., and Yeo, D.H. (2011). "Testing of residential homes under wind loads." *J. Nat. Hazards Rev.*, 12(4), 166-170.

Simiu, E. and Scanlan, R.H. (1996). *Wind Effects on Structures*, Wiley, New York

Stathopoulos, T., Marathe, R., and Wu, H. (1999). "Mean wind pressure on flat roof corners affected by parapets: field and wind tunnel studies." *J. Eng. Struct.*, 21, 629-638.

Suaris, W., and Irwin, P. (2010). "Effect of roof-edge parapets on mitigating extreme roof suctions." *J. Wind Eng. Ind. Aerodyn.*, 98, 483–491.

Suresh, Kumar, K., and Stathopoulos, T. (1998), "Power spectra of wind pressures on low building roofs", *J. Wind Eng. Ind. Aerodyn.*, 74-76, 665-674.

Surry D. and Lin, X. J. (1995). "The effect of surroundings and roof corner geometric modifications on roof pressures on low-rise buildings." *J. Wind Eng. Ind. Aerodyn.*, 58, 113-138.

Tecle, A., Bitsuamlak, G., Suksawang N., Gan Chowdhury, A., and Fuez, S. (2013). "Ridge and field tile aerodynamics for a low-rise building: a full-scale study." *Wind and Struct.,* 16(4), 301-322.

Tieleman, H. W. (2003). "Wind tunnel simulation of wind loading on low-rise structures: a review." *J. Wind Eng. Ind. Aerod.*, 91, 1627-1649.

Tieleman, H. W., Hajj, M. R., and Reinhold, T. A. (1998). "Wind tunnel simulation requirements to asses wind loads on low-rise buildings." *J. Wind Eng. Ind. Aerod.*, 74-76, 675-685.

Yamada, H., and Katsuchi, H. (2008). "Wind-tunnel study on effects of small-scale turbulence on flow patterns around rectangular cylinder." *Proc. of the 4th International Colloquium on Bluff Bodies Aerodynamics & Applications*, Italy.

Yeo, D., and Gan Chowdhury, A. (2013). "A simplified wind flow model for the estimation of aerodynamic effects on small structures." *J. Eng. Mech.*, 139, 367-375.

**CHAPTER VI**

SUMMARY AND CONCLUSION

# CHAPTER VI

## SUMMARY AND CONCLUSION

This chapter summarizes the conclusions of this dissertation. The achievements in this dissertation are summarized into 3 parts: 1. A partial turbulence simulation methodology using an iterative procedure was successfully developed to yield good agreement of the high frequency portion with the ABL flow. 2. Pressure results obtained using large-scale models at the WOW facility compared well to both the full-scale TTU and Silsoe building and small-scale wind tunnel model measurements. This validated the partial turbulence simulation methodology. 3. The effectiveness of discontinuous perforated parapets in alleviating high suction pressure at critical roof locations was demonstrated by testing typical two-story residential buildings in the WOW using the partial turbulence simulation method. The details are described in the following sections.

### 6.1 Flow simulation

A partial turbulence simulation methodology using an iterative procedure was developed. The simulation was shown to be appropriate for testing of large-scale models in aerodynamic facilities. Such simulation with deficient low-frequency spectral content is freed of integral length scale constraints so that model length scales are only limited by blockage considerations. This is a major advantage, because it allows for both testing at higher Reynolds number and greater spatial resolution of the pressure taps in high pressure zones. The methodology was applied successfully in the 12-fan WOW open-jet wind testing facility and partial simulation results were obtained. Flow management devices were used in an open-jet 12-fan WOW facility to generate turbulence spectrum with high frequency components similar to those of ABL flows. A methodology was presented for

testing large-scale models of low-rise buildings in flows that replicate only the high frequency fluctuations of the longitudinal wind velocity. It was hypothesized that two flows – characterized, respectively, by a full turbulence spectrum (achieved in an ABL wind tunnel flow) and by a partial turbulence spectrum with missing low frequency fluctuations (achieved in the WOW flow) – will induce similar wind effects if both flows have (1) similar high frequency content, and (2) mean wind speed in the flow with weak low frequency fluctuations is augmented by an increment to compensate for the missing fluctuations. A numerical iteration procedure was shown to yield good agreement of the high frequency portion of the partial spectrum obtained in the laboratory on the one hand and the ABL spectrum model on the other. The high frequency portion of the partial spectrum obtained in the WOW compared well with the full spectrum in an ABL wind tunnel and prototype full spectrum for the TTU and Silsoe site.

## 6.2 Pressure validation

Pressure measurements and comparisons of mean and peak pressure coefficient estimates were performed for (1) the partial turbulence flow in small and large-scale 12-Fan WOW, and (2) the full turbulence flow in the ABL wind tunnel and field data for TTU and Silsoe sites. For four gable and hip roof low rise building models it was shown that both the wind tunnel and the small-scale WOW produced comparable high suctions (high peak pressure coefficients) for critical locations near the leading edge for low-slope roof, leeward edge,  gable end ridge, and downwind of sloped hips. The results showed that similar high suction can occur near the gable end ridge for cornering wind and the downwind side of the sloped hip for both cornering wind and wind perpendicular to the eave. The findings provide an explanation to why failures initiate mostly at these ridge

and hip locations. Besides using small-scale WOW to validate the pressure field, the large-scale 12-Fan WOW was also used to perform and verify the effectiveness of partial turbulence simulation by comparing the WOW pressure coefficients with their full-scale (TTU and Silsoe buildings) and smaller model-scale (wind tunnel) counterparts. For the open terrain, 1:6 TTU building model and 1:5 Silsoe building model were tested and the pressure coefficients were compared with their benchmark prototype counterpart. For most cases, the pressure results obtained from WOW partial simulation for taps experiencing high mean and peak suctions were in reasonable agreement with their full-scale counterparts. For the suburban terrain, 3:12 gable and hip roof building models were tested and the pressure coefficients were compared with those obtained in full turbulence spectrum flow in an ABL wind tunnel. The mean and peak pressure coefficients obtained in the two facilities were in reasonable agreement for most cases. All the pressure comparisons showed that the partial turbulence simulation approach was effective aerodynamically.

## 6.3 Uplift pressure mitigation

WOW experimentation was performed to study the effectiveness of discontinuous perforated parapets in alleviating high suction pressure at critical roof locations. For the 3:12 gable roof, a maximum reduction of 72% in peak pressure coefficient was observed for a gable end ridge tap when using the parapet. For the 3:12 hip roof, a maximum reduction of 58% was observed for a corner tap near the sloped ridge line. Significant reductions in area averaged peak pressures for high suction zones were obtained for both roofs when using discontinuous parapets (up to 48% and 38% for gable and hip roofs, respectively). Overall, the discontinuous porous parapets, which can be also used as ar-

chitectural features, performed well in reducing high suctions at critical roof locations. These simple architectural features can be retrofitted in existing buildings or constructed on new low-rise buildings to improve roof performance. Limited comparisons showed that the percentage reductions in area-averaged pressures using the discontinuous porous parapets were in most cases higher in the WOW large-scale testing than those obtained in the wind tunnel small-scale testing. In addition, the experiments performed for testing the effects on parapets showed that the partial simulation methodology can be effective in validating mitigation techniques to reduce wind damage to low-rise buildings.

# CHAPTER VII

## RECOMMENDATIONS FOR FUTURE RESEARCH

# CHAPTER VII

# RECOMMENDATIONS FOR FUTURE RESEARCH

Future tests should be planned to refine the partial turbulence simulation technique and validate it for a wide range of model-to-full-scale ratios. These tests should address the effects of Reynolds Number (Re), the effects of sudden change of internal pressure, and the effects of no-stationary gusts.

## 7.1 Reynolds number

Hoxey (1998) described that bluff body aerodynamic effects can be highly depended on Reynolds Number (Re). In 2001, Schewe also carried out a series of tests and discovered that Re had significant effects on the mean pressure coefficients ($C_p$) for the structures with sharp edges. The Re number in Schewe's study ranged between $10^4$ and $10^7$. In general, the Re values of conventional wind tunnel tests and WOW tests are about $10^4$ and $10^6$, respectively. It is necessary to further investigate Re effects on civil engineering structures. Moreover, different from the global Re mentioned above, the effects of local Re could be also important. These Re effects are due to the local aerodynamic loads generated by architectural details. In most cases, the testing of buildings in small-scale experimentation is usually simplified. However, architectural features are important in terms of local aerodynamic loads. Thus there is a need to perform partial turbulence simulation experiments using large-scale testing models to find local Re effects.

## 7.2 Internal pressure

The net wind pressures acting on building envelopes are the combination of external and internal pressures. The opening sizes and locations are the most important factors influencing internal pressures. During hurricanes wind-borne debris may create a siz-

able opening suddenly and result in abrupt change of the internal pressure. There is a need to study the effect of partial simulation flows on internal pressures due to sudden breach of envelope.

**7.3 Non-Stationary gusts and rapid directionality changes**

During extreme events such as hurricane, strong wind gust and rapid directionality changes may occur. Such transient effects may have significant influence on wind loading which can exceed quasi-steady loading. Partial turbulence simulation methodology can be used to perform research on non-stationary phenomena and their effects on structures.

# VITA

## EDUCATION

2007-Present   Doctoral Candidate,
Department of Civil and Environmental Engineering,
Florida International University, Miami, FL.

2004            M.S., Department of Civil and Environmental Engineering,
West Virginia University, Morgantown, WV.

2000            B.E., Department of Civil and Environmental Engineering,
National Central University, Taoyuan, Taiwan

## PROFESSIONAL EXPERIENCE

2008-2013   Research Assistant, International Hurricane Research Center,
Florida International University, Miami, FL.
2007-2008   Teaching Assistant, Department of Civil and Environmental Engineering,
Florida International University, Miami, FL.

## PUBLICATIONS AND PRESENTATIONS

Fu, T.C., Aly, A.M., Bitsuamlak, G., Gan Chowdhury, A., Simiu, E. (2010) "Flow Simulation in 12-Fan Wall of Wind Testing Facility" The 2nd American Association for Wind Engineering Workshop (2AAWE), Marco Island, Florida, USA, August 18-20, 2010.

Fu, T.C., Aly, A.M., Gan Chowdhury, A., Bitsuamlak, G., Yeo, D.H. and Simiu, E. (2011), "Simplified wind flow and aerodynamic response of residential homes: Laboratory and Computational Fluid Dynamics simulations," 4 International Conference on Experimental Vibration Analysis for Civil Engineering Structures (EVACES 2011), Varenna, Italy, October 3-5, 2011.

Fu, T.C., Aly, A. M., Gan Chowdhury, A., Bitsuamlak, G., Yeo, D., and Simiu, E. (2012), "A Proposed Technique for Determining Aerodynamic Pressure on Residential Homes", Wind and Structures, 15(1), 27-41.

Fu, T.C., Gan Chowdhury, A., Bitsuamlak, G., Li, R. and Aly, A.M., (2011), "Wall of wind facility: low-rise buildings roof pressure validation," The EMI 2011 Engineering Mechanics Institute Conference, Northeastern University, Boston, MA, USA, June 2-4, 2011.

Fu, T.C, Gan Chowdhury, A., and Bitsuamlak, G., (2012) "An Open-Jet Test Facility Validation Using Comparison of Pressure Field on Buildings", ASCE Advances in Hurricane Engineering Conference (ATC & SEC), Miami, United States, October 24-26, 2012.

Fu, T.C., Gan Chowdhury, A., Bitsuamlak G., Simiu, E. "Pressure Validation for an Open-Jet Wind Testing Facility", submitted to Wind and Structures, Jul. 2013, in progress.

Fu, T.C., Gan Chowdhury, A., Smith D., Zisis I., Irwin P., Simiu E. "Experimental Simulation of Wind Pressures on Large-Scale Building Models and Comparisons with Field Measurements', submitted to Journal of Wind Engineering and Industrial Aerodynamics, Sep. 2013, in progress.

Fu, T.C., Gan Chowdhury, A., Zisis I., Irwin P., "Experimental Simulation of Wind Pressures on Large-Scale Building Models and Comparisons with Field Measurements', submitted to Engineering Structures, Nov. 2103, in progress.

Gan Chowdhury, A., Bitsuamlak, G., Fu, T., and Kawade, P. (2011), "Study on Roof Vents Subjected to Simulated Hurricane Effects." ASCE, Nat. Hazards Rev. 12, SPECIAL ISSUE: Hurricanes and Insurance, 158–165.


**TRAINING/PROFESSIONAL MEMBERSHIPS**

2011-Present        Membership of Chi-Epsilon Honor Society of Civil Engineering
                    Honor Society